ABSTRACT

Title of Thesis: OPTICAL PROPERTIES OF MARINE AND PICOCYANOBACTERIA-DERIVED DISSOLVED ORGANIC MATTER IN THE ATLANTIC, PACIFIC AND DURING LONG-TERM INCUBATION EXPERIMENTS

Madeline Amelia Lahm, Master of Science, 2022

Thesis directed by: Dr. Michael Gonsior
University of Maryland Center for Environmental Science
Marine-Estuarine and Environmental Science

Marine dissolved organic matter (DOM) is a large, dynamic, and complex pool of carbon, comparable in size to the carbon dioxide pool in the atmosphere, yet it is arguably the least understood component of the global carbon cycle. DOM deriving from picocyanobacterial cells via situationally unique mechanisms, such as viral lysis and metazoan grazing, complicate the picture as the resident pool present reflects sequestration processes that occur at time scales ranging from days to hundreds of thousands of years. Recently virus induced cell lysis released from the globally distributed picocyanobacteria, such as *Synechococcus* and *Prochlorococcus,* have been shown to release optically active DOM known as Chromophoric DOM (CDOM) that closely matches the “humic-like” appearance of marine CDOM raising questions about our understanding of this carbon pool given the reliance on spectral measures to assess its composition. Hence, this thesis is seeking to understand CDOM released by lysed picocyanobacteria and to investigate the molecular chemical composition of picocyanobacteria-

derived DOM in general. A special focus will be to confirm the refractory nature of chromophores released by lysed picocyanobacteria (*Synechococcus*) given the reliance on optical properties of recalcitrant DOM being used in the investigation of timescales of carbon storage and biological processing of carbon. As we consider the outcomes of the current global carbon inventory with a sizable error in flux, linking products of microbial processes to chromophore structures and spectrometry is a capstone in understanding the global carbon cycle for decades of research. This study offers a direct comparison of fluorescence signatures from the Bermuda Atlantic Time-Series (BATS) and the Hawai'i Ocean Time-series (HOT), observes optical and nutrient profiles tracking long-term incubation experiments of oligotrophic microbial communities amended with *Synechococcus*-derived DOM, and explores new techniques in DOM solid-phase extraction (SPE). This work is part of a National Science Foundation project - *The Fate of Lysis Products of Picocyanobacteria Contributes to Marine Humic-like Chromophoric Dissolved Organic Matter* – linking the accumulating evidence of picocyanobacterial-derived DOM to our understanding of marine organic carbon. Furthermore, we seek to understand how picocyanobacteria-derived DOM is degraded and what role changing heterotrophic microbial communities plays. This research is important to the concept of a microbial carbon pump that supplies a constrained and constant source of DOM which has important implications for the marine carbon cycle and its role in global climate.

OPTICAL PROPERTIES OF MARINE AND PICOCYANOBACTERIA-DERIVED DISSOLVED ORGANIC MATTER IN THE ATLANTIC, PACIFIC AND DURING LONG-TERM INCUBATION EXPERIMENTS

by

Madeline Amelia Lahm

Thesis submitted to the Faculty of the Graduate School of the
University of Maryland, College Park in partial fulfillment of the
requirements for the degree of
Master of Science
2022

Advisory Committee:

Associate Professor Dr. Michael Gonsior, UMCES CBL, Chair
Professor Dr. Feng Chen, UMCES IMET
Associate Research Professor Dr. Andrew Heyes, UMCES CBL

Preface

This work is part of the National Science Foundation project # 1829888: *The Fate of Lysis Products of Picocyanobacteria Contributes to Marine Humic-like Chromophoric Dissolved Organic Matte*r.

Acknowledgments

When I started my work at the Chesapeake Biological Laboratory (CBL) in Solomons, Maryland in July of 2019, I would never have imagined that my master's experience would be disrupted by the Coronavirus global pandemic. I would like to begin by expressing my gratitude for the CBL facilities and maintenance teams for their essential work in ensuring that our work could safely continue in these times of crisis.

I would like to thank and acknowledge the funding that made the project and my growth as a scientist possible through the National Science Foundation grant awarded to Michael Gonsior and Feng Chen as principal investigators of the fate of lysis products of picocyanobacteria contributes to marine humic-like chromophoric dissolved organic matter. Thanks to additional funding from Anne Harrison and the CBL Graduate Education Committee, I was able to attend the 2020 Ocean Sciences Meeting in San Diego, California to engage in professional development and present my research.

Next, I want to recognize Dr. Michael Gonsior who took a chance on me – without his offer to join this project and the last three years of support as my advisor, I would not know what I am capable of. Michael has taught me so much about what it means to be a scientist by pushing me outside of my comfort zone and encouraging me to participate in my passion, fieldwork, for and outside of the project. I would also like to thank my remarkable lab mates over the years – Dr. Leanne Powers, Dr. Alec Armstrong, Dr. Katie Martin, Alexandra Gibbs. Special extra thanks to Dr. Leanne Powers and Dr. Alec Armstrong who were tremendously helpful as they worked on their own post-doc and Ph.D. respectively in the Gonsior Lab. I'd also especially like

to thank Andrew Heyes as an honorary member of the Gonsior Lab since he was always there whenever I needed something when Michael was gone. Their guidance and support boosted my own abilities and were instrumental in hurdling roadblocks in my research and analysis. Outside the members of the Gonsior Lab, this research would not have been possible without the other main collaborators on this project: committee member Dr. Feng Chen and Ph.D. student Yufeng "Freddy" Jia. I would also like to acknowledge the work contributed by the Chen Lab research assistant Lauren Wagner and graduate students Dr. Daniel Fucich and Dr. Ana Sosa.

Finally, I would like to thank everyone who supported me in my pursuit of this degree. I am indebted to my friends, roommates, family, and undergraduate mentors – Professors Dr. Matthew Evans and Dr. Janina Benoit of Wheaton College. Here I would also like to express my gratitude for my assistant coach David Wenrich, the Jets White 2021-22 squad, and the Southern Maryland Jets Lacrosse Program. I am extremely grateful for the outlet that being a lacrosse coach and referee has given me but also for the community it gave me during my time here in Southern Maryland. Extra special thanks to Stefenie Shenoy, Lauren Rodriguez and her dog, Lady for keeping me sane.

I truly never thought that I would be sitting here writing these acknowledgements for this thesis. Reflecting back on my time at CBL, I have grown tremendously during these last three years, and I will always be grateful for it. Thank you so much to all.

Table of Contents

List of Tables

List of Figures

List of Abbreviations

a (300) – absorbance at 300 nm
ALOHA - Long-Term Oligotrophic Habitat Assessment
AOU – apparent oxygen utilization
AQY - apparent fluorescence quantum yield
BATS – Bermuda Atlantic Time Series
BGE - Bacterial Growth Efficiency
CBL – Chesapeake Biological Laboratory
CDOM – chromophoric DOM
chl-*a* - chlorophyll-a
CO_2 – Carbon Dioxide
CTD – conductivity, temperature, depth
DIC – dissolved inorganic carbon
DOC – dissolved organic carbon
DOM – dissolved organic matter
DON – Dissolved Organic Nitrogen
DOP – dissolved organic phosphorous
E2/E3 (a(250)/a(365))
EEM – excitation and emission matrix
EPA – Environmental Protection Agency
ESI - electrospray ionization
FA – Formic Acid
FDOM – fluorescent DOM
$FDOM_H$ - "humic-like" FDOM
$FDOM_P$ – "protein-like" FDOM
Fmax – Fluorescence Maximum
FT-ICR MS - Fourier-transform ion cyclotron resonance mass spectrometry
HCl - Hydrochloric Acid
HMW – high molecular weight
HOT – Hawai'i Oceanic Time-Series
HPLC - high performance liquid chromatography
m/z – mass to charge ratio
MCP – microbial carbon Pump
MeOH – Methanol
MS – mass spectrometry
MS/MS - tandem mass spectrometry
MW- Molecular Weight
NASL - Nutrient Analytical Services Laboratory
NH_4 – Ammonium
NH_4OH – Ammonium-Hydroxide
NM – nominal mass
NO_2 - Nitrite
NO_3 - Nitrate
NSF – National Science Foundation
ODV – Ocean Data View

OMZ - oxygen minimum zone
PARAFAC – Parallel Factor Analysis
PO_4 - Phosphate
POM – particulate organic matter
PPL - proprietary polystyrene vinyl resin
QqQ - triple quadrupole
RDOM – refractory DOM
RU - Raman units
$S_{275–295}$ - spectral slope of 275 nm – 295 nm
$S_{350–400}$ – spectral slope of 350 nm – 400 nm
SCOR - Scientific Committee on Ocean Research
SD – standard deviation
SDOM – *Synechococcus* DOM
SPE - solid-phase extraction
SR – slope ratio
TDN – total dissolved nitrogen
TDP – total dissolved phosphorous
UV-Vis – Ultra-Violet visible spectrum
WAX – weak anion exchange

Chapter 1: Introduction

1.1 The Significance of Marine Dissolved Organic Matter and its Composition

Carbon dioxide (CO_2) is an important constituent of our atmosphere and global biogeochemical processes involving CO_2 play a significant role in the Earth's life cycles and in controlling the global climate. Since the industrial era, the chemistry of the atmosphere has been altered as a direct result of increased CO_2 concentrations generated by human activities. Nearly 50% of anthropogenic CO_2 is absorbed in marine systems as they act as a major CO_2 sink. The air-sea interface is one of the most chemically active environments on earth because enormous quantities of oxygen and CO_2 are exchanged between the atmosphere and the ocean. This CO_2 is fixed by photosynthesizing autotrophic organisms which create biomass with a very complex suite of organic compounds. This biomass is then consumed and transformed into more stable organic molecules of largely unknown composition. It can be broadly defined as particulate organic matter (POM), which may partially sink through the water column and may further degrade into Dissolved Organic Matter (DOM) at depth. Several approaches have been developed to identify the DOM sources and its composition, which include stable carbon isotope analyses, use of molecular biomarkers, and spectroscopic and spectrometric techniques - specifically including optical properties[1] as a proxy for deep-ocean DOM. The mechanisms responsible for the formation of DOM remain vague and even less is known about the more stable or so-called refractory DOM. Generally speaking, DOM in aquatic systems is considered to have distinctive aspects, but vast chemical transformation makes it difficult to characterize them in detail. Broadly defined sources include allochthonous and autochthonous material. Allochthonous material originates from terrestrial environments and transported into the specific

water bodies. Autochthonous material is derived from primary producers (algae), but can be further altered by heterotrophic bacteria and zoo plankton, that produce it within a system, and anthropogenic sources[2]. Marine DOM is a complex mixture of chemical compounds considered to be mostly produced by photosynthetic plankton in the surface layers and serves as a substrate to heterotrophic microbial populations and as a nutrient source. Cycled DOM is eventually exported to the interior ocean through biogeochemical processes involving a complex array of biological and microbial processes such as transformation via bacterial degradation, protozoan grazing, and viral lysis[3] and transport via physical oceanic mechanisms. The biological pump is considered the main transport mechanism of organic carbon to the deep ocean, where particles aggregate in the photic zone and become sufficiently heavy to sink through the water column[4]. While the exact mechanism of POM dissolution remains a challenging research area, it is estimated that greater than 99% of the POM is consumed and mineralized to CO_2 or converted to DOM during the sinking process[4]. Therefore, less than 1% POM reaches the ocean floor in the oligotrophic open ocean[4]. Investigating the efficiency of CO_2 fixation by phytoplankton and the transformation from phytoplankton produced organic matter to heterotrophic microorganisms and the link between microbial functions and DOM degradation can help us understanding the carbon cycling and storage capacity of the ocean. However, the research on DOM reactivity and turnover in the deep ocean remains a challenge for the scientific community, largely driven by the complexity of the DOM pool in a given sample. Previously, marine DOM has been divided into fractions determined by its reactivity as labile, semi-labile, and Refractory Dissolved Organic Matter (RDOM)[5]. These DOM pools have respective storage timescales of minutes to days (labile), months to years (semi-labile), to hundreds of years to millennia (RDOM). RDOM refers to the large, yet undefined DOM fraction of this Dissolved Organic Carbon (DOC) pool is

"non-accessible" or "resistant" to rapid microbial degradation[5] that stores DOC for great periods of time. DOC refers to the dissolved organic forms of carbon defined as organic matter that is able to pass through a filter and is a potential source of carbon and energy for heterotrophic organisms[6]. Direct comprehensive decomposition studies of source material are logistically problematic given the large range in time scales involved for the different processes involved. This large proportion of DOM has not been characterized at the molecular level, but correlations of optical data suggested that long-wavelength absorbing and fluorescent organic compounds are part of this pool[7].

Despite the importance of marine carbon – one of the most dynamic and complex carbon pools on earth, our understanding on oceanic storage capacity in a changing climate is limited. The sources, characterization, and structural nature of this material within the oceans remains unclear and continues to be a subject of debate across research[1,8,9]. While it is well established that most marine DOM is derived from marine photoautotrophic carbon fixation and the resulting biomass degradation, chemoautotrophs may also fix substantial amounts of dissolved inorganic carbon (DIC)[10,11] but DOM arising from theses deep ocean primary producers remains a mystery. DOM turnover rates have been inferred from chemical proxies, metabolic measurements, and C flux budgets but it is debated and these postulated assessments do not consider sources and transformations outside the photic zone such as chemotrophic DOM[8]. To gain further fundamental understanding of DOM concentrations and its reactivity, biological carbon pump efficiency and the autotrophic communities that are the ultimate but variable sources of marine DOM need to be studied in greater detail to reveal the complex dynamics of DOM transformations in marine systems.

1.2 The Biological Carbon Pump and Microbial Degradation

Microbes play critical roles in global biogeochemical cycling. Marine autotrophs are responsible for synthesizing half of the global photosynthetic biomass through photosynthetic carbon fixation[12]. (Sentence on bacterial respiration). The role DOM plays in the marine carbon cycle is dependent on whether it is fully mineralized through bacterial respiration[13]. As mentioned, the biological pump is considered the main transport mechanism of organic carbon to the deep ocean where substrates such as DOM are consumed by heterotrophic bacteria and zoo plankton and cycle through remineralization. DOM that is not immediately remineralized accumulates in the surface ocean as biologically semi-labile DOM and has presumably still active chemical properties, meaning it can be further degraded at slightly longer time scales. DOM exportation via thermohaline circulation or oceanic water circulation are currently assumed to be important contributors to deep-ocean biogenic carbon sequestration and affects DOM distribution throughout the water column[5].Our general understanding of DOM distribution suggests that deep-ocean DOM concentrations vary with residence time – slow ventilation results in lower minimum DOM concentrations and vice-versa. The ongoing pursuit of deciphering the molecular composition of DOM and our understanding of its reactivity is still evolving, but we have recognized DOM as an important export term in the biological pump[5].

Historically, our understanding of the marine carbon cycle has been severely constrained by the limited analytical tools and the difficulties in running long-term experiments or mesocosm experiments. As the technology and research techniques developed along with our understanding of the genomic diversity of marine microorganisms and their processes, we can consider the far more intricate mechanisms at play than just the kinetics of chemical degradation of known metabolites. It is widely accepted that the production, transformation, and consumption of

marine DOM is strongly dependent on the source as well as the structure of the microbial communities present, both of which change as DOM is processed over time[14]. The processes leading to the diversification of DOM compounds have not been fully identified, but previous studies suggested that prokaryotic microorganisms play a key role in contributing to source material due to evidence of differences in the community structures influence on population[15,16]. Recently, Chen et al. highlighted their finding that DOM variations were more crucial in shaping microbial communities than vice versa[17]. Recent studies have provided further evidence for the potential role of microorganisms in influencing DOM composition using incubation experiments where they compared mass spectrometric data characterizing exometabolomes with ecological diversity measurements[18,19]. In summary, DOM flux is dependent on the accumulation of trophic interactions, biotic, and abiotic transformations, it is then dependent on the local metabolic functional diversity, which means that microbial communities play a major role in producing and sustaining the observed chemodiversity of marine DOM. To quote Moran et al.[1], *"when the question of why deep ocean DOM persists is finally resolved, the answer is likely to be a combination of concentration, chemical structure, bioenergetics, and microbial diversity"*. Moran et al.[1] found that the percentage of microbial genes with no known functions increased with depth in the ocean and suggested that the metabolic pathways degrade refractory molecules hidden within these unidentified genes. Noriega-Ortega et al.[19] showed the impact that active marine microbial communities have on DOM chemodiversity using the vast genetic repertoire of natural microbial communities, the multitude of available substrates and the complex interactions found in marine environments. The majority of these studies have indicated that these differences are likely the result of further processes, presumably mostly microbial and consistent with the concept of the microbial carbon pump (MCP)[15]. This MCP is a conceptual addition to the

biological pump conceived in 2010 by an international working group of Scientific Committee on Ocean Research (SCOR) [15]. SCOR was formed to discuss the role of microbes in the cycling of labile, semi-labile and recalcitrant DOM and aimed to describe specific roles of microbes in the formation of recalcitrant DOM and its transport into the deep ocean[15]. This group also specifically considered the extent of the impact of marine viruses and viral lysis on microbial activity in DOM processing by regulating microbial population structure, horizontal gene transfer between microbes, and the release of cellular material from infected cells[15]. The MCP has been recognized as the leading concept to explain the accumulation of recalcitrant DOM in the deep ocean and the production of more stable organic matter caused by microbial degradation through laboratory and mesocosm experiments[16]. Given the gravity of all that is unknown, it is critical to synthesize existing data on marine microbial processing to help outline an overall concept of DOM reactivity within the marine carbon cycle.

Using projections of increased sea surface temperature it is theorized that global warming will increase the carbon flow through the microbial food web[20]. Flombaum et al. projected increases in cyanobacterial cell numbers of 29% and 14% for Prochlorococcus and *Synechococcus*, respectively[20]. These changes would be geographically uneven, varying widely across different physical environments, but will likely contribute to an overall increase in productivity and bacterial growth efficiency (BGE), at least in the oligotrophic ocean, but also coastal regions. The assessment of BGE is critical to understanding microbial metabolism and determining ecological and biogeochemical roles of bacteria in aquatic ecosystems, especially in carbon cycling[5]. Oceanic microbial communities that will experience the impact of anthropogenic climate change and contribute to complex changes on ocean ecosystems such as large-scale changes in phytoplankton communities as evidence is presented in Flombaum et al.[20]

1.3 Optical Properties of marine DOM and Picocyanobacterial DOM

The importance of Chromophoric Dissolved Organic Matter (CDOM) to marine and freshwater ecosystems has been firmly established over the last several decades[21,22], but the sources and structural nature of this material within the oceans remains unclear and continues to be a subject of debate. Estimations of about 20–70% of oceanic DOM absorbs light over the ultraviolet-visible (UV-Vis) wavelengths due to chromophores present in DOM[21]. Higher UV-Vis ranges are often found in coastal regions and lower ranges are found further from terrestrial DOM input[21,23]. DOM dynamics are often traced via changes of the CDOM portion which strongly absorbs light in the UV and visible light spectrum[24,25]. CDOM is active in a wide range of photochemical reactions, including but not limited to the production of CO_2 and DIC[24,25], low molecular weight organic acids[26], and reactive intermediates[27,28]. Photo-bleaching has been recognized as the most important sink for CDOM in the ocean and can lead to the mineralization and potential transformation of CDOM to smaller and more bio-available forms[29]. Theoretical photo-reactivity has been shown to increase with depth[22,30] but the photochemical transformations can lead to either an enhancement or reduction in its bioavailability[26,31].

The fraction of CDOM that fluoresces is referred to as fluorescent DOM (FDOM) and is known to be the most photo-reactive sub-fraction found throughout the oceans. The biogeochemical origins of the CDOM, along with the subjectivity of CDOM and FDOM forms to photobleaching, affect its lability and thus any subsequent molecular transformations. In areas of upwelling and high biological productivity, it has been found that the decreased irradiance, meaning less absorbance of the light energy that triggers photochemical reactions, results in higher CDOM and FDOM content[22]. Additionally, deep water DOM that has not been exposed

to light for extended periods of time may be more photosensitive, and therefore degrades faster when exposed to sunlight, than DOM that has already undergone photobleaching[32].

Given the distribution of FDOM in marine DOC pool and the global autochthonous DOM production[15], sources must be ubiquitous. Some marine *in situ* sources of FDOM have been suggested and some have been confirmed, but thus far none could explain the ubiquitous appearance of the so called "humic-like" fluorophores ($FDOM_H$) with its unusual exponential behavior in UV-Vis absorbance[21,33]. $FDOM_H$ can be detected using excitation-emission matrix (EEM) fluorescence, with an excitation wavelength extending well above 400 nm, and a large Stoke's shift (the difference in excitation and emission maxima of fluorophores in fluorescence spectroscopy)[34].

It has been found that picocyanobacteria are ubiquitous in the World's Oceans and make up 50% of the autotrophic marine primary production[20]. Preliminary results of research by Zhao et al.[16] showed that picocyanobacteria *Synechococcus* released CDOM that matched the $FDOM_H$ appearance of globally observed marine CDOM after virus-induced lysis. Their findings support the notion that picocyanobacteria are well suited to be one important source of organic fluorophores in the World's Deep Ocean.

1.4 Rationale for Study

As the reactivity and ongoing debate of sources of marine DOM remain at the forefront of global carbon research, a strong correlation between FDOM fluorescence with apparent oxygen utilization (AOU) was demonstrated for the Pacific Ocean suggesting that this relationship is indicative of *in situ* production of bio-refractory FDOM at depth[35]. However, other studies found that this correlation does not hold in the North Atlantic Ocean[22] further

fueling the discussion of FDOM production and its link to microbial processing. Preliminary results of our research group[16] revealed that CDOM from cell lysis released DOM closely matches the $FDOM_H$ appearances of marine CDOM. This study is a part of a novel path for integrating chemical property of DOM with microbial structure and activity with the goal of assessing the long-term stability of chromophores. The longevity of which has implications for marine carbon cycling in assessing large-scale biogeochemical processes. One focus of this study is linking the microbial processes with production of complex, refractory DOM with $FDOM_H$ chromophores from a defined source.

Providing early chemical signatures of picocyanobacterial-derived DOM using ultrahigh resolution mass spectrometry coupled with the deep sequencing of bacterial communities to link microbial diversity with chemical diversity of DOM has the potential to fundamentally advance our understanding of CDOM sources, microbial interactions, and transformation of DOM, and address key issues in proposed marine carbon cycling concepts. Advancing our understanding of an important marine CDOM source will help us address key uncertainties in marine carbon cycling and carbon storage capacity.

1.5 Thesis Outline

The focus of this study is the characterization of the optical properties and molecular composition of CDOM collected from the Atlantic and Pacific Ocean and the dynamics and degradability of *Synechococcus*-derived DOM (SDOM) and its changes of optical properties during long-term incubation experiments.

Chapter two describes and compares DOM profiles from the Atlantic and Pacific oceans in a high-resolution depth profile for the first time. The analysis focuses on the specific chromophores released that share properties amongst samples collected on research cruises from

the Bermuda Atlantic Time-Series (BATS) and Hawai'i Oceanic Time-series (HOT) stations. Aboard vessels, we collected water samples from the bottom to the surface at 200 m depth intervals and solid phase extracted them for analysis back at the Chesapeake Biological Laboratory (CBL). At CBL, the samples were analyzed using 3D florescence spectroscopy scans and statistical Parallel Factor Analysis (PARAFAC) modeling techniques. PARAFAC is used in the chemical sciences to decompose trilinear multi-way data arrays and facilitate the quantification of statistically reoccurring underlying signals, termed 'components'[36]. This chapter aims to use the data collected from the field to discuss our understanding of the relationship between marine CDOM and FDOM and their distribution and whether or not major differences in DOM and its optical properties exist between the Pacific and Atlantic Ocean sampling stations.

Chapter three provides results from a comprehensive decomposition incubation study of SDOM. Samples were collected over a long incubation on days 0, 1, 3, 10, 30, 90, 360, and 540 and were used for subsequent analyses, including community structure, metagenomics, optical properties, DOC concentrations and cell counts, as well as comprehensive optical properties analyses and Fourier-transform ion cyclotron resonance mass spectrometry (FT-ICR MS). However, my focus was on the transformations of optical properties found in sample extracts and measured using 3D florescence spectroscopy scans for statistical PARAFAC modeling. This chapter aims to confirm the refractory nature of SDOM and investigate chemical transformations of SDOM fluorescence over time.

Chapter four provides a brief look at a fragmentation study of presumed aromatic glycosides found in the BATS sample extracts using weak anion exchange solid-phase extraction (WAX-SPE) and compare it to samples collected at station HOT, in the Pacific. Diluted WAX

sample extracts were compared by using high performance liquid chromatography (HPLC) paired with electrospray ionization (ESI) triple quadrupole (QqQ) tandem mass spectrometry (MS/MS) to detect ion transitions and investigate compounds of interest. This chapter aims to discuss molecular signatures and transitions of interest and to describe differences in DOM composition extractable by this unique anion exchange fraction of DOM between the Pacific and Atlantic Ocean basins.

Chapter 2: High-Resolution Optical Properties Profiles of DOM at the Bermuda Atlantic Time-Series and Hawai'i Ocean Time-series Stations

Abstract

Despite the importance or marine DOM and significant advances made in deciphering its dynamics, the sources, distribution, and chemical composition of optically active components, namely marine CDOM and FDOM, are still uncertain. CDOM and FDOM have been used as proxies for processes with implications without much supportive evidence for understanding carbon turnover in the World's Oceans. This study is a part of a larger project integrating the chemical properties of DOM with microbial structure and activity. We collected and analyzed high-resolution depth profiles of DOM throughout the water column in the North Atlantic at the BATS in August 2019 and the HOT in July 2021. Water samples were collected at 200 m depth intervals from 4,530 m at BATS and 4,700 m at HOT before using solid phase extraction techniques to isolate sample DOM. Sample analysis consisted of UV-vis spectroscopy and fluorescence measurements to investigate depth-related changes in abundance and photochemical reactivity of FDOM. The overall absorption was higher at BATS than at HOT, further spectroscopy spectral slope and absorption ratio trends supported evidence that molecular weight of compounds was overall higher in the Atlantic and lower in the Pacific. Parallel factor analysis modeled EEM fluorescence revealed changes of "humic-like" and "protein-like" FDOM ($FDOM_H$ and $FDOM_P$ respectively) throughout the water column. The fluorescence values were higher in the Pacific than in the Atlantic despite the higher absorbance in the Atlantic. When comparing $FDOM_H$ and AOU relationships, the correlation between Fmax 1 (446 nm) and Fmax 2 (322 nm) increases at depths at HOT but decreases at BATS indicating that DOM at HOT is likely to be subjected to mineralization. Increases in AOU with depths at HOT supports this

observation. Strong correlations between $FDOM_H$ component Fmax 4 (453 nm) and AOU were found at both stations, potentially indicating common compounds contribute to the observed changes in Fmax 4 (453nm) at depth across ocean basins. The $FDOM_P$ component Fmax 3 (264 nm) showed weak overall negative correlation with AOU except for depths below 1,000 m at HOTs which trended positive suggesting further heterotrophic processing linked to changes in this FDOM component at depth. Findings from the water column profiles, UV-Vis absorbance, PARAFAC model fluorescence values, and AOU analyses supported the idea that DOM in the Atlantic and Pacific oceanic basins contained substantial differences that would impact FDOM production and structure. This collaborative study and future work will hopefully lead to a better understanding on the role of microbial carbon pump processing and transport of recalcitrant DOM into the deep ocean.

2.1 Introduction

This chapter focuses on the detailed analyses of optical properties from the waters of the sub-tropical Atlantic and Pacific Oceans. High-resolution depth profiles were collected from the BATS in the Atlantic Ocean and the HOT in the Pacific Ocean. The first set of samples were collected aboard the R.V. Atlantic Explorer in August of 2019 and transported back to CBL for subsequent analysis in following months. The second set of samples were collected in July of 2021 aboard the R.V. Kilo Moana and transported back to CBL for analysis.

The UV range of light is where most CDOM components of DOM have their maximum absorption and where differences in CDOM have been observed that correspond to changes driven by microbial degradation and photochemical alteration[37]. While several spectral parameters have been examined to extract information about CDOM properties, primarily absorption ratios, have been used, which are independent of CDOM concentrations. UV-visible spectra for CDOM increases approximately exponentially with decreasing wavelengths[38] and is used here to assess marine CDOM, but direct measurements in seawater are problematic due to low signal intensities. One specific parameter derived from marine CDOM UV-Vis spectroscopy is the spectral slope (S), which has been used to provide insight into the chemical composition and extrapolated to source and diagenesis state of DOM[39]. Calculating S over specific wavelength ranges, such as between 270-295 nm, has been used to examine CDOM transformations during transport and through photochemical alterations[37]. Other wavelength ranges have been used for monitoring CDOM degradative processes[40]. De Haan and De Boer[41] used the ratio of absorption at 250 to 365 nm (called E2/E3) to track changes in the relative size of DOM molecules[41,42]. As molecular sizes increased, E2/E3 decreased because of stronger light

absorption by high-molecular-weight CDOM at longer wavelengths. CDOM UV-Vis spectroscopy is used in this study to describe CDOM depth distribution.

Fluorescence spectroscopy (FDOM) is another tool used to describe marine CDOM and it is much more sensitive than UV-Vis spectroscopy. Measurements of FDOM are cheap, fast, and convenient ways to provide meaningful information about DOM sources, composition, or biodegradability[7] – even from low levels of fluorescence[21]. Experimental evidence showed that pure bacteria strains or heterotrophic bacterial communities can transform substrates to different types of FDOM[43–45], including the previously discussed $FDOM_H$[16]. $FDOM_H$ is currently considered to be a component of RDOM because it remains relatively stable in the dark ocean once it is formed and it appeared to have a longer turnover time[46]. Investigations into $FDOM_H$ are often undertaken using EEM fluorescence. EEM spectroscopy is sensitive enough to analyze low concentrations of DOM in bulk seawater[47]. Several fluorescent regions within the contour plots of EEM data have been previously described using additional tools such as the previously mentioned PARAFAC modeling technique[36]. While direct comparisons of EEMs is an important qualitative (and semi-quantitative) tool, PARAFAC is used to compare large datasets of EEMs to deconvolutes them into components for analysis. An example of a relationship between EEM PARAFAC component distribution and molecular composition in the ocean is the defined $FDOM_H$ region has been linked to marine biota through PARAFAC modeling[16,35,36]. Previous studies using ultrahigh resolution ESI-FT-ICR- MS have been used to characterize marine DOM with limited success[29,48–54]. Studies of DOM-rich boreal rivers and lakes likewise compared EEM-PARAFAC components with FT-ICR-MS derived molecular formulas, identifying similar relationships between longer wavelength, “humic-like” fluorescent components and oxidized aromatic compounds[55,56]. Timko et al.[30] investigated the depth-related changes in abundance and

photochemical reactivity of FDOM in the North Atlantic Ocean. EEM-PARAFAC components measured in samples were fit to a five-component model including components containing "humic-like" components[30]. As previously discussed, "humic-like" properties are characterized by showing fluorescence in the visible region, as well as components in the UV portion of the spectrum. This UV fluorescence is characteristic of small aromatic molecules, including the amino acids tryptophan and tyrosine[30]. The similarities found provide a strong validation that the modeling of the EEMs collected during photo-irradiation experiments are indicative of fluorescence changes occurring in the water column[30]. The authors also noted that since the observed results on the photochemical changes in marine FDOM are not limited to the Sargasso Sea, but can presumably generalized, at least to the greater Atlantic Ocean[30].

In order to better understand the processing and distribution of FDOM in the North Atlantic and North Pacific Oceans, we investigated depth-related changes of FDOM. Spectroscopy, PARAFAC derived component analysis, and profile comparisons were utilized here to help characterize and explore how FDOM changed at these sites throughout the water column. Temperature, depth, salinity, oxygen, and chlorophyll fluorescence were also measured using a conductivity, temperature, depth (CTD) profiler aboard the vessels. The focus of this study was to compare the changes observed by the EEM-PARAFAC and investigate the DOM depth profiles at the BATS and HOT stations.

2.2 Materials and Methods

In the sample preparation for subsequent analysis, water samples were taken using an established technique for extracting seawater DOM though SPE on a proprietary polystyrene vinyl resin (PPL). PPL SPE is commonly used for the relatively high DOC extraction efficiency of about 40-50% of oceanic DOM, and PPL can retain more polar compounds than other

commonly used reverse phase resins[57]. Small organic acids and highly polar compounds are still not retained using this technique. Therefore, WAX cartridges were attached to each PPL cartridge in the first profile at each site to recover additional DOM constituents that were not extractable by the PPL resin. This is the first time that this sequential method has been used in a high-resolution marine-DOM profile study and this approach has the potential to extend the molecular level characterization to this highly specific weak anion exchange amendable fraction of marine DOM. All these procedures and techniques used are described below.

2.2.1 Sample collection

Two research cruise expeditions were launched for the NSF project "*The fate of lysis products of picocyanobacteria contributes to marine humic-like chromophoric dissolved organic matter"* and DOM samples were collected from two long-term time-series stations: BATS and HOT. BATS and HOT were chosen to represent locations in both ocean basins that are roughly at similar latitude and that are accessible (Figure 2.1A). Further, a tremendous amount of historical data exists for both stations. However, they may not be representative for the entire North Atlantic or North Pacific Gyres, respectively. For example, BATS is influenced by eddies of the Gulf Stream and HOT is known to have relatively high primary production, which is unusual for oceanic gyres. The bottom panel B and C of Figure 2.1 gives a closer look at the stations of each time-series stations used for sampling in relation to the local archipelagos of the Hawai'i (B) and Bermuda (C).

2.2.1a R/V Atlantic Explorer 2019 – Atlantic Sample Collection

The R/V Atlantic Explorer hosted the scientific team and collaborators in August of 2019 on an expedition to BATS (Figure 2.1 C). BATS is located at the coordinates 31°40′N

and 64°10′W, approximately eighty-two kilometers southeast of Bermuda's island of St. George. BATS has been in operation since 1988 and is often used to represent the western North Atlantic subtropical gyre and is located within the Sargasso Sea. Three full depth profiles were carried out collecting 10 L water samples for each sample depth at 200 m depth intervals from surface to the seafloor at 4,530 m using Niskin water collection bottles for a total of seventy-five samples. A CTD profiler was attached to the rosette holding the Niskin sampling bottles and the attached sensors measured depth (m), temperature (°C), oxygen (mg O/L) and chlorophyll *a* fluorescence.

2.2.1b R/V Kilo Moana 2021 – Pacific Sample Collection

The R/V Kilo Moana hosted the scientific team in July of 2021 on an expedition to the Long-Term Oligotrophic Habitat Assessment (ALOHA) station of HOT (Figure 2.1 B). ALOHA is nominally located around a 10-kilometer radius circle centered at 22 45'N and 158 W, approximately 100 kilometers north of O'ahu of the Hawai'ian Islands. The HOT study has been in operation since 1988 for oceanographic research and data from which is considered to represent the oligotrophic North Pacific Ocean. Three full profiles collecting 10 L water samples were taken at 200 m depth intervals from surface to the seafloor at 4,730 m using Niskin water collection bottles for a total of seventy-eight samples. A similar CTD profiler attached to the water sampling rosette was used as described for BATS.

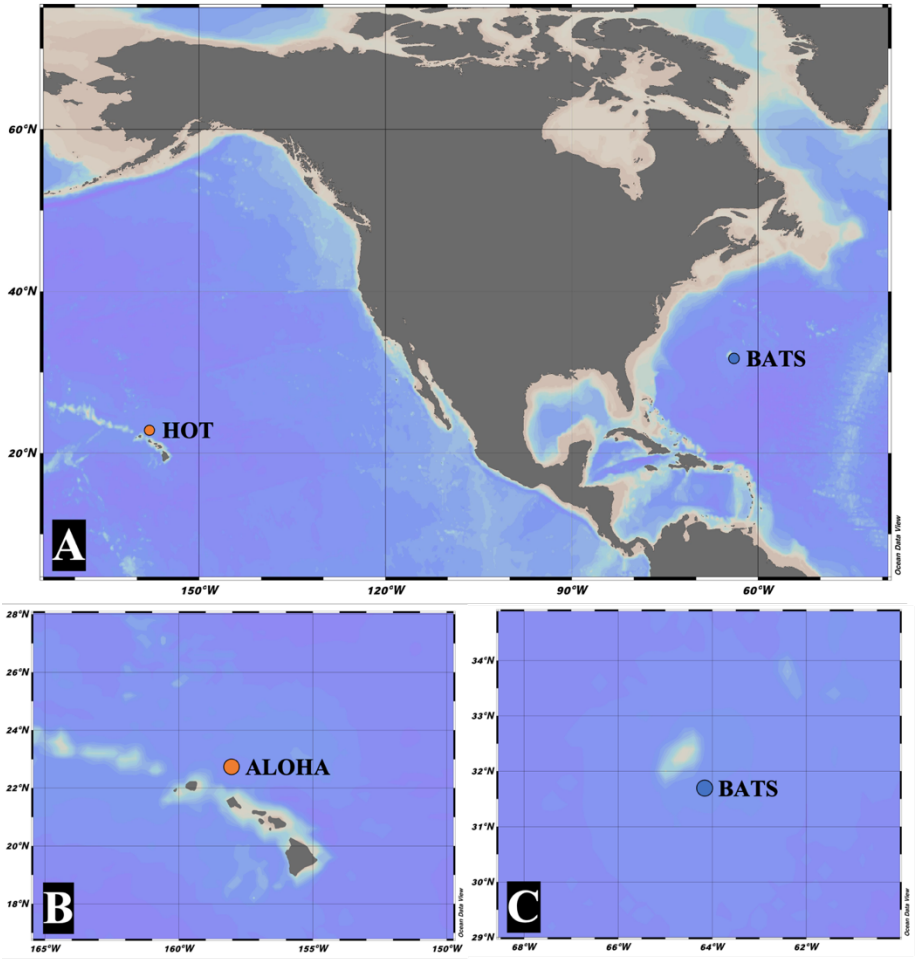

Figure 2.1 (A) Northwestern hemisphere bathymetry map of sampling sites used for this study. (B) Location of station ALOHA part of the HOT time-series study in relation to the Hawai'ian archipelago. (C) Location of BATS station part of the time-series study in relation to the Bermuda archipelago. Bathypelagic maps created in ODV software.

Aboard both cruises, 10 L samples were collected into five-gallon polycarbonate drinking water containers after rinsing three times using seawater samples. Standard bottles were marked using measured volumes of 10L for volume reference. Sample sets likely had slight variations in volumes due to using two different bottle types on each cruise and human error in volume filling approximations. Samples were then acidified with pure grade 32% hydrochloric acid from Acros Organics to pH of 2 prior to filtration and SPE.

2.2.2 Solid phase extraction (SPE) of water samples

DOM samples for this study were isolated through two fundamentally different types of solid phase extraction. The collected 10L water samples were in-line filtered through pre-ashed 47 mm and 0.7 μm Whatman GF/F glass microfiber filters. Solid-phase extraction was conducted sequentially using 1g of Agilent Bond Elut PPL in 6mL cartridges and 500 mg of Waters Oasis WAX resin also in 6mL cartridges. All methanol (MeOH), 0.1% (v/v) formic acid (FA) water used for SPE in the field were LC/MS grade and the ultrapure water (RO water) used to rinse in the field was from systems maintained aboard the research vessels. Details about each extraction is given below.

2.2.3a Solid Phase Extraction using Proprietary Polystyrene Vinyl Resin (PPL)

Agilent Bond Elut 1g PPL cartridges were first activated with 10 mL MeOH, rinsed with 5 mL 0.1% FA water, then loaded via lines running through pre-ashed 0.7 μm glass microfiber filters by gravity or a peristaltic pump as necessary at a flow rate of less than 10 mL min^{-1}. After sample loading, the cartridge exterior was rinsed with ultrapure water and the sorbent was thoroughly rinsed with 20 mL 0.1% FA water to completely remove salts. Cartridges were then dried, and eluted with 10 mL MeOH into new, trace contaminant certified or acid-washed and combusted 40 mL glass vials.

2.2.3b Weak Anion-Exchange

WAX cartridges were added beneath the PPL cartridges for the first full profile. Oasis Waters WAX cartridges were activated using 5 mL 2% NH_4OH methanol and 5 mL 0.1% FA water before being loaded with the filtered and acidified sample by gravity after it had passed through the PPL resin. After sample loading, cartridge exteriors were rinsed with ultrapure water and the sorbent was rinsed with 10 mL 0.1% FA water to remove salts. Cartridges were eluted

with 10 mL 2% NH_4OH methanol into new, trace contaminant certified or acid-washed and combusted 40 mL glass vials.

The methanolic SPE extracts of DOM (SPE-DOM) were stored in the dark at -20 ˚C before transported back to CBL. At CBL, all extracts were stored in the dark at -20 ˚C prior to further analyses.

2.2.3 Characterization of Optical Properties

Samples of the methanolic SPE extracts were re-dissolved in 5 mL of ultrapure water for optical properties analysis after drying of 0.5 mL of the methanolic SPE sample using ultrahigh purity nitrogen. UV-Vis absorbance spectra and fluorescence EEMs were measured over a 10s integration time at an excitation wavelength range of 250-700 nm and emission wavelength range of 240-600 nm at 3 nm intervals using a Horiba Aqualog Spectrofluorometer, which is capable to measure UV-Vis absorbance and EEMs simultaneously. All absorbance and fluorescence spectra were blanked using scans of ultrapure water. Absorbance spectra ($A(\lambda)$) were converted to Napierian absorption coefficients ($a(\lambda)$) using the equation $a(\lambda) = 2.303*A(\lambda)/L$, where L is the pathlength of the cuvette in m (0.01 m), and A is the raw measured absorbance[38]. Rayleigh scattering and inner filter effects were corrected using the Aqualog software and custom-designed post-processing scripts programmed in MATLAB. Spectra were normalized using the water Raman scattering of pure water and Water Raman Units. SPE-DOM EEMs were analyzed using statistical PARAFAC modeling using the MATLAB DrEEM toolbox[36].Three outliers were removed because of high leverages which suggests contamination. A 4-component model was generated to explain the data, which was split-half validated using four random splits and met other validation requirements[36]. Unit normalization was reversed to

recover true scores of components. The maximum fluorescence (Fmax) values of components were summed for each sample and each Fmax value was calculated to explain representation by these statistical components.

2.2.4 Calculations and statistical analyses

AOU calculations were conducted by using the Ocean Data View (ODV) software by subtracting the *in-situ* oxygen measurements from oxygen saturation calculations and using CTD data. AOU was calculated using the equation AOU = O'_2 - O_2 by subtracting the measured *in-situ* oxygen concentration (O_2) from the theoretical oxygen saturation (O'_2) at any given temperature and pressure (depth). Neutral density was also calculated by ODV software using measured *in-situ* temperature and salinity derived from conductivity via CTD instrumentation[58]. Neutral density ($\nabla\gamma^n$) was calculated using the equation $\nabla\gamma^n = b\rho(\beta\nabla S - \alpha\nabla\theta) + R$ where S is salinity, θ is potential temperature (°C), α is the thermal expansion coefficient, β is the salinity contraction coefficient, b is the integrating factor, and R is the residue number which is not zero[59]. Datasets were fitted with linear and polynomial regressions using Microsoft Excel.

Spectral slopes $S_{(275–295\ nm)}$, $S_{(350–400\ nm)}$, their slope ratio (*SR)* ($S_{(275–295\ nm)}/S_{(350–400\ nm)}$) and absorption ratio *E2/E3* (a(250)/a(365))were calculated using the reference wavelength and applied a nonlinear least-squares curve fitting procedure to the absorption spectrum exponential model[37].

2.3 Results and Discussion

CTD measurements from BATS and HOT depth profiles are given in Figure 2.2. Temperature measurements were found to be higher at BATS surface before decreasing more gradually than the sharp decrease at HOT (Figure 2.2 A). Salinity at BATS was overall higher than HOT and did not overlap with the BATS profile (Figure 2.2 B).

BATS salinity reached a higher maximum near the surface and decreased more gradually at depths below the mixed layer. At each site, oxygen measurements showed a decrease in oxygen below the euphotic zone and reached a minimum. At BATS, the oxygen minimum at 785m only reached 132.20 μmol/kg whereas the 670m minimum at HOT reached 26.92 μmol/kg (Figure 2.2 C). The oxygen saturation at BATS was 49.34% and at HOT it was 8.72% (Appendix 2.1) Below the oxygen minimum layer, there is often an increase in dissolved oxygen at depth for two reasons: one because oxygen-rich water is denser and sinks, and two because as the temperature decreases, and the pressure increases the solubility of dissolved gases such as oxygen increases[60]. Dense, oxygen rich waters form in the polar regions of the Atlantic and circulates to the Pacific where oxygen is removed through respiration which is why the dissolved oxygen levels are significantly lower[60]. The oxygen levels at HOT gradually increased with depth whereas at BATS, they increased quicker and remained steady at higher levels before slightly decreasing near the bottom. The pronounced much lower oxygen minimum at HOT indicated that oxygen was removed through respiration and therefore the water column at HOT has higher microbial respiration when compared to BATS, as also reflected in the AOU.

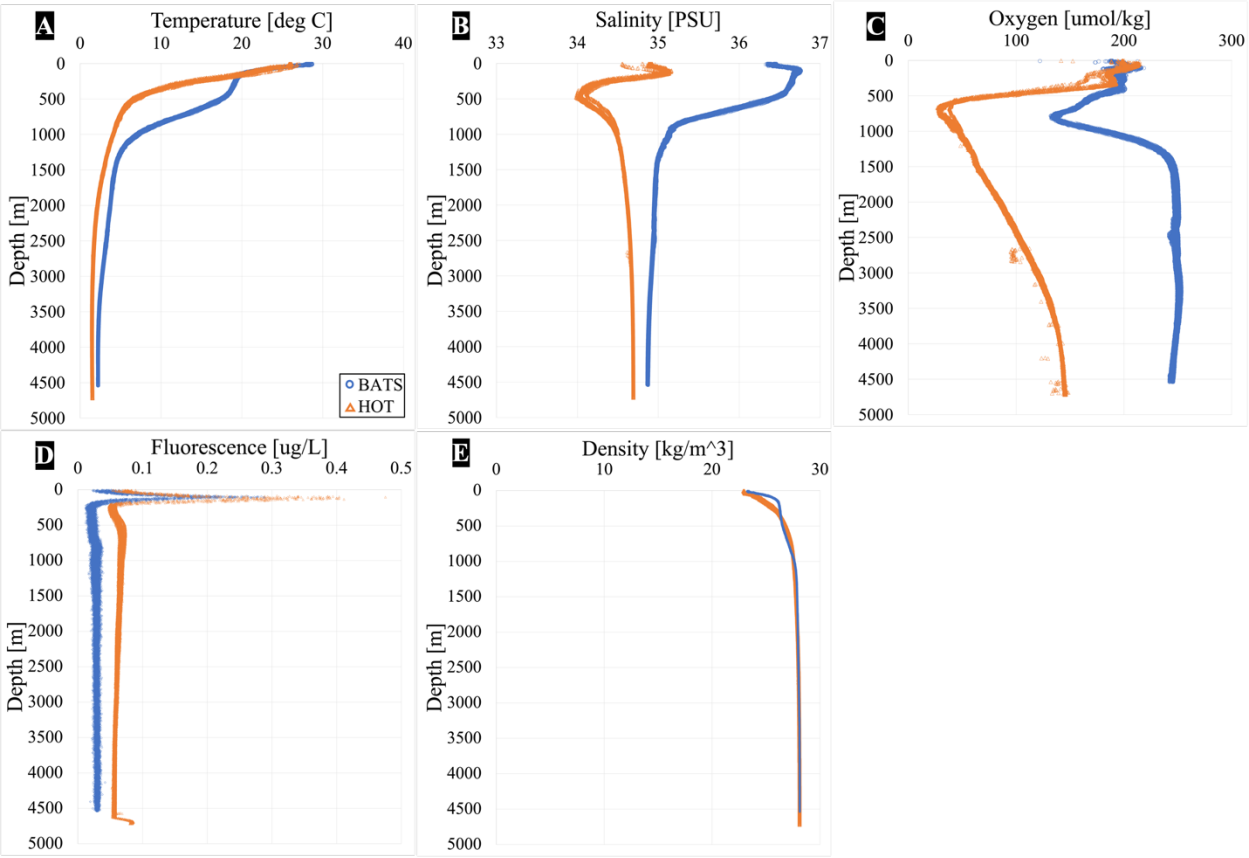

Figure 2.2 Comparing station BATS in the Atlantic (blue) and HOT in the Pacific (orange) water column CTD profiles. (A) Temperature [°C] at depth. (B) Salinity [PSU] at depth. (C) Oxygen [μmol/kg] at depth. (D) Chlorophyl-*a* [ug/L] at depth. (E) Neutral density [kg/m^3] at depth.

Fluorescence calibrated for chlorophyll-*a* (chl-*a*) showed a maximum of bio-photosynthetic activity producing chl-*a* at 105 m at BATS and HOT (Figure 2.2 D). The overall higher chl-*a* levels at HOT with a maximum of 0.48 ug/L than the 0.29 ug/L at BATS indicated an overall higher primary production (Figure 2.2 D), further building evidence of more biological activity at HOT. Correlations between DOM fluorescence and chl-*a* has been previously found to correlate positively with the $FDOM_H$ components and negatively with the $FDOM_P$[33,46,61] components in fluorescence data of surface waters but was not supported in this study. There was a greater initial rate of increase in water density at BATS from 23.34 kg/m^3 at 5 m to 26.09 kg/m^3 at 150 m (Figure 2.2 E), whereas HOT only increased from 22.98 kg/m^3 to 24.81 kg/m^3. The increase in density at the surface of BATS is more gradual until about 1,000 m whereas HOT continued to increase down the water column. Previous studies have demonstrated

that absorption at 300 nm and spectral slopes are indicators of CDOM molecular information[62–65]. The UV-band absorptions (i.e., 250–440 nm) are studied because some aromatic compounds have their absorption maxima in the UV range and are believed to contain more chemical information of CDOM composition than the visible wavelengths[62,66]. The UV range is where most CDOM components have their maximum absorptivity and the absorption spectra increases approximately exponentially with decreasing wavelengths [37,38].

Figure 2.3 A showed the initial absorbance at 300 nm (*a (300 nm)*) at BATS to be at a minimum of 8.33 nm m^{-1} at the 5 m of depth before increasing to 12.90 nm m^{-1} at 75 m. After which, the absorbance decreased to a local minima of 11.35 nm m^{-1} at 600 m before increasing back to 14.34 nm m^{-1} at 1,000 m and fluctuating within a standard deviation of $^{+}/_{-}$0.56 nm m^{-1} until reaching the maximum of 15.44 nm m^{-1} at 4,000 m. After the maximum, the absorbance dips and increases once more before reaching a minima of 12.93 nm m^{-1} at the final depth of 4,530 m. Figure 2.3 A shows the initial a(300nm) at HOT to be at a minimum of 6.13 nm m^{-1} at the 5 m of depth before increasing to 10.18 nm m^{-1} at 75 m. After which, the absorbance slightly decreases before increasing to a local maxima of 13.68 nm m^{-1} at 600 m. At depths greater than 600 m, the absorbance showed a fluctuating decreasing trend with a standard deviation of 0.83 nm m^{-1} and a local minima of 9.41 nm m^{-1} at the final depth of 4,530 m. Figure 2.3 A shows that the overall absorption was consistently higher at BATS than at HOT other than at 600 m where BATS decreased and HOT increased in absorbance. Table 2.1 supported these observations with regression analysis results. In Figure 2.3 A, BATS showed higher absorption coefficient at 300 nm while Table 2.1 showed that BATS also had narrower range of absorption and lower standard deviation.

In addition to the findings in Figure 2.3 A, it is worth noting that Figure 2.2 B showed a minimum in salinity at HOT just before 500 m, right where the a300 for HOT jumps from 11.32 nm m^{-1} at 400 m to 13.68 nm m^{-1} at 600 m. Grebel et al.[67] found that seawater concentrations of chloride and bromide ions enhance absorbance photobleaching reaction rates by approximately 40%, regardless of DOM source or the presence or absence of carbonate ions. Drastic changes in ionic strength and DIC can fundamentally change the degradation of CDOM with increasing salinity[67], therefore these shifts in absorbance could be explained by fundamental differences in ocean basin DIC processing resulting in divergent FDOM formation. The different salinity concentrations at BATS and HOT indirectly control factors that change the photochemical impact on the different metabolite transformations occurring in these ocean basins, but further research must be conducted to understand its leverage over other factors.

Figure 2.3 B showed the initial spectral slope of 275 nm – 295 nm ($S_{275–295}$), at BATS to be at a maximum of 0.041 nm at 5 m before decreasing to 0.032 nm at 75 m and increasing to a local maxima of 0.034 at 400 m. At depths greater than 400 m, $S_{275–295}$ at BATS showed a decreasing trend in absorbance until 0.027 nm at 4,400 m where it increased to a local maxima of 0.028 nm at the final depth of 4,530 m. The $S_{275–295}$ profiles in Figure 2.3 B showed consistently higher slopes at depths but the $S_{275–295}$ decreased with depth at BATS. At HOT, while the initial $S_{275–295}$ was the overall greatest in this dataset, the following decrease had slopes consistently lower than BATS, but increased with depth. Helms et al.[37] concluded from their experiments that the shifts in SR and $S_{275–295}$ were related to shifts in molecular weight (MW)[37]. Lower $S_{275–295}$ and SR values generally reflected a higher MW and reflected a lower MW vice versa[37]. Figure 2.3 B showed trends that were consistent with the Helms et al.[37] suggestion that the lower $S_{275–295}$ values at HOT than BATS indicated that FDOM compounds had higher a MW at HOT than at

BATS. This would also imply the gradual increase in $S_{275–295}$ at HOT from 0.023 nm at 1200 m to a local maxima of 0.026 nm at the final depth of 4,530 m was indicative of a decreasing trend in MW with depth. With the same reasoning, the decreasing trend in absorbance from 1,200 m until 4,400 m would indicate an increasing trend in MW with depth at BATS.

The spectral slopes of UV-Vis absorption spectra were indicative of distinct differences in the molecular composition of CDOM. Specific slopes $S_{275–295}$ (Figure 2.3 B) and $S_{350–400}$ (Figure 2.3 C) indicated these molecular changes throughout the depth profiles and between ocean basins. Different spectral ranges produced different spectral slopes, because the CDOM absorption spectra did not follow a continuous exponential decay with increasing wavelengths. Previous works have highlighted the distinction that samples that were mostly marine in character had a higher sample $S_{275–295}$ than $S_{350–400}$[37], which was true for both sub-sample sets at BATS and HOT. Helms et al.[37] also suggested that the primary factor controlling CDOM optical properties is the intramolecular charge transfer capability of CDOM[68], then a decrease in MW would alter the potential for intramolecular charge transfer interactions. This would shift the absorption spectrum toward shorter wavelengths, causing steeper $S_{275–295}$, shallower $S_{350–400}$, and increased SR[37,68]. Figure 2.3 B-D reflected this by showing steeper $S_{275–295}$ values, shallower $S_{350–400}$, and increased SR values at both BATS and HOT.

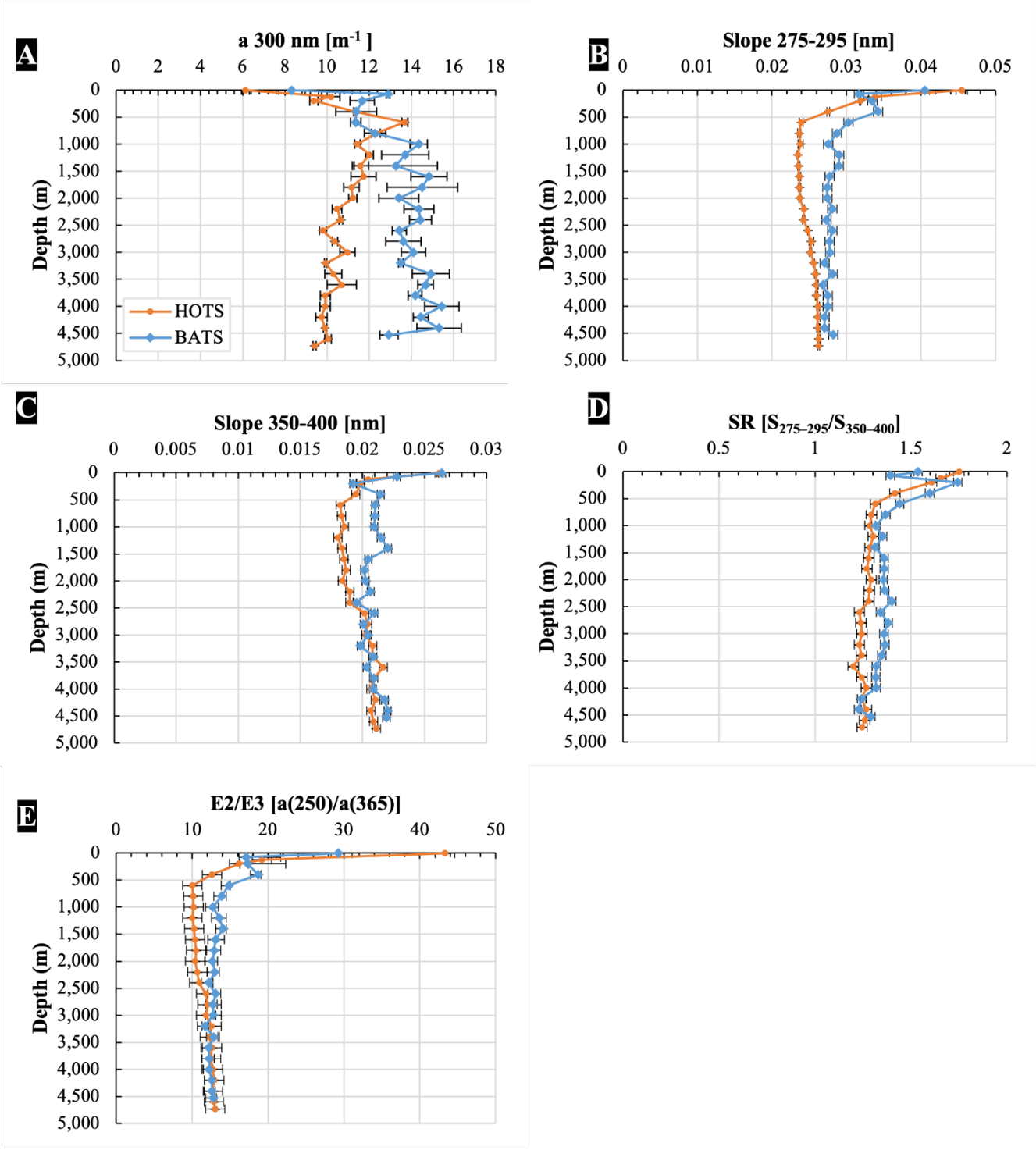

Figure 2.3 Depth profiles of the HOT and BATS analyzed using PPL SPE-DOM (A) absorption coefficient at 300 nm (a (300)); spectral slopes (B) $S_{275–295,}$ and (C) $S_{350–400}$; (D) spectral slope ratio SR ($S_{275–295}/S_{350–400}$); and (E) absorption ratio E2/E3 (a (250)/a (365)).

Table 2.1 The range, mean value, and standard deviation (SD) of the HOT and BATS PPL SPE-DOM absorption coefficient at 300 nm (a (300)); spectral slopes $S_{275–295}$, and $S_{350–400}$; spectral slope ratio SR ($S_{275–295}/S_{350–400}$); and absorption ratio E2/E3 (a (250)/a (365)).

	HOT			BATS		
	Range	Mean	SD	Range	Mean	SD
a(300) (1/m)	6.13-13.68	10.5482306	1.34875309	8.33-15.44	13.4917414	1.56359765
s275-295 (1/nm)	0.023-0.045	0.02641209	0.00457873	0.026-0.041	0.02902284	0.00307481
s350-400 (1/nm)	0.018-0.026	0.02001869	0.0016904	0.019-0.026	0.02110769	0.00138565
Slope Ratio	1.19-1.75	1.31602788	0.13789749	1.22-1.74	1.37558617	0.1085833
E2/E3	10.04-43.33	13.2632004	6.45748872	12.17-29.28	14.1369202	3.60277245

The absorption ratio E2/E3 (a(250)/a(365)) is typically negatively correlated with CDOM MW[41,42,69], hence a decrease of E2/E3 could indicate an increase in CDOM molecular size[37], however this assumption may not hold for marine DOM, because this correlation has been only confirmed to date for freshwater samples. The E2/E3 increased at HOT between 500 m and roughly 3,000 m, was not observed at BATS. Table 2.1 showed a considerably larger range of the E2/E3 values for HOT, with much higher values at the surface and substantially lower values between 500 m and 3,000 m at HOT further supporting evidence of fundamental molecular differences between HOT and BATS. Understanding DOM behavior at depths is critical in understanding the substantial differences in marine DOM. Because the overall absorption coefficients at 300 nm (a300) were higher at BATS and lower at HOT, the UV-Vis absorption derived parameters exhibited a much more dynamic pool of FDOM at HOT, meaning that the higher absorbance is not translating to higher fluorescence.

EEM fluorescence components of the PPL SPE-DOM showed variations that fitted best to a four component EEM-PARAFAC model (Figure 2.4 A). Three out of the four validated components with maximum emission wavelengths following the signal: Fmax 1 (446 nm), Fmax 2 (322 nm), and Fmax 4 (453 nm) fit the $FDOM_H$ descriptions from literature[33,47,70]. These EEM-

PARAFAC components showed similar patterns including the large Stokes shift of the previously defined $FDOM_H$ fluorescence peaks. The Fmax 3 (264 nm) component with maximum emission wavelength of 264 nm exhibited similar optical appearance as what was historically considered to be the $FDOM_P$ or protein-like component[47,71].

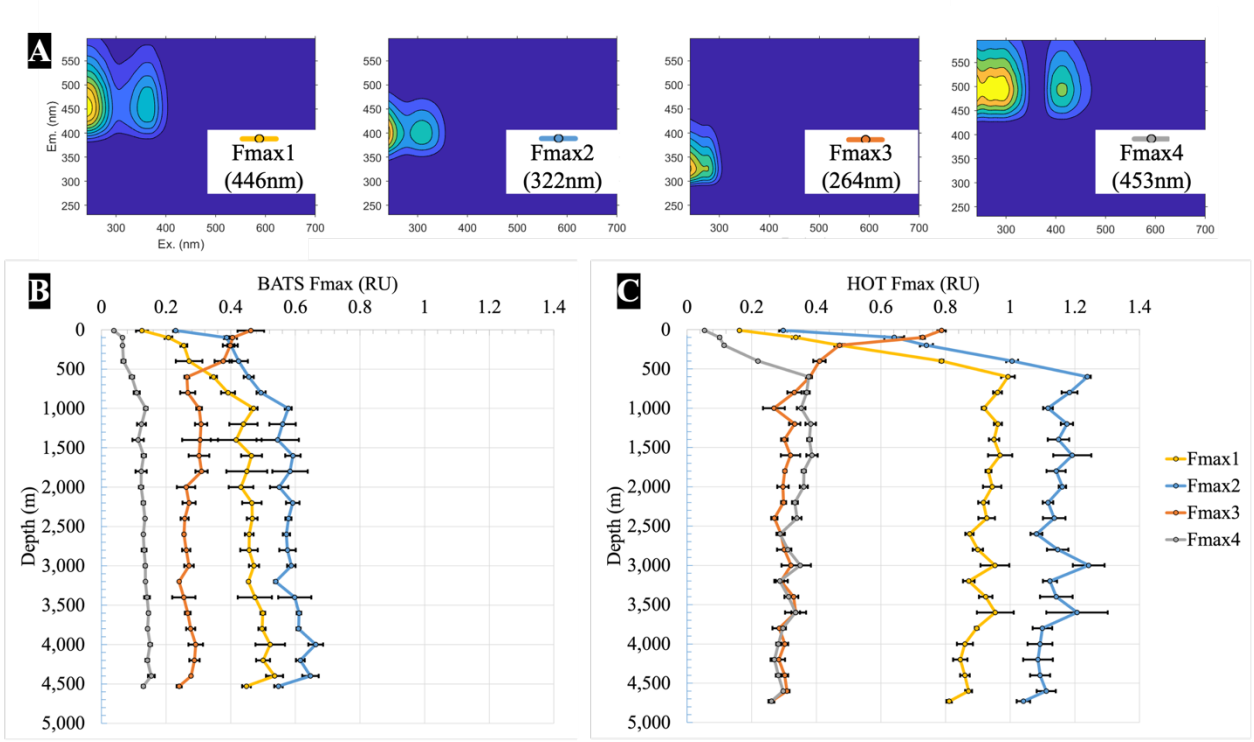

Figure 2.4 (A) Optical Properties of PPL SPE-DOM PARAFAC component EEMs for BATS, Atlantic and HOT, Pacific with each maximum emission wavelength. (B) Fluorescent maximum of PARAFAC components 1-4 at depths of BATS, Atlantic in Raman Units [RU] (C) Fluorescent maximum of PARAFAC components 1-4 at depths of HOT, Pacific [RU].

Fmax components were plotted against sample in the water column at BATS (Figure 2.4 B) and HOT (Figure 2.4 C). Fmax 1 (446 nm) at BATS showed an increase in fluorescence from the surface to a local maxima of 0.47 RU at 1,000 m before incrementally increasing at depths to a maximum of 0.54 RU at 4,400 m but decreased to a local minima of 0.45 RU just above the seafloor and a depth of 4,530 m. Fmax 1 (446 nm) at HOT showed a greater increase in fluorescence from the surface to 600 m to a maximum of 0.99 RU before gradually decreasing to the minimum of 0.81 RU at the seafloor, but also showing a further distinct decrease between

4,600 m and the seafloor at 4,720 m, similar to the observed trend at BATS. Notable increases in fluorescence at 3,000 m and 3,600 m at HOT are unexplained. There is some indication of notable behavior at 3,000 m and 3,600 m in the UV-vis absorbance at 300nm (Figure 2.3 A) but nothing that would indicate an explanation in the depth profile (Figure 2.2). Fmax 2 (322 nm) at BATS at HOT showed overall similar patterns. Fmax 2 (322 nm) at BATS increased from the surface to a local maxima of 0.58 RU at 1,000 m and a maximum of 0.66 RU at 4,000 m and decreasing to 0.54 RU at the bottom. Fmax 2 (322 nm) at HOT increased from the surface to a maximum of 1.24 RU at 600 m before gradually decreasing to a local minima at 1.04 RU at the bottom. Fmax 3 (264 nm) at BATS decreased from a maximum of 0.46 RU at the surface to 0.26 RU at 600 m before remaining relatively consistent at depths to a local maximum of 0.29 RU at 4,000 m and decreasing to a local minimum of 0.24 at the bottom. Fmax 3 (264 nm) at HOT decreased from the maximum of 0.79 RU at the surface to a local minima at 0.27 RU at 1,000 m and remained relatively constant at depths before decreasing to the minimum of 0.26 RU at the bottom. The additional decrease between the bottom samples collected just 10 m above the sediment was again observed for both stations here. Fmax 4 (453 nm) at BATS increased from 0.04 RU from the surface to the local maxima of 0.14 RU at 1,000 m before increasing gradually to the maximum at 0.15 RU at 4,400 m and decreasing to 0.13 RU at the bottom. Fmax 4 (453 nm) at HOT increased from 0.05 RU to local maxima at 0.38 RU at 600 m before gradually decreasing but with an increase to the maximum of 0.39 RU at 1,600 m and local minima of 0.26 RU at the bottom. Once again, this component also showed this additional decrease just above the seafloor. Hence, all $FDOM_H$ components behaved similarly with depth.

Overall, among these time-series study stations, the $FDOM_H$ EEM fluorescence intensity at surface waters were found to be depleted, while the $FDOM_P$ component was enriched,

consistent with previous studies[30]. The relative changes in the EEM fluorescence data and Fmax values in the water column indicated that FDOM was not simply produced in the euphotic zone because these relative changes persist throughout the water column. It is likely that the relative changes were indications of FDOM undergoing further transformations while exhibiting similar fluorescence components throughout the water column beyond the euphotic zone and mixed layer transported metabolites while maintaining the $FDOM_H$ characteristics. As depth increases, the observed humic-like and protein-like optical properties increased for $FDOM_H$ components at both stations. These typical $FDOM_H$ peaks have been previously shown to increase with depth and exhibited in these earlier studies relatively stable behavior below 1000-1400m in bathypelagic layers of the global ocean[22,30,72]. The $FDOM_P$ or protein-like component decreased in fluorescence with depth at both BATS and HOT. These results were also consistent with findings of previous studies[33]. However, after demonstrating the strength of the statistical EEM-PARAFAC analysis of the fluorescence data, a detailed assessment of the results further illuminated the intricate relationships of marine FDOM between and within the Atlantic and Pacific oceans. Specifically, the contrary behavior of $FDOM_H$ at depth and the continued decrease at HOT and increase at BATS below 1,000 m is intriguing and warrants further investigations.

To elaborate in greater detail the already observed substantial differences between HOT and BATS deep samples, we combined the data below 1,000 m for the UV-Vis absorbance data and the EEM-PARAFAC component data (Figure. 2.5). Given that high molecular weight (HMW) CDOM typically has higher absorption at longer wavelengths, CDOM at BATS is presumed to have a HMW when compared to HOT samples. This might be related to the special case of deep water formation in the North Atlantic and the subduction of Arctic DOM, that is

enriched in terrestrially-derived DOM[33]. Figure 2.5 A showed the much higher absorption coefficient at BATS than at HOT at 300nm. Figure 2.5 B showed the slightly higher $S_{275–295}$ at BATS than at HOT, indicating substantial differences in the quality of the CDOM composition. Figure 2.5 C showed the $S_{350–400}$ values to be overlapping but higher overall at BATS than HOT. Figure 2.5 D showed an overall higher SR at BATS than HOT, once again indicative for substantial differences in the CDOM composition. Figure 2.5 E showed an overlapping E2/E3 ratio but overall higher values at BATS than at HOT.

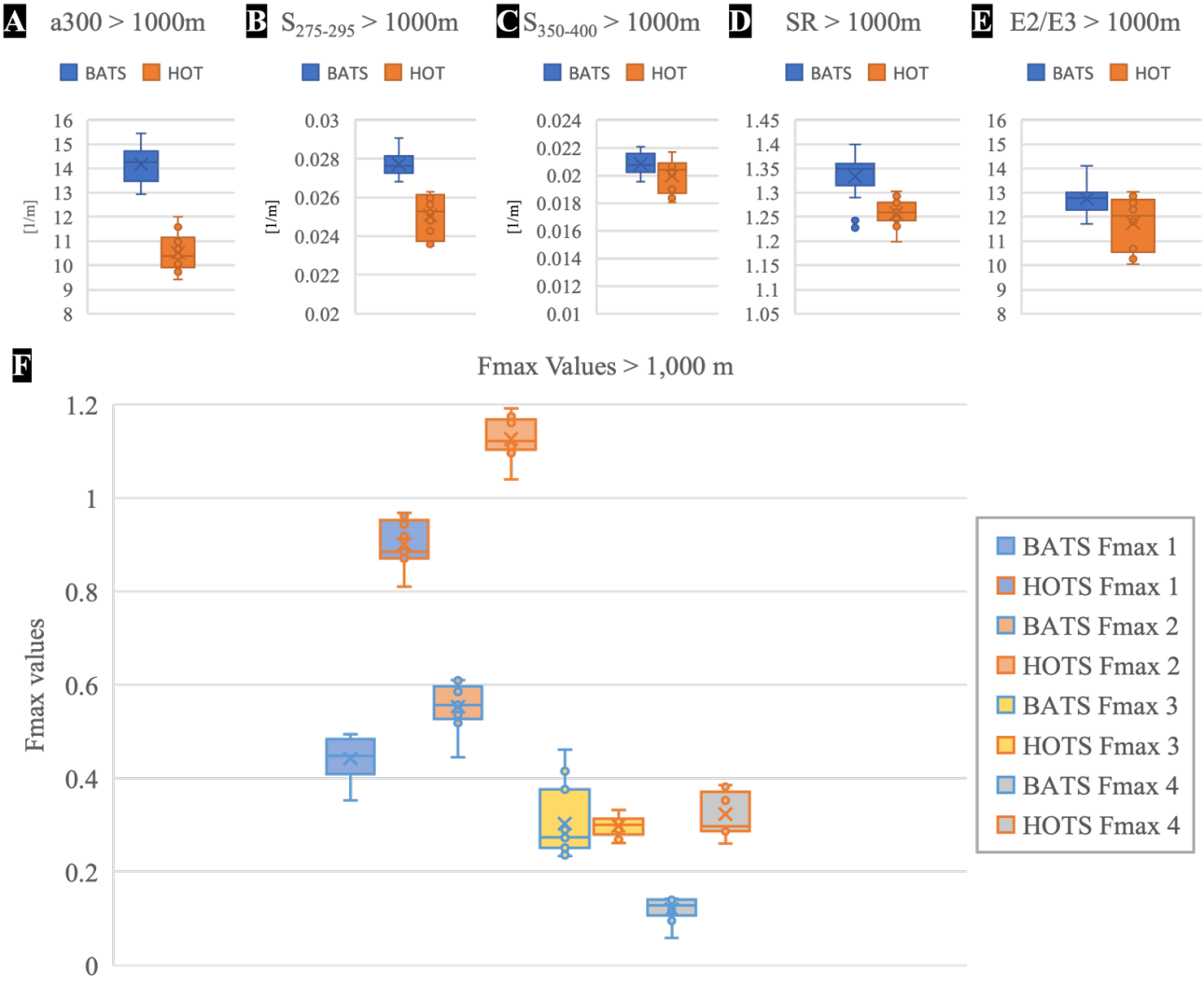

Figure 2.5 Ocean basin comparisons of UV-absorbance and PARAFAC component Fmax values analyzed from PPL SPE-DOM below 1000m. (A) absorption coefficient at 300 nm (a(300)); spectral slopes (B) $S_{275–295}$, and (C) $S_{350–400}$; (D) spectral slope ratio SR ($S_{275–295}/S_{350–400}$); and (E) absorption ratio E2/E3 (a(250)/a(365)). (F) PARAFAC component 1-4 Fmax values at each site.

Figure 2.5 F showed the significantly higher fluorescence of all $FDOM_H$ components. CDOM and FDOM are directly linked by apparent fluorescence quantum yield (AQY) of DOM, which reflects the efficiency of chromophores emitting fluorescence light after absorbing it[73]. It became abundantly clear that fundamental differences in AQY have to be present and was further indicated by the correlation between Fmax values and a300 (Figure 2.6 A) and also spectral slope values (Figure. 2.6 B).

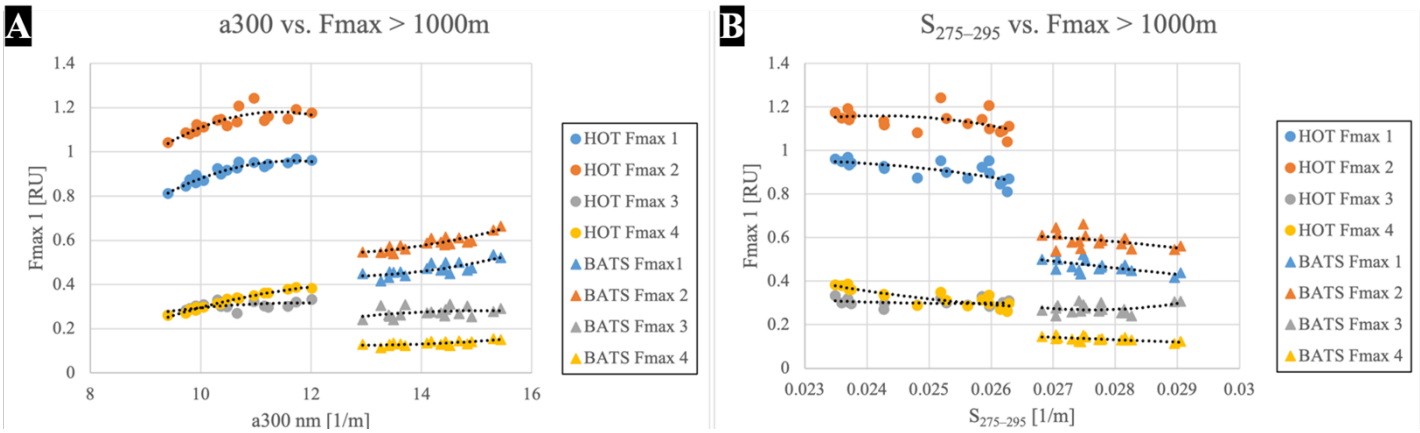

Figure 2.6 Comparing UV-Vis absorbance at 300 nm (A) and the spectral slope of $S_{275–295}$ (B) with PARAFAC component Fmax values analyzed from PPL SPE-DOM below 1000 m.

Directly comparing the UV-Vis absorbance data with the PARAFAC modeled fluorescence showed distinct differences in the two sample profiles. There was no overlap of absorbance or slope values between sites (Figure 2.6; Table 2.2). The *a*300 at HOT showed negative nonlinear slopes with downward pointing parabola of Fmax 1 (446 nm) and Fmax 2 (322 nm) whereas BATS showed positive slopes with upward facing parabola. Indicating that the fluorescence increased as absorbance decreased at HOT, but the fluorescence increased as absorbance increased at BATS. Overall, these two components showed similar trends within their respective oceanic basins and provided insights on the different FDOM processing occurring that yielded the changes in fluorescence. Earlier, the nature of the spectral slope

parameter was noted to indicate MW[41,42]. The overall decreasing trends in fluorescence as spectral slope increased hinted that the MW increased as absorbance increased, which was also consistent with the higher absorbance values at the surface seen in Figure 2.3 A.

Table 2.2 Regression analysis of the HOT and BATS PPL SPE-DOM absorption coefficient at 300 nm (a (300)) and spectral slope $S_{275–295}$ with each PARAFAC component fmax values.

		BATS			HOT		
Parameter	Fmax	Slope	R^2	Regression	Slope	R^2	Regression
a300	1	-0.23	0.81	$0.0097x^2 - 0.23x + 1.94$	0.82	0.72	$-0.036x^2 + 0.82x - 3.48$
	2	-0.24	0.65	$0.0098x^2 - 0.24x + 1.95$	0.65	0.92	$-0.028x^2 + 0.65x - 2.83$
	3	0.17	0.12	-0.0057x2+0.17x-1	0.16	0.33	-0.0068x2 + 0.16x - 0.63
	4	0.10	0.54	$0.0039x^2 - 0.10x + 0.77$	0.27	0.98	-0.01x2 + 0.27x - 1.37
$S_{275-295}$	1	248.18	0.21	$-4879.3x^2 + 248.18x - 2.54$	677.96	0.24	$-14013x^2 + 677.96x - 7.0401$
	2	-72.23	0.38	$749.95x^2 - 72.23x + 1.89$	277.8	0.53	$-6188.7x^2 + 277.8x - 2.1612$
	3	-826.28	0.16	$14961x^2 - 826.28x + 11.67$	-145	0.03	$2852.4x^2 - 145x + 2.1411$
	4	-9.05	0.41	$-30.5x^2 - 9.05x + 0.41$	-303.12	0.76	$5432x^2 - 303.12x + 4.5017$

In further investigating the statistical EEM-PARAFAC analysis, all Fmax values were correlated to each other for the entire depth profiles (Figure 2.7 A, C, E), but also on samples that were all taken below 3,000 m (Figure 2.7 B, D, F) to better compare the FDOM in the abyssal

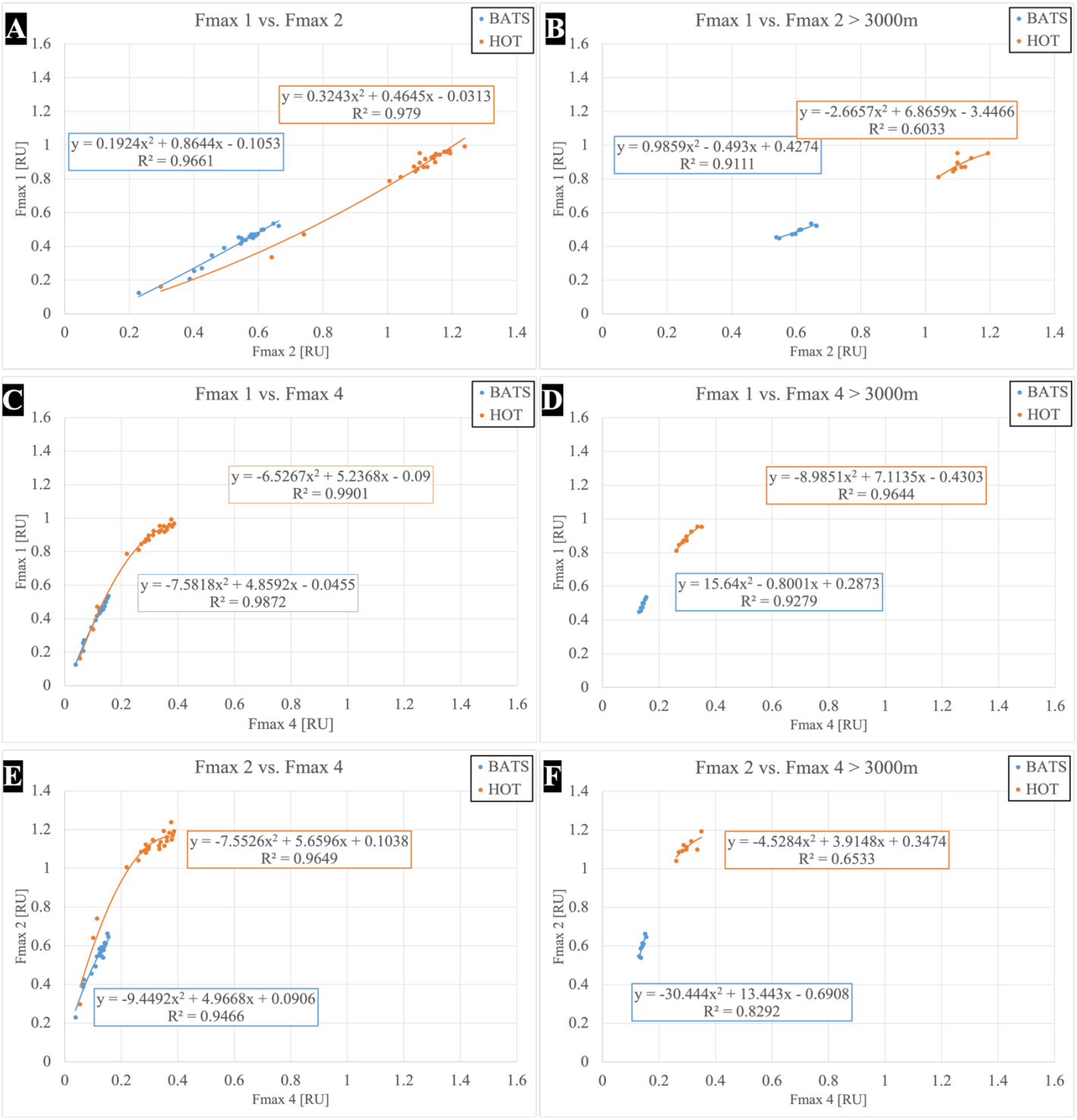

Figure 2.7 Fmax values and their correlations to each other. (A) Fmax 1 (446nm) vs. Fmax 2 (322nm) throughout the water column and (B) Fmax 1 (446nm) vs. Fmax 2 (322nm) below 3,000 m. (C) Fmax 1 (446nm) vs. Fmax 4 (453nm) throughout the water column and (D) Fmax 1 (446nm) vs. Fmax 4 (453nm) below 3,000 m. (E) Fmax 2 (322nm) vs. Fmax 4 (453nm) throughout the water column and (F) Fmax 2 (322nm) vs. Fmax 4 (453nm) below 3,000 m.

Atlantic and Pacific Oceans. Fmax 1 (446 nm) was compared to Fmax 2 (322 nm) and showed a strong non-linear correlation of all $FDOM_H$ components at HOT and a much more linear relationship at BATS throughout the entire water column (Figure 2.7 A). Fmax 1 (446 nm) was compared to Fmax 4 (453 nm) and showed the overall strongest relationship between components at both sites (Figure 2.7 B). Fmax 2 (322 nm) compared to emission maxima of Fmax 4 (453 nm) also showed strong correlation in the full profile at both sites (Figure 2.7 C). However, the Fmax 1 (446 nm): Fmax 2 (322 nm) and Fmax 2 (322 nm): Fmax 4 (453 nm) relationships fell apart at depths below 3,000 m (Figure 2.7 B & F). This indicated that the common component, Fmax 2 (322 nm), was likely more labile and thus subject to more remineralization than the other components. These comparisons gave good insight to the overall fluorescence intensity patterns in these statistically derived components to help determine component changes throughout the profiles. It is often assumed that DOM is highly conserved[52], and that its chemical character is similar across many marine environments[9]. This study is in contrast to these assumptions. The fundamental differences in behavior of $FDOM_H$ at HOT versus BATS suggested that fundamental compositional differences must exist in FDOM from BATS and HOT.

In further investigating the statistical EEM-PARAFAC analysis of the fluorescence data, the output of fluorescent PARAFAC components Fmax1 (446 nm), Fmax2 (322 nm) and Fmax 4 (453 nm) were compared to the $FDOM_P$ component Fmax3 (264 nm) (Figure 2.8 A-F). This analysis was undertaken to better understand the interrelationships of statistically derived fluorescent components throughout the water columns and specifically between the Pacific and Atlantic Ocean Basins. $FDOM_H$ Fmax 1 (446 nm), Fmax2 (322 nm), and Fmax4 (453 nm) were compared to $FDOM_P$ Fmax3 (264 nm) from a full depth profile (Figure 2.8 A-B), below the

mixed layer) (>1,000 m) (Figure 2.8 C-D, and at greater depths (>3,000 m) (Figure 2.8 E-F). The abundance of FDOMP components has typically been considered to be controlled by biological productivity and microbial consumption because protein-like components in marine

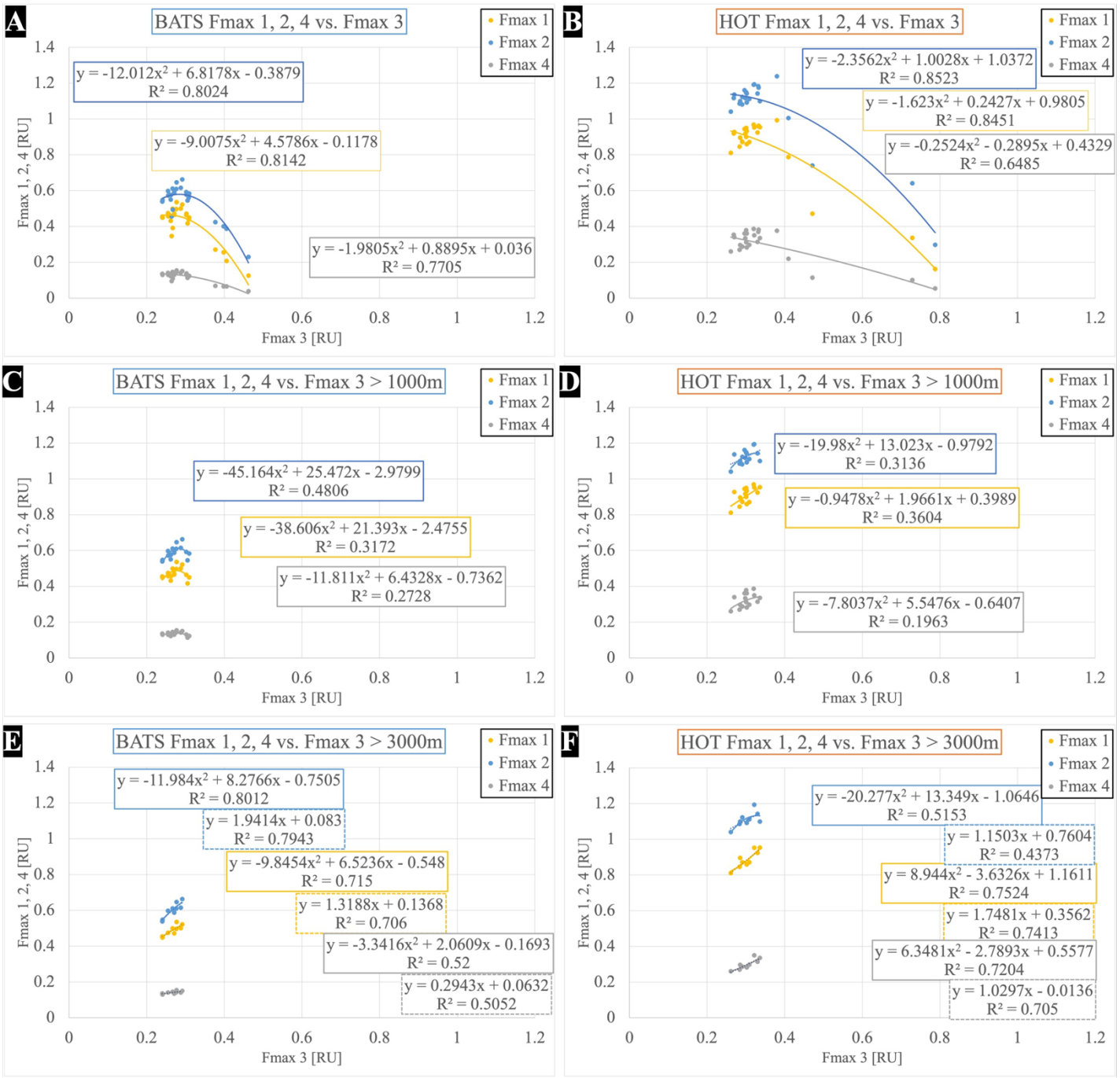

Figure 2.8 PARAFAC model component comparison of optical behavior [RU] based on sampling site, and depth using PPL SPE-DOM. Fmax 1 (464nm), 2 (322nm), 4 (453nm) with emission maxima of Fmax 1(446nm), Fmax 2 (322nm), Fmax 4 (453nm) respectively compared with Fmax 3 (264nm) at BATS (A) and HOT (B) above and below 1200m.

environments are presumed to be derived from aromatic amino acids, such as tryptophan and/or tyrosine [71,74]. The substantial shifts in correlations amongst components at depths below 1,000 m and 3,000 m across the basins confirmed the complicated relationship between $FDOM_P$ and $FDOM_H$. Specifically, the weak correlation of $FDOM_H$ with the $FDOM_P$ components below 1000 m, but a better correlation at depth cannot be easily explained and needs further research, which is beyond this study. Comparable trends were observed at HOT in the Pacific than at BATS in the Atlantic, however the slopes were distinctly different indicating that Pacific and Atlantic DOM underwent fundamentally different transformations resulting in these different relationships summarized in Figure 2.8, or have fundamental differences in structure and hence reactivity, yet maintaining similar fluorescence pattern.

AOU was calculated from the measured oxygen concentration and saturation derived from CTD measurements (Figure 2.9 A). Substantial differences in AOU between BATS and HOT were observed and once again point to fundamental differences in DOM processing or composition. AOU at HOT showed a greater increase in oxygen utilization. which is a proxy for heterotrophic respiration, from the surface to the oxygen minimum around 750 m depth as seen

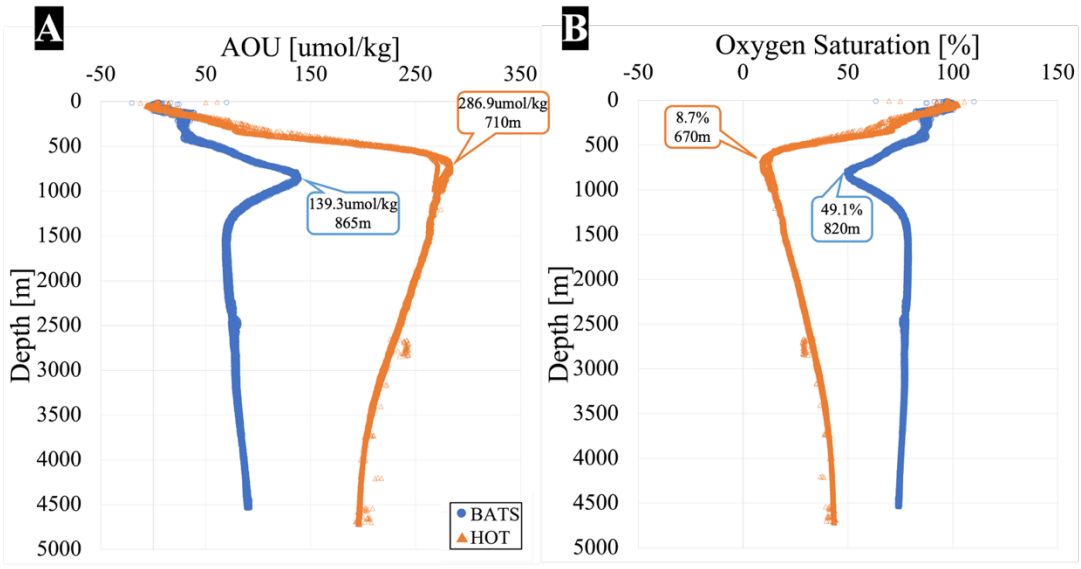

Figure 2.9 (A) Apparent oxygen utilization and (B) oxygen saturation depth profiles at BATS, Atlantic and HOT, Pacific Oceans.

in the oxygen saturation profile (Figure 2.9 B). The oxygen minimum reached as low as 7.8% oxygen saturation, which is low and indicated an extensive oxygen minimum zone (OMZ). AOU in the Atlantic at BATS showed a much more gradual and smaller increase from the surface to the oxygen minimum around 865m reaching only a minimal value of 49.1% oxygen saturation (Figure 2.8 B). Below the oxygen minimum in the Pacific, AOU gradually decreased with depths whereas in the Atlantic, AOU sharply decreased below the oxygen minimum and then gradually increases with depths, indicative again of drastic differences between BATS and HOT in microbial respiration derived from AOU calculations. These results supported previous findings of historical data from BATS and HOT studies with consistent AOU and oxygen saturation patterns[75,76]. Recently, a study of BATS oceanographic observations have been analyzed and indicated an accelerated deoxygenation in the surface at BATS due to ocean warming, salinification, and acidification that can impact controls on community productivity[75]. At HOT, shallower, more intense OMZ off the eastern North Pacific were shown to be increasing despite declining midwater oxygen concentrations and becoming increasingly dominant[77].

Because AOU has been used as an indicator of microbial activity in the dark ocean[78,79], and FDOM has been previously correlated to AOU[33,80], Fmax values were compared with AOU in the water column at each site and provided new insights based on the high resolution data (Figure 2.10). The linear regressions between AOU and the presumed biologically refractory $FDOM_H$ gave interesting insights in this relationship. On the left side of Figure 2.10, the $FDOM_H$ components: Fmax 1 (446 nm) in Figure 2.10 A, Fmax 2 (322 nm) in Figure 2.10 B and Fmax 4 (453nm) in Figure 2.10 D showed overall strong, positive correlations with AOU in the HOT profile but less in the BATS profile, which is supported by previous studies[75,81].

Fmax 1 (446 nm), Fmax 2 (322 nm), and Fmax 4 (453 nm) all showed stronger positive correlation with AOU at HOT than at BATS throughout the water column and show weaker correlations below 1,000 m. The $FDOM_P$ component: Fmax 3 (264 nm) in Figure 2.10 C showed negative and weak correlations with AOU in the depth profile, but below 1,000 m, HOT showed a weak, and positive correlation and BATS showed a weak, negative correlation. This suggested that the processes producing and transforming $FDOM_P$ were different at each of the sampling stations.

A closer look of data from below 1,000 m, showed that the correlation between Fmax 1 (446 nm) and AOU appeared to be different between BATS and HOT (Figure. 10 A, right panel). The other $FDOM_H$ Fmax 2 (322 nm) in Figure 2.10 B, left panel showed also an overall strong positive correlation with AOU in the combined data set. Below 1,000m, a similar divergence than in Fmax 1 (446 nm) was also apparent with this component (Figure. 10 B, right panel). Because AOU usually is used as an indicator of microbial activity in the dark ocean[78], higher values imply high amount of dissolved oxygen consumption by remineralization processes. The linear regression indicated that $FDOM_H$ was produced as organic matter is oxidized biologically. In both $FDOM_H$ component comparisons, the high resolution of these profiles showed that the slope of the linear regression was significantly higher at HOT than BATS, at which could be explained by a higher FDOM production at HOT due to increased remineralization because of the rich, dense, oxygen-rich bottom waters in the Pacific[33]. In figure 2.10 E-F showed $FDOM_P$ Fmax 3 (264 nm) compared to AOU which trended negatively in the BATS and HOT profiles: HOT showed a greater slope of -488.68 whereas the slope at BATS was -391.34. At depths below 1,000 m, the $FDOM_P$ Fmax 3 (264 nm) and AOU linearity disappears and the trending slope at HOT is positive (Figure. 10 F) The deeper samples were

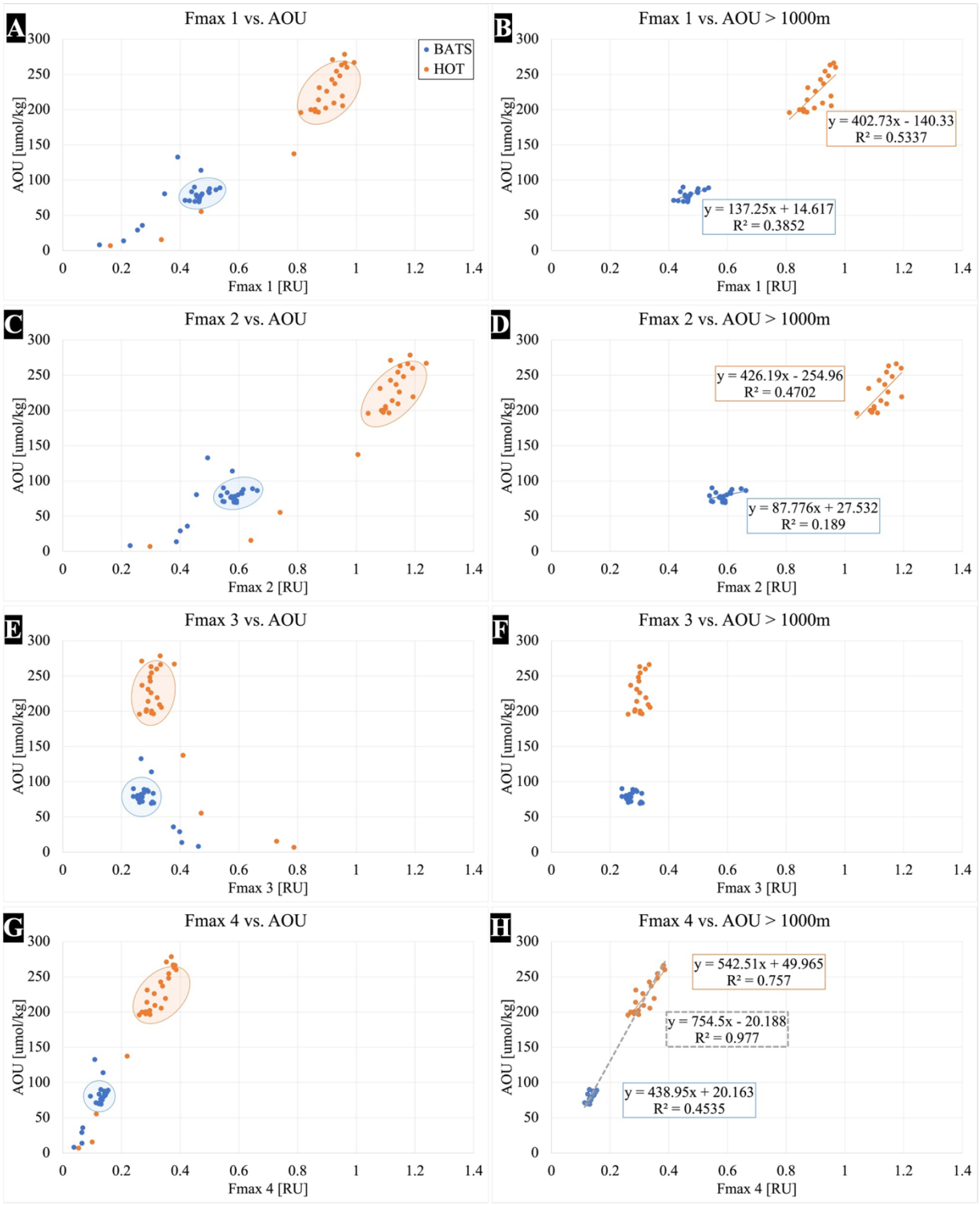

Figure 2.10 A-D Correlations between AOU and PARAFAC fluorescence components Fmax1-4 in the entire water column (left panels) and below 1,200m depth (right panel) at BATS and HOT.

highlighted with circles and did not show any correlation at all. The third $FDOM_H$ component, Fmax 4 (453 nm) showed an even stronger overall positive correlation with AOU at BATS and HOT (Figure 2.10 G-H) than Fmax 1 (464 nm) and Fmax 2 (322 nm). Interestingly, samples collected below 1,000 m and showed strong linear regression of all data collected from both BATS and HOT seen as the dotted line in Figure 10 H. A strong correlation between FDOM fluorescence with AOU was demonstrated for the Pacific Ocean with a coefficient of determination of 0.757 at HOT suggesting that this relationship is indicative of *in situ* production of refractory FDOM at depth[35]. . Our results agree with generalizations of previous findings and indicated that there is a stronger correlation of AOU at depth with $FDOM_H$ at HOT in the Pacific than at BATS in the Atlantic. Levels of $FDOM_H$ components Fmax 1 (446 nm), Fmax 2 (322nm) and Fmax 4 (453 nm) were linearly correlated to AOU in the bathypelagic layer, implying that all $FDOM_H$ components were likely *in situ* produced during microbial degradation processes of organic matter. The poor linear regression fit of the $FDOM_P$ component, Fmax 3 (264 nm), of both sites below depths of 1,000 m supports evidence that the production of $FDOM_P$ is similar in not correlating with AOU and the processes associated with oxygen utilization (Figure 2.10 C). The notable strong correlation between AOU and Fmax 4 (453 nm) at both stations in Figure 2.10 D has not been previously described and might indicate the specifically usefulness of this EEM-PARAFAC component in describing AOU-FDOM relationships. This study described in detail the optical properties of two high resolution depth profiles at BATS and HOT and revealed novel and nuanced relationships between FDOM fluorescence and AOU in the Atlantic and Pacific Oceans using directly comparable sample collections and processing protocols.

In addition to the PPL SPE-DOM samples, the WAX extract also showed some interesting behavior in optical properties with depth at BATS and HOT. The biggest difference

was that the WAX resin collected much less CDOM than PPL, which was expected and reflected in the much lower absorbance at 300 nm for BATS and HOT (Figure 2.11 A). Interestingly, the WAX extracts showed higher values for the spectral slope $S_{275\text{-}295}$ at BATS than at HOT. These differences provide further evidence that the WAX extracts were also fundamentally different between BATS and HOT and continued to support the finding that BATS and HOT CDOM is remarkably different at the molecular level.

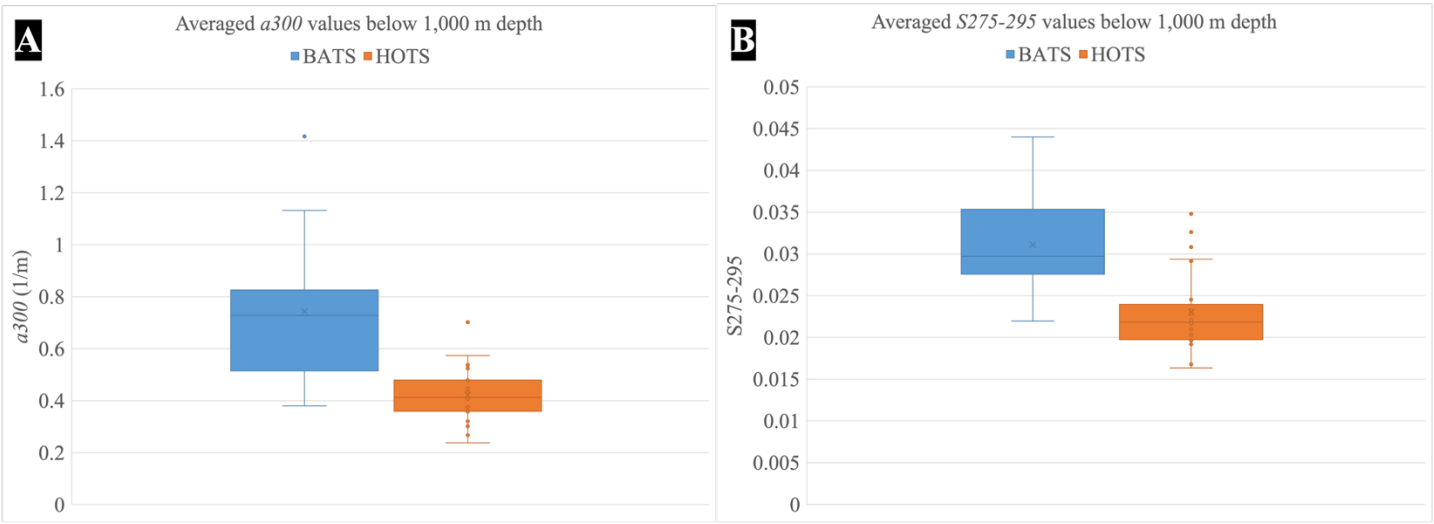

Figure 2.11 Comparing WAX SPE-DOM sample absorbance collected at BATS and HOT. (A) Box plot comparison of averaged WAX absorbance at 300 nm values below 1,000m depth. (B) Box plot comparison of averaged WAX spectral slope $S_{275\text{-}295}$ values below 1,000 m depth.

The fluorescence of the WAX SPE-DOM showed variations that fitted best to a four component EEM-PARAFAC model (Figure 2.12 A). Three out of the four validated components fitted again the $FDOM_H$ descriptions from literature[33,47,70] while the fourth likely accounted for contamination caused by protein-like fluorescence. Fmax values below 1,000 m for each site plotted side by side revealed only significant differences in Fmax 2 (322nm) (Figure. 2.12 B). Overall BATS seemed to also have higher fluorescent AQY in this fraction, but it should be noted that the scales here were much smaller than the magnitude of the PPL SPE-DOM findings. In conclusion, the absorbance and fluorescence data in the fundamentally different fractions

isolated by PPL and WAX converge and tell similar stories about fundamental DOM differences between these two ocean basins.

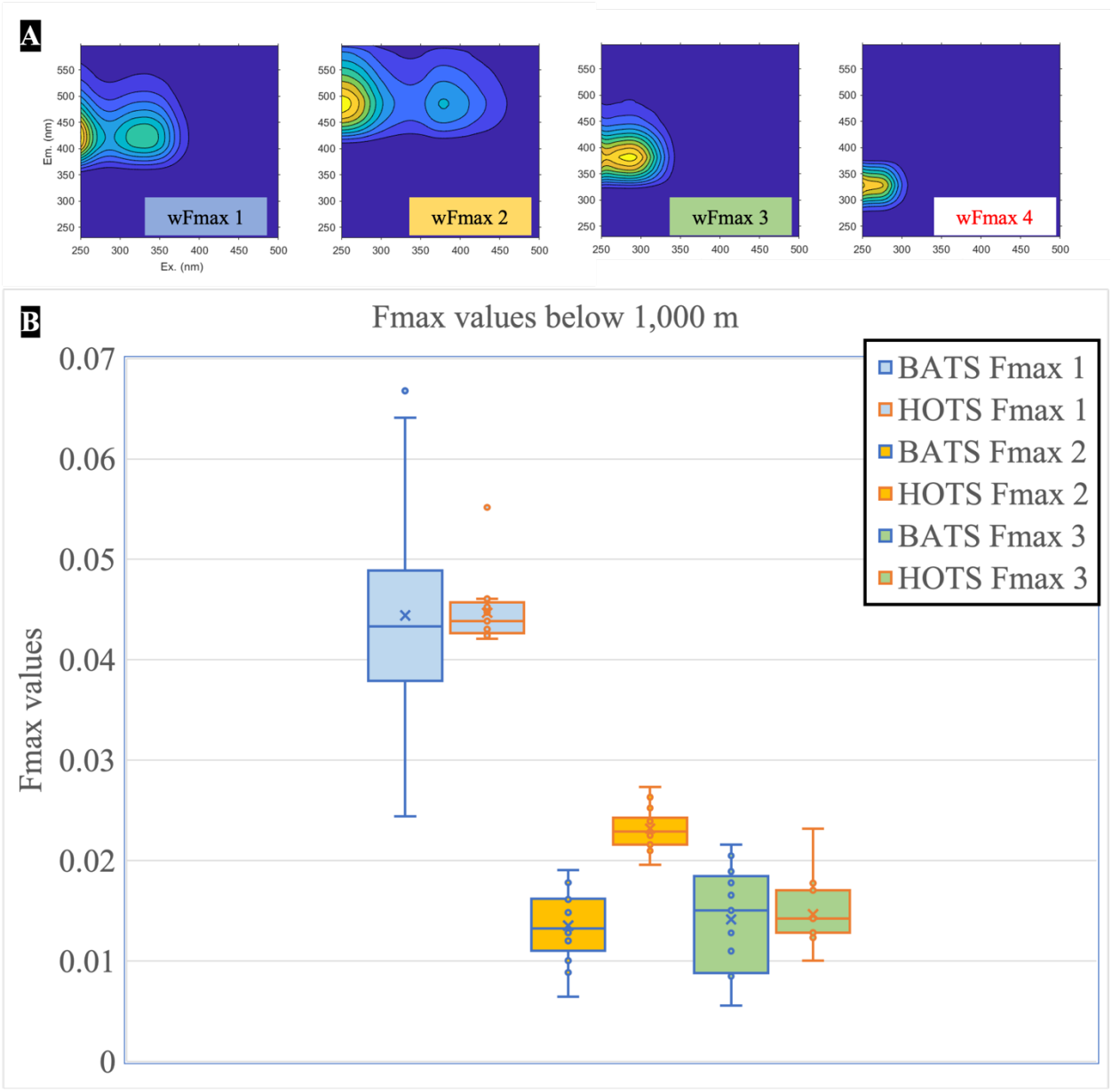

Figure 2.12 (A) WAX SPE-DOM PARAFAC component EEMs for BATS and HOT. (B) Fluorescent maximum of PARAFAC components 1-3 values below 1,000 m at BATS and HOT.

2.4 Conclusions

In this study, I used absorption and fluorescence spectroscopy to compare DOM composition between depth profiles of HOT and BATS ocean transects. The overall absorption was consistently higher at BATS than at HOT other than at 600 m where BATS samples decreased, and HOT samples increased in absorbance (Figure 2.3 A). Trends of $S_{275–295}$ and SR values increased at depths for HOT, supporting the evidence that the MW of compounds were overall decreasing in the Pacific given the inversely proportional findings of previous studies (Figure 2.3 B & D). The higher absorption ratio E2/E3 at the HOT surface indicated that the CDOM MW was smaller in the Pacific (Figure 2.3 E). PARAFAC modeled EEM fluorescence showed evidence of consistent $FDOM_H$ and $FDOM_P$ throughout the water column. The fluorescence values were higher in the Pacific than in the Atlantic (Figure 2.4 B & C) despite the overall greater absorbance and E2/E3 ratio values in the Atlantic. At HOT, the relationships between Fmax 1 (446 nm): Fmax 2 (322 nm) and Fmax 2 (322 nm): Fmax 4 (453 nm) fall apart at depths indicating that the common component was likely subjected to remineralization (Figure 2.7 B & F). A ubiquitous strong correlation was found between all of the Fmax 4 (453nm) samples at BATS and HOT at depths below 1,000m and AOU (Figure 2.10 H). $FDOM_H$ component comparisons showed high resolution profiles with higher linear regression slope at HOT than BATS, at which could be explained by a higher FDOM production at HOT due to increased remineralization because of the dense, oxygen-rich bottom waters in the Pacific[33]. The $FDOM_P$ Fmax 3 (264 nm) showed only a weak overall negative correlation with AOU in the BATS and HOT profiles, but this seemed only to be present at shallower depth (<1,000 m) (Figure. 10 E). Findings from the water column profiles, UV-Vis absorbance, PARAFAC model fluorescence values and AOU analyses supported the idea that DOM in the Atlantic and Pacific oceanic basins are composed of fundamentally different molecules, differences in FDOM

production, and remineralization between basins - sometimes structured by depth. Hence FDOM production and reactivity are key in explaining the observed differences in bulk DOC in understanding marine carbon cycling.

Chapter 3: Comparing Optical Profiles and Nutrient Analyses of *Synechococcus*-Derived Dissolved Organic Matter during Long-Term Incubation Experiments

Abstract

Marine carbon is a key component of the Earth's active carbon cycle and marine microbial communities play a critical role in processing carbon in global biogeochemical cycles. DOM deriving from picocyanobacterial cells via situationally unique mechanisms such as viral lysis and metazoan grazing complicate carbon can be stored in the oceans at time scales ranging from days to hundreds or thousands of years. Optical properties of DOM are commonly used as proxies to identify and quantify refractory or accumulating DOM in the deep ocean. Therefore, there is a need to assess the impact of microbial process on the chemical nature of DOM. We added *Synechococcus*-derived DOM to an oligotrophic microbial community and followed the changes by measuring and modeling the changes in fluorescence patterns over time. Bacterial community structure, nutrients, DOC, and optical properties of pressure system lysed *Synechococcus* degradation products were monitored in three dark-incubation experiments and three controls over a year-long incubation period. The addition of SDOM resulted in dramatic changes based on the nutrients, DOC and microbial community profiles, especially in the early days of incubation. This analysis of changes in nutrient speciation, and optical properties over the course of a year revealed nuanced changes in the inorganic nitrogen speciation along with fundamental shifts in the microbial community structure as well as the dynamic changes of the FDOM derived from lysed *Synechococcus* cells. Overall, the experimental analyses found that the microbial communities transformed the SDOM and confirmed the production of refractory FDOM from the initial materials. Linking products of microbial processes to chromophore

optical signatures and spectroscopy is a capstone in understanding parts of the global carbon cycle over decades of research.

3.1 Introduction

3.1.1 Microbial Carbon Processing

The oceans play an important part of the Earth's carbon cycle and DOM is one of the biggest pools of reduced and complex carbon on Earth. Marine DOM is a complex mixture of chemical compounds that is typically compartmentalized into pools determined by their reactivity: labile, semi-labile, or refractory with respective storage timescales of days, months to years, to hundreds of years to millennium as mentioned earlier, but this traditional view has been recently challenged[8].

Marine microbial communities and specifically photo-autotrophs play a critical role in global biogeochemical cycling by converting sunlight energy into chemical energy through fixing large amounts of atmospheric carbon dioxide in the photosynthetic process and synthesizing half of the global photosynthetic biomass[12]. Autochthonous DOM is then either directly released from photosynthetic eukaryotic organisms or produced during a cascade of trophic interactions[13]. The quantity and composition of microbial communities likely determines the rate of atmospheric CO_2 sequestering and the chemical structure of resulting DOM. Therefore, there is a need to examine the marine microbial communities that produce and interact with DOM to further our understanding of the dynamics of these processes and impact on long-term carbon storage. DOM and microbial community structures depend on each other and perhaps can be phrased as a chemical-biological symbiosis.

The biologically labile fraction of DOC produced by photoautotrophs is routed through rapid bacterial production and mineralized and represents a large flux of the oceans' carbon. DOC that is not immediately mineralized accumulates as biologically semi-labile and refractory DOC and has conservative spectroscopic and chemical properties, often used to trace DOC

composition changes related to biolability[5]. Removal of refractory DOC via abiotic processes equates to only a fraction of sinking particulate organic carbon but is four times the rate of organic carbon sequestration in deep ocean sediments[5]. This disconnection between the AOU rates continues to challenge our current understanding of the marine carbon cycle that requires a more accurate assessment of fundamental biogeochemical drivers of surface water DOM concentrations and reactivity, biological carbon pump efficiency, and the autotrophic communities that are the ultimate but variable sources of marine DOM. Exploring the microbial and physiochemical constraints of DOM reactivity and microbial degradation is necessary for a more accurate assessment of the active and dynamic role marine DOM plays in the global carbon cycle in a changing world.

Global warming and increased ocean temperatures will increase carbon flow through the microbial carbon pump[82]. Large-scale changes in phytoplankton communities as shown in Flombaum et al.[20] could create a cascade of changes in the microbial community along with the higher marine carbon-flux with unknown consequences with regard to carbon storage. Hence, the importance of picocyanobacteria as a large and ubiquitous source of DOM should not be ignored, but little is known today about stable metabolites or stable degradation products from these very important primary producers, that account for the majority of primary production in the oligotrophic ocean[16]. Estimates indicate that these microorganisms provide 45.2% of the total primary productivity accounted for in the Pacific Ocean[83], but global estimates find that about picocyanobacteria make up 39% of the planktonic primary production in the world's oceans[84].

3.1.2 Investigating In-Situ Sources of Fluorescent Dissolved Organic Matter

Sources of *in situ* production of marine CDOM has been a topic of research for some time, but linking marine biota with specific fluorescent optical properties has recently been

explored in more detail[33,70,35,80,16,85], but no fluorophore has been discovered to date that is microbially recalcitrant and hence could explain the observed fluorescence of deep ocean DOM. However, marine fluorescent material has been recently linked to picocyanobacteria[16] and it was found that cultured marine picocyanobacteria, *Synechococcus* and *Prochlorococcus*, released FDOM that closely matched the typical fluorescent signals found in oceanic environments. *Synechococcus* and *Prochlorococcus* being some of the most abundant and widely distributed photoautotrophs in the global oceans[86,87], have the potential to be an ubiquitous source of FDOM. The lysis and degradation of picocyanobacterial cells supply DOM to the abyssal ocean, but picocyanobacterial-derived DOM and its optical properties have not been previously characterized in detail or directly compared to FDOM present in the deep ocean prior to our group's effort. As stated earlier, picocyanobacteria have been predicted to have large impacts on the future ocean environment, with 10–20% increase of abundance globally by the end of 2100[20]. Identifying the processes in which *in-situ* DOM sources, such as those derived from picocyanobacteria, undergo chemical transformations that produce fluorophore metabolites identified as FDOM is the key to further investigation. Picocyanobacteria-derived DOM degradation processes yield intriguing stable FDOM, but it remained vague how stable this material really is over time. Other sources of FDOM derived from pure culture of heterotrophic bacteria, phytoplankton or zooplankton remain not well defined explaining specifically the $FDOM_H$ that has been found in the deep ocean as discussed in the previous chapter.

This chapter is based on describing and investigating lysed picocyanobacteria released DOM and specifically FDOM during long-term incubation experiments that has the potential to explain in part the marine $FDOM_H$ signals observed globally[16].

3.1.3 Objective of Study

Chapter 3 focuses on the data collected from a long-term incubation experiment using lysed *Synechococcus* cells to investigate the microbial degradation and chemical transformations of SDOM fluorescence. The results from this work are discussed using a combination of microbial, optical, and chemical analyses as we continue to shape our understanding of microbial and physiochemical constraints on marine biogeochemical fluxes and the challenges that lie ahead.

3.2 Materials and Methods

3.2.1 Incubation Experiment

The *Synechococcus* culture, incubation experimental set up, subsampling procedures and chemical analyses described here were all derived from preliminary work undertaken by Zhao et al[85].

Ph.D. candidate, Yufeng Jia and the Chen laboratory at the Institute of Marine and Environmental Technology (IMET) were responsible for cultivating the *Synechococcus* culture, building and maintaining the incubation set up, and conducting subsampling on the pre-determined dates over the course of 150 days. Briefly, the following descriptions have been shared from Ph.D. candidate Jia's notes. The *Synechococcus* strain WH7803 was cultivated to 25 L (~10^8 cells/mL) in the SN30 medium (Waterbury et al. 1986) at 25 ˚C under constant cool white light (20 to 30 μE m^{-2} s^{-1}) before centrifugation harvesting (10,000 rpm for 10 min) and washed twice with DOM-free artificial seawater (salinity 30). The harvested cells were stored at -20 ˚C until being lysed using French Press (Glen Mills®). The pressed cell material was filtered through a GF/F (Whatman®) glass fiber filter (pore size 0.7μm) to remove large cell debris,

generating 150 mL of concentrated *Synechococcus*-derived DOM which was kept in 4 ˚C for 3 days until further use.

Seawater was collected on R/V Seahawk of University of North Carolina Wilmington at an open ocean station located within the Gulf Stream in the North Atlantic (37 ˚N, -70 ˚E, surface water). The water sample was filtered and transferred to six acid washed 20 L glass bottles (triplicates for control and for *Synechococcus*-derived DOM treatment). Eighteen liters of filtered seawater was transferred to the incubation bottles and were kept in the dark for 4 days to lower background labile DOC level and to stabilize the microbial community[85].

Synechococcus-derived DOM was added to 3 incubation bottles as triplicates for treatment, and no alteration was applied to the control triplicates. All 6 incubation samples were kept in the dark with ventilation at room temperature for the entirety of the experiment.

Sub-samples of 700 mL were taken on days 0, 1, 3, 5, 7, 10, 15, 22, 30, 59, 75, 90, 181 and 367 for analyses of microbial abundance, microbial community composition, total organic carbon (TOC), dissolved organic carbon (DOC) and nutrients. For DOC measurement, sub-samples were filtered through a pre-combusted GF/F filter (Whatman®), of which 20 mL filtrate was transferred to an acid-rinsed and pre-combusted VOA vial (Restek, USA), followed by an addition of 2 mL 32% high purity HCl. Nutrients were collected from the filtrate of sub-samples through 0.22 μm poly carbonate (PC) filter, where 40 mL of filtrate was transferred to a 50 mL centrifuge tube and stored at 4 ˚C until chemical measurements.

Sub-samples were transported on ice to Gonsior laboratory at the CBL. Samples taken for nutrient analyses were submitted to the Nutrient Analytical Services Laboratory (NASL) at CBL measured DOC, Ammonium, Nitrite + Nitrate, Nitrite, Phosphate, TDN, TDP and calculated

dissolved organic nitrogen (DON) using Environmental Protection Agency (EPA) and standard methods. Acidified sub samples were immediately solid phase extracted, as described below.

3.2.2 DOM Sample Collection

The DOM samples for the study were isolated through two types of solid phase extraction. Solid-phase extraction was conducted for the 300mL of sub-samples collected using 200mg of Agilent Bond Elut proprietary polystyrene vinyl resin (PPL) in 3mL cartridges and 150 mg of Waters Oasis WAX resin in 6mL cartridges. The MeOH, 0.1% (v/v) FA water used for SPE in the field were LC/MS grade and the ultrapure water used to rinse. Details about each extraction is given below.

Agilent Bond Elut 0.5g PPL cartridges were first activated with 5 mL MeOH, rinsed with 5 mL 0.1% FA water, then loaded via lines running through pre-ashed 0.7 μm glass microfiber filters by gravity or a peristaltic pump as necessary. After sample loading, the cartridge exterior was rinsed with ultrapure water and the sorbent was thoroughly rinsed with 5 mL 0.1% FA water to completely remove salts. Cartridges were dried, and eluted with 3 mL MeOH into new, trace contaminant certified or acid-washed and combusted glass vials. WAX cartridges were added subsequently beneath the PPL cartridges for the first full profile or one third of the sample collection. Oasis Waters WAX cartridges were activated using 5mL 2% NH_4OH methanol and 5mL 0.1% FA water before being loaded with the filtered and acidified sample by gravity or a peristaltic pump as necessary. After sample loading, cartridge exteriors were rinsed with ultrapure water and the sorbent was rinsed with 5 mL 0.1% FA water to remove salts. Cartridges were eluted with 3 mL 2% NH_4OH methanol into new, trace contaminant certified or acid-washed and combusted glass vials. 1 mL of RO water was subsequently added to prevent

flocculation. The methanolic SPE-DOM extracts were stored in the dark at -20°C following extraction and between analyses.

Samples of the methanolic SPE extracts were dried and re-dissolved for optical properties analysis by drying 0.5 mL using ultrahigh purity nitrogen and re-dissolving in 5 mL of ultrapure water. UV-Vis absorbance spectra and fluorescence excitation-emission matrices (EEMs) were measured over a 10s integration time at an excitation wavelength range of 250-700 nm and emission wavelength range of 240-600 nm at 3 nm intervals using a Horiba Aqualog spectrofluorometer, which is capable to measure UV-Vis absorbance and EEMs simultaneously. All absorbance and fluorescence spectra were blank corrected using scans of ultrapure water. Absorbance spectra (A(λ)) were converted to decadic absorption coefficient spectra (a(λ)) using the equation $a(\lambda) = A(\lambda)/L$, where L is the pathlength of the cuvette (0.01 m). Rayleigh scattering and inner filter effects were corrected using the Aqualog software. Spectra were normalized using the water Raman scattering of pure water and Water Raman Units. SPE-DOM EEMs were analyzed using statistical parallel factor analysis (PARAFAC) modeling using the MATLAB DrEEM toolbox[36,70]. Three outliers were removed because of high leverages which indicated contamination. A five-component model was generated to explain the data, which was split-half validated using four random splits and met other validation requirements[36]. Unit normalization was reversed to recover true scores of components. The maximum fluorescence values of components were summed for each sample and the relative contribution in % of each Fmax value were calculated to explain representation by these statistical components.

3.3 Results and Discussion

EEM fluorescence of the PPL SPE-DOM were integrated to show transformations over the course of the experiment and best fit a four component EEM-PARAFAC model (Figure. 3.1

A). Two out of the four validated components with maximum emission wavelengths of 464 nm (Fmax 1 (464 nm)) and 404 nm (Fmax 3 (404 nm)) fit the $FDOM_H$ descriptions from literature[33,47,70]. The characteristics of these components showed similar patterns including the large Stoke's shift at about 250 nm excitation and 450 nm emission and fit the previously defined $FDOM_H$ fluorescence peak description with absorbance extending well above 400 nm. Fmax 4 (310nm), the component with maximum emission wavelength of 310 nm, exhibited similar optical behavior as what has been historically considered to be $FDOM_P$ chromophore with a single peak ranging emission from 275-340 and excitation around 275[47,71]. Fmax 2 with a maximum emission wavelength of 319 nm displays similar optical behavior to a $FDOM_P$ chromophore as well but it was flagged as a typical contamination signal from human handling and the result of very long integration times, so the data from this component was discarded.

Figure 3.1 B showed PARAFAC Fmax values distributed across the component model and showed a high-resolution time series profile of FDOM samples over the course of the incubation experiment for the control samples as well as the SDOM-treated subsamples plotted against incubation sampling dates. Compared to those in the SDOM-treated subsamples, the control subsamples showed overall lower fluorescence intensity – expressed as Raman unit [RU] – and low variations as seen in the small values shown in Table 3.1.

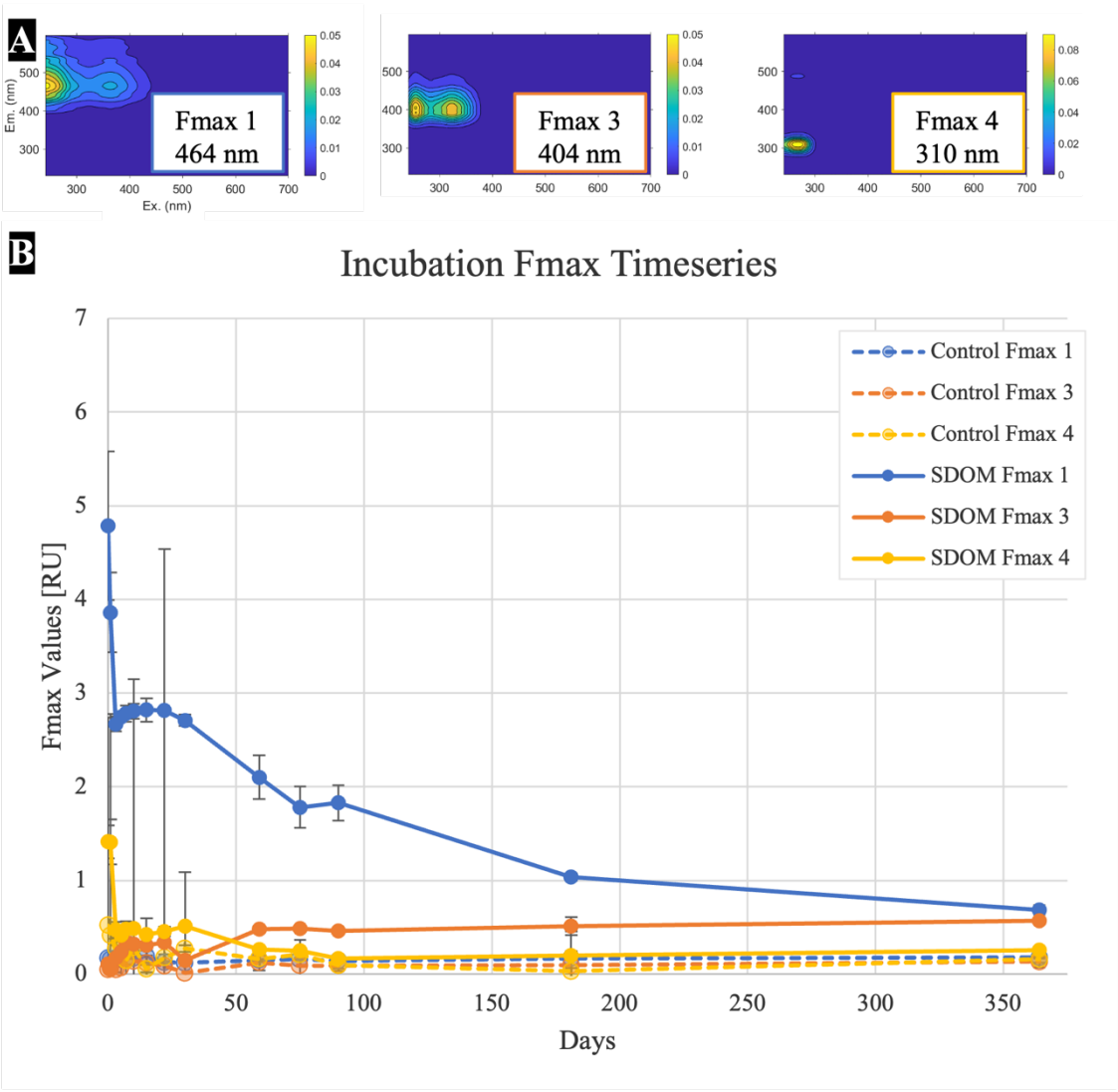

Figure 3.1 (A) Optical Properties of PPL SPE-DOM PARAFAC component EEMs for the incubation experiment. (B) Fluorescent maximum of PARAFAC components 1, 3, & 4 for both the control (dashed lines) and SDOM (solid lines) treated groups over time.

Table 3.1 Overall experimental averages and standard deviation of each set of control and SDOM-treated subsamples for each component for the duration of the year-long incubation experiment.

	Fmax 1 (464 nm)		Fmax 3 (404 nm)		Fmax 4 (310 nm)	
	Control	SDOM	Control	SDOM	Control	SDOM
Avg	0.168	2.531	0.091	0.324	0.221	0.513
SD	0.035	1.043	0.041	0.162	0.136	

The control subsample fluorescence properties that were identified as Fmax 1 (464nm) had a measured average value of 0.167 RU at day zero of the incubation experiment whereas the SDOM-treated subsample properties identified as Fmax 1 (464 nm) had a much higher measured average value of 4.786 RU, indicating a very high contribution from the lysed material. Control Fmax 1 (464 nm) and Fmax 3 (404 nm) showed a minimal range of variation throughout the year-long incubation indicating negligible fluorescent organic material produced from the culture medium alone that was added to the controls (Table 3.1). SDOM Fmax 1 (464 nm) sharply decreased in the first three days before reaching a local minimum of 2.670 RU and increasing to a local maximum of 2.819 RU and decreasing gradually and stepwise over the rest of the incubation period. Fmax 1 (464 nm) showed the biggest difference in fluorescence between the start of the incubation and at the one-year mark across all the samples.

The control sub-samples identified as Fmax 3 (404 nm) had an initial measured average of 0.049 RU whereas the SDOM-treated Fmax 3 (404 nm) had an initial measured average of 0.110 RU, while greater than the intensity of the controls, but at the minimum intensity for the beginning of the experiment. The SDOM-treated Fmax 3 (404 nm) signal decreased in intensity in the first day but then increased to a local maximum of 0.348 RU on day seven. Then Fmax 3 (404 nm) decreased to a local minimum of 0.306 RU on day fifteen before another local maximum of 0.336 RU on day twenty-two. Fmax 3 (404 nm) repeated the same pattern again with a local minimum of 0.144 RU on day thirty before gradually increasing for the remainder of the experiment. The Fmax 3 (404 nm) signal one-year mark of the experiment reached a maximum of 0.569 RU, approaching the 0.685 RU minimum of SDOM Fmax 1 (464 nm).

The control sub-samples identified as Fmax 4 (310 nm) had an initial measured maximum of 0.521 RU and gradually decreased to 0.141 RU on day seven. The control Fmax 4

(310 nm) showed the most variation in fluorescence intensity over the course of the experiment but decreased overall before reaching a local maximum of 0.158 RU at the end of the year-long experiment. In contrast, SDOM Fmax 4 (310 nm) averaged value around 1.411 RU for days zero and one before decreasing to 0.474 RU on day three. Fmax 4 (310 nm) increased to a local maximum of 0.484 RU on day ten before reaching a local minimum at 0.421 RU on day fifteen and increased again to 0.510 RU on day thirty.

The initial high fluorescence followed by an immediate sharp decrease in intensity seen in the SDOM-treated Fmax 1 (464 nm) and 4 (310 nm) values does seem counterintuitive given their $FDOM_H$ classification. Perhaps some of these $FDOM_H$ are microbially labile under the right conditions given that Zhao et al. found that the $FDOM_H$ also behaved like that for their 15-day cyanophage incubation. The lack of initial Fmax 3 (404 nm) signal detected at the start of the experiment and its accumulation over time implied that it was produced as organic matter was recycled and transformed from compounds that initially produced Fmax 1 (464 nm) and 4 (310 nm) signals. Figure 3.1 B illustrated that Fmax 3 (404 nm) signal slightly mirrored patterns of Fmax 1 (464 nm) as it was degraded over time, which supported the suggestion that the SDOM degradation process caused chemical transformations that can be tracked optically. Additionally, the continued increase in Fmax 3 (404 nm) signal throughout the experiment demonstrated the stability of FDOM characterized by this component confirming the refractory nature of SDOM from lysed *Synechococcus*.

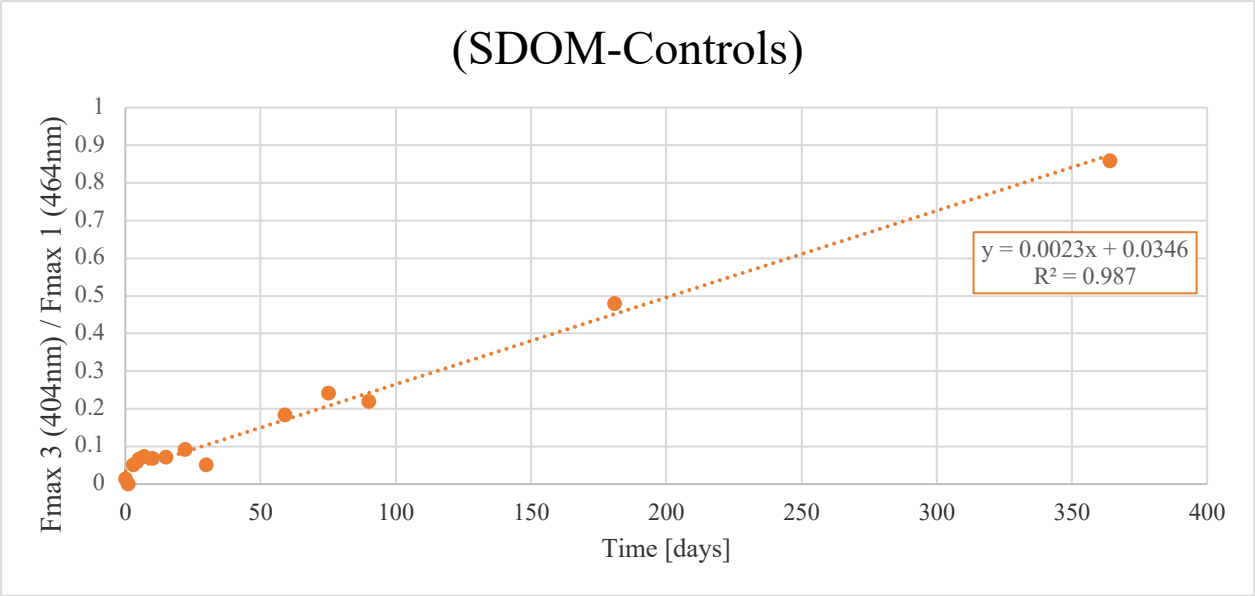

Figure 3.2 Optical Properties of PPL SPE-DOM PARAFAC component SDOM Fmax 3 (404nm) – control Fmax 3 (404nm) over SDOM Fmax 1 (464nm) – control Fmax 1 (464nm) over the course of the incubation experimental period.

Figure 3.2 showed the ratio of SDOM-treated Fmax 3 (404 nm) over Fmax 1 (464 nm) values after subtracting the Fmax values produced by the controlled group. The ratio plotted over the incubation experimental period showed a positive linear regression with a strong correlation (R^2=0.987). This indicated that a direct relationship between Fmax 3 (404 nm) and Fmax 1 (464 nm) was very likely.

The microbial cell abundance was enumerated using an Accuri C6 flow cytometer over the course of the incubation experiment by Yufeng Jia. Upon the addition of SDOM, bacterial cell counts sharply increased during T0-3, then sharply decreased during T3-10, and remained stable in later days (Fig. 3.3). The initial sharp intensity of the fluorescence seen in the Fmax 1 (464 nm) and Fmax 3 (404 nm) peaks on T0 is evidently the result of the addition of SDOM. Therefore the heterotrophic microbes utilized DOM represented by those two optical properties, which resulted in the drop of the Fmax values and the increase of cell count during T0-3 (Fig.

3.1). The sustained abundance over the course of the experiment indicated continued renewal of microbial community productivity and the likely case of further transformations of fluorophores.

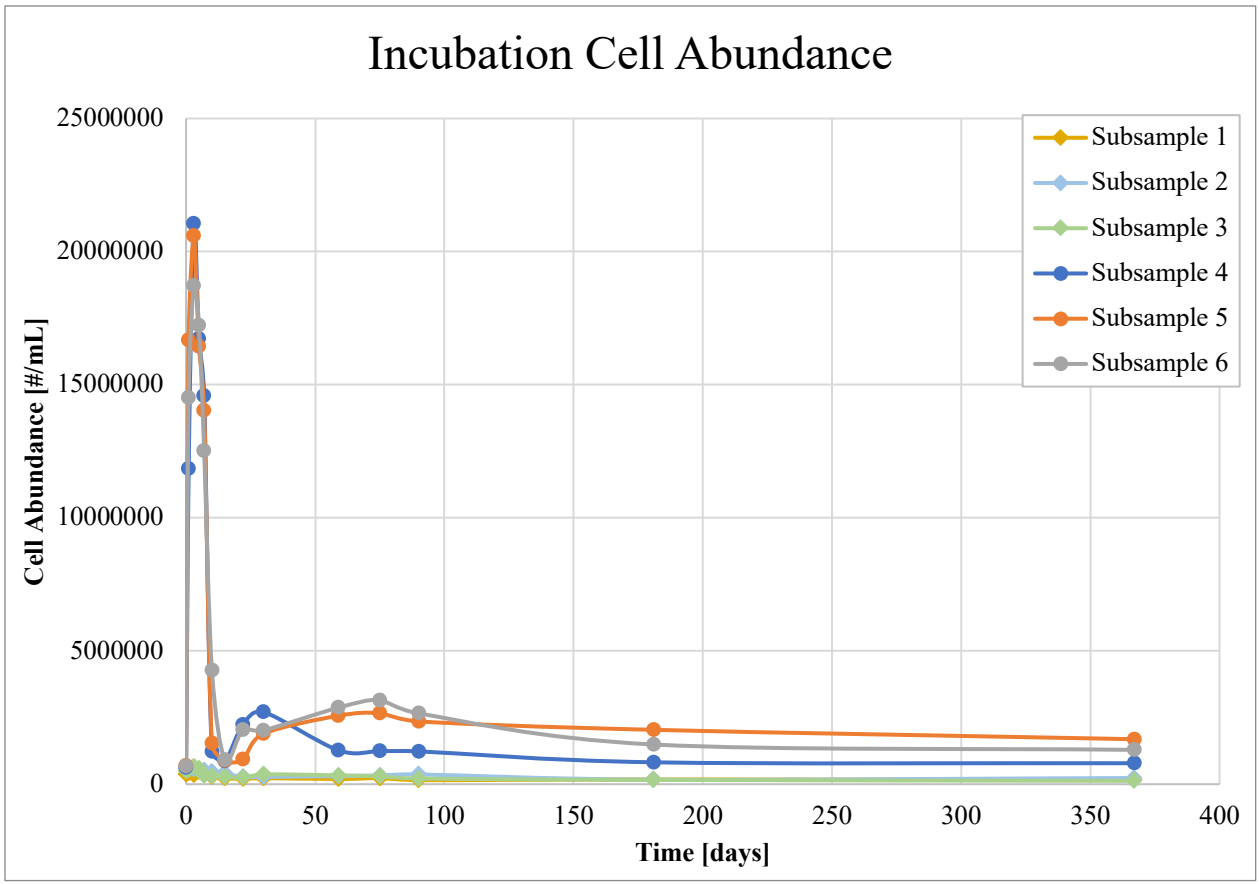

Figure 3.3 Incubation experiment cell abundance measured in each of the samples over time.

In the incubation control subsample group, nitrogen levels incorporating the DON nitrate, nitrite, ammonia, and TDN remained low as expected for the experimental control (Figure. 3.4 A). The average concentration of SDOM treated subsamples were higher over the course of the experiment (Figure. 3.4 B). As materials were utilized at the start of the incubation, the TDN in the control subsamples increased from the 0.11 mg N/L measured on day zero to a maximum of 0.12 mg N/L on day one. In contrast, the SDOM treated subsamples started at a local maximum of 0.72 mg N/L before sharply decreasing to a local minimum of 0.55 mg N/L by day five. The

control subsample group TDN levels remained relatively constant with a standard deviation of 0.01 mg N/L over the course of the experiment. The SDOM treated subsample group increased significantly from a local minimum on day twenty-two to level off over a two-month period with an average of .70 mg N/L and maximum of 0.73 mg N/L on day seventy-five. Day ninety showed the beginning of the gradual decreasing trend from 0.663 mg N/L to a minimum of 0.387 mg N/L on T181 and increased before the end of the experiment at T364.

In the SDOM subsamples, DON was initially high at a maximum of 0.69 mg N/L but decreased sharply shortly after the beginning of the incubation. By day seven, the DON levels reached a local minimum of 0.26 mg N/L before increasing again to 0.37 mg N/L on T30. The increase in DON after T7 occurred due to the crash of bacterial biomass. After which DON once again decreased to a new low of 0.11 mg N/L on day T75. After this period, DON decreased before diminishing on T181 at the six month-mark of the incubation experiment with a slight increase at T364. The control subsamples followed a similar pattern, but a reduced magnitude indicated that the SDOM treatment containing labile organic matter fueled significant microbial productivity.

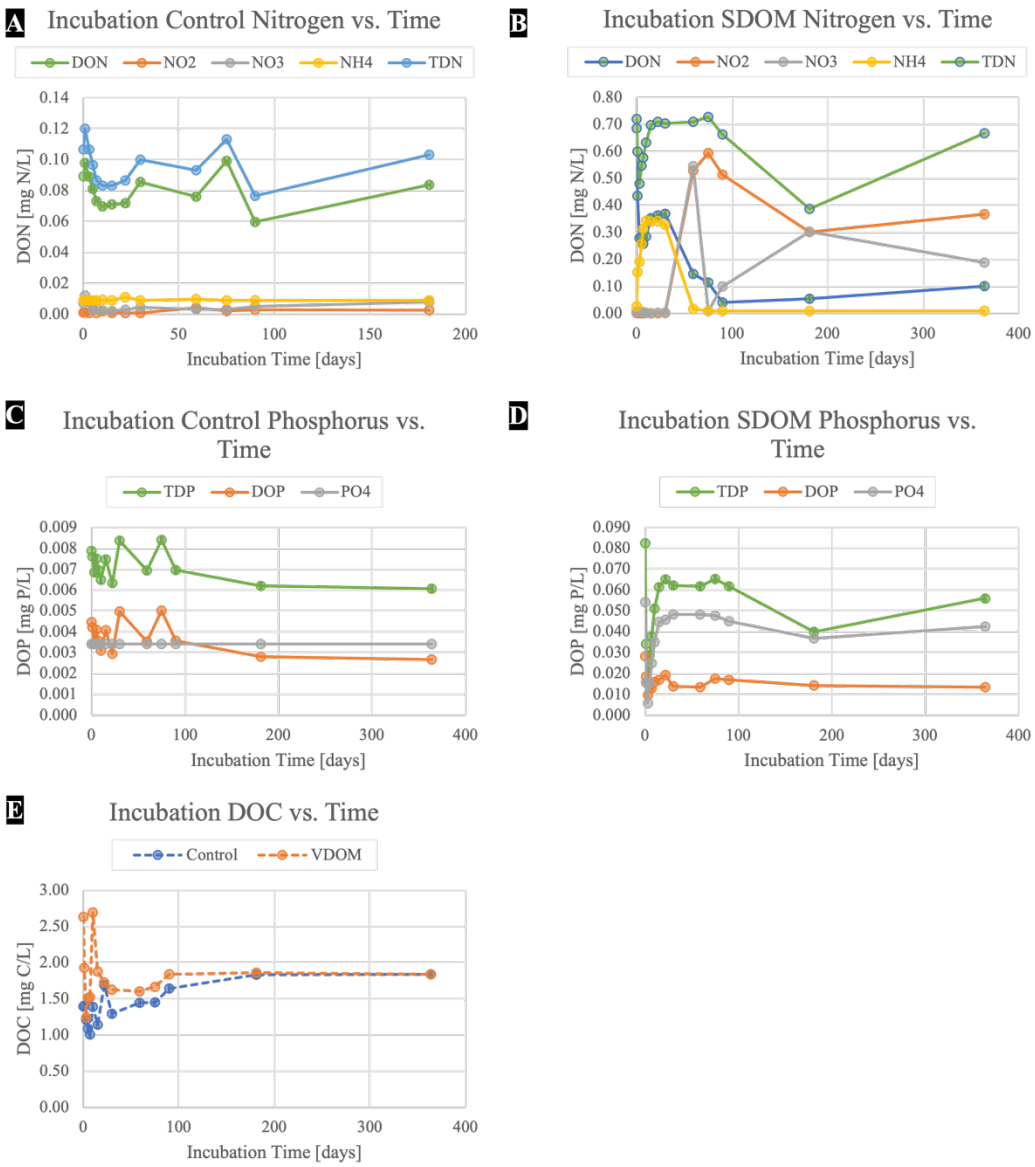

Figure 3.4 A-E: Nutrient profiles of incubation experiment over time. A shows the nitrogen species of the control subsamples (subsamples #1-3) and B shows the nitrogen species of the SDOM subsamples (subsamples #4-6). C shows the phosphorous species of the control subsamples (subsamples #1-3), and D shows the phosphorous species of the SDOM subsamples (subsamples #4-6). E shows the dissolved organic carbon levels over time.

The inorganic nitrogen species continued to show higher average concentrations in the SDOM treated subsamples than the control subsamples, except for both treatment groups showing identical low levels of NH_4 after day seventy-five. The control subsample NH_4 levels maximized at an average of 0.01 mg N/L after the first three weeks and had a standard deviation

of 0.001 mg N/L over the first six months of the experiment. Meanwhile, the SDOM treated subsamples had an initial concentration of 0.03 mg N/L NH_4 and showed an instantaneous increase that maximized at 0.34 mg N/L at the same sampling point as the control group maximum after the first three weeks. After this, the average concentration decreased to 0.02 mg N/L on day fifty-nine and remained at 0.01 mg N/L until the one-year mark when it reached the detection limit. The minimum average NH_4 for the control subsamples was also at the detection limit at the end of the incubation.

Nitrite and nitrate concentrations showed nominal levels at the beginning of the incubation experiment in both the control and SDOM treated subsample groups. This remained until nitrite levels in the SDOM treated subsamples started to increase gradually after day thirty to 0.53 mg N/L on day fifty-nine and peaking at 0.59 mg N/L on day seventy-five. This increment matched the decrease in average NH_4 after day thirty and subsequently illustrated the initial ammonification and accumulation of ammonia and the delayed nitrification of NH_4 to nitrite in the incubation experiments. The nitrite levels began to drop shortly after day ninety and reached a local minimum of 0.30 mg N/L at the six-month mark of the experiment before gradually increasing to 0.37 mg N/L over the remainder of the experiment. This increment can be explained using the nitrate levels which increased when nitrite decreased, indicative of nitrite oxidation. The average SDOM-treated subsample nitrate levels increased to 0.10 mg N/L by day ninety and to 0.3 mg N/L by the six-month mark of the experiment before decreasing to 0.19 mg N/L over the remainder of the experiment. The nitrate levels mirroring the nitrite levels after day ninety can be explained by the oxidation of nitrite into nitrate, as stated above and seen clearly in Figure. 3.4 B, it is not clear whether this oxidation is microbial mediated or of a pure chemical nature.

The phosphorus species monitored over the course of the incubation experiment showed a similar story to the nitrogen species based on the similarity of activity in Figure 3.4 C and D and in the comparison of the control subsample and the SDOM-treated subsample group averages. The control subsample TDP remained below 0.01 mg P/L and the average dissolved organic phosphorous (DOP) was 0.004 mg P/L with a standard deviation lower than 0.001 mg P/L over the course of the experiment. Without the organic phosphorous from detritus, the phosphate levels remained unchanged at an average of 0.003 mg P/L throughout the entire year. The SDOM-treated subsample showed maxima of phosphorous species with an average TDP of 0.082 mg P/L, DOP of 0.028 mg P/L, and PO_4 of 0.054 mg P/L at the beginning of the incubation. The SDOM treatment provided not only fuel in the form of decomposing lysed cells to be remineralized but inorganic phosphorous as well for biological uptake and recycling. All three phosphorus species decreased immediately after the experiment began and all three species reached a minimum by day three with TDP averaging 0.016 mg P/L, DOP averaging 0.010 mg P/L, and PO_4 averaging 0.006 mg P/L indicating that the material was highly labile and fueled microbial productivity. The TDP levels reflected the combination of the DOP and PO_4 averages throughout the experiment until T181 at the six-month mark of the experiment, at which the TDP levels averaged at 0.040 mg P/L instead of the 0.051 mg P/L expected based on the combined DOP and PO_4 averages. DOP increased from the minimum on day three to a local maximum of 0.019 mg P/L after three weeks after which then showed a small convex curve with local minima of 0.014 mg P/L on days thirty and fifty-nine before recovering to 0.018 mg P/L on day seventy-five and gradually decreasing for the remainder of the experiment. At the same time, PO_4 reached 0.046 mg P/L after three weeks and after which then showed a slight concave curve with a local maximum at 0.048 mg P/L before returning to 0.045 mg P/L on day ninety and decreasing to

0.037 mg P/L by the six-month mark. Figure. 3.4 D showed that the DOP and PO_4 levels mirroring each other in the curves shown after day twenty-two. The increase in PO_4 levels in the last six months of the experiment further indicated sustained remineralization and microbial productivity throughout the experiment.

Averaged DOC levels shown in Figure. 3.4 E further supported the dominance of increased microbial productivity and chemical transformations in the SDOM-treated subsamples. DOC levels were consistently higher in the SDOM subsamples than in the control subsamples for the incubation period and showed that the shifting patterns are different. In general, the treatment moved downwards, and the control moved upwards. The SDOM-treated subsamples averaged a DOC maximum of 2.63 mg C/L on day zero and the control subsamples averaged 1.39 mg C/L on day zero. All DOC levels decreased until day five where SDOM-treated average DOC reached a minimum of 1.51 mg C/L and control average reached only a local minimum of 1.09 mg C/L. In the increment from day T3 to T10, control samples reached its averaged maximum at 1.39 mg C/L, but SDOM-treated DOC average reached only a local maximum of 2.70 mg C/L. After T10, control samples dropped at T15 and increased at T22 before decreasing until increases at T90 and T181. After T10, SDOM samples decreased until T90 and T181 similarly to the control. On day thirty, the control DOC reached its minimum of 0.98 mg C/L, but SDOM-treated DOC concentration only reached 1.62 mg C/L while continuing to decrease to a local minimum of 1.60 mg C/L until day fifty-nine. At this point, the control average has accumulated to 1.44 mg C/L which could be interpreted as less-labile, diminished DOC returning from the microbial loop. For the remainder of the experiment, the DOC levels in the control subsamples averaged at only slightly lower range of concentrations than the SDOM-treated subsample as both gradually increased. On T181, at the six-month mark, the SDOM-treated

DOC was at 1.86 mg C/L whereas the control DOC was 1.83 mg C/L. Minimal differences between SDOM and control samples in DOC was observed at the end of the incubation experiment at T364. The overall demonstration of the SDOM treated subsamples in Figure 3.4 showed greater magnitude in comparison to the control subsample group, confirming that the microbial productivity is fueled by the labile SDOM treatments.

The SDOM subsamples compared against DOC showed a difference in fluorescence behavior (Figure. 3.5) across PARAFAC components. The Fmax 1 (464 nm) and 4 signals showed positive correlations, but the Fmax 3 (404 nm) signals showed negative correlations with DOC accumulation. This suggested that Fmax 3 (404 nm) signals were produced when DOM lability was low and was presumably produced from degradation products of other metabolites.

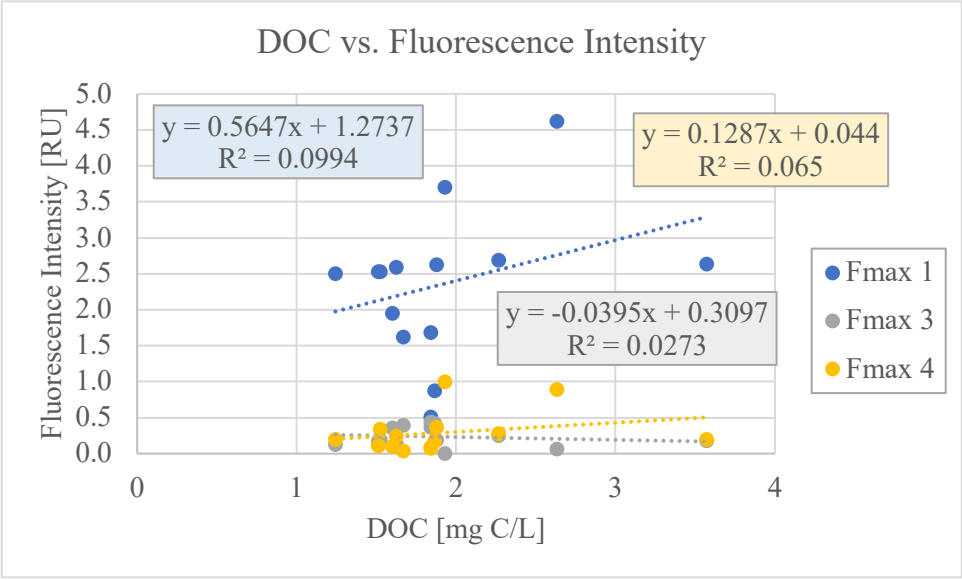

Figure 3.5 SDOM Fmax Values vs. DOC concentrations over incubation experimental period.

Similar trends of correlations between DON and EEM-PARAFAC components were found when compared to the DOC to EEM-PARAFAC correlations (Figure 3.6).

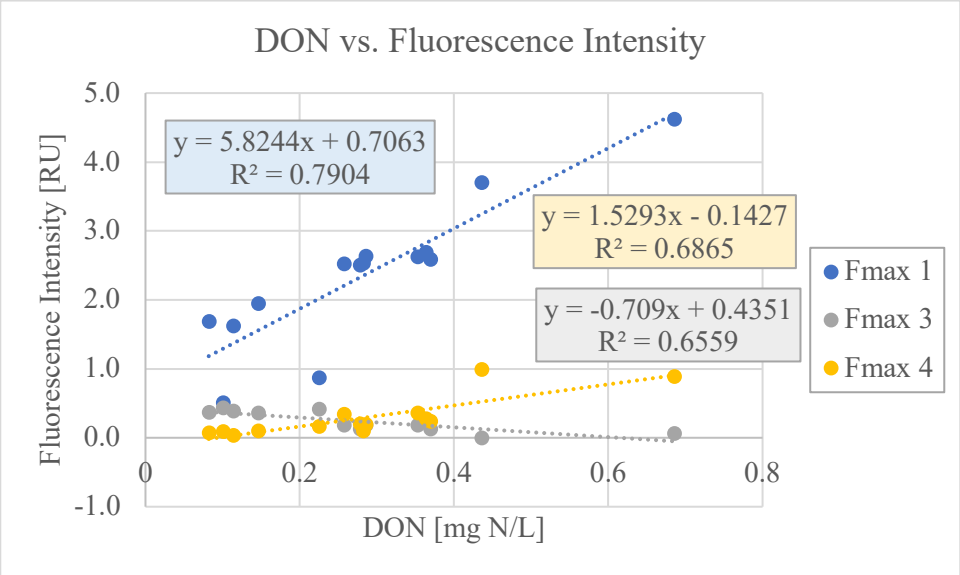

Figure 3.6 SDOM Fmax Values vs. DON concentrations over incubation experimental period.

3.4 Conclusions

This chapter described the refractory nature of *Synechococcus*-derived DOM metabolites in the incubation treatments and observed the overall metabolite degradation process over time in the experiment. In this study, we investigated how microbial community in surface oligotrophic ocean water responded to the addition of *Synechococcus*-derived DOM based on a year-long incubation experiment. In response to the French-press lysed cyanobacterial DOM and observed through FDOM patterns, the bacterial community response varied drastically during the experiment in contrast to much more subtle changes were observed in the control. The optical profiles of samples taken from the incubation experiment showed initial high fluorescence followed by an immediate sharp decrease in intensity seen in the SDOM-treated Fmax values is an indication of the rapid utilization of the organic matter and its high lability despite assumptions made based on previously shown $FDOM_H$ behaviors. The continued increase in

Fmax 3 (404 nm) signal throughout the experiment demonstrated the stability of FDOM characterized by this component confirming the refractory nature of SDOM from lysed *Synechococcus* cells. The lack of initial Fmax 3 (404 nm) signal at the start of the experiment and its accumulation over time implied that heterotrophic activity produces refractory DOM signals from labile FDOM precursors. The ratio of SDOM-treated Fmax 3 (404 nm) over Fmax 1 (464 nm) indicated that a direct relationship between Fmax 3 (404 nm) and Fmax 1 (464 nm) is very likely. In response to the pulse of SDOM, microbial abundance showed strong responses within the first three days of marine microbial abundance which has also been observed in previous studies[85]. This increase in microbial biomass in the first three days corresponded with the sharp decrease of control of DOC, DON, and DOP levels, suggesting that microbes quickly take up nearly all the added cyanobacterial DOM (Figure 3.3 and 3.4 A-E). This result conflicts with the similar previous incubation experiment of coastal microbial community where quick consumption of DOC produced more DON and DOP[85]. Many aspects could factor in the dynamic difference of *S*DOM utilization in our experiment. For instance, nitrate concentration was extremely low (Figure 3.4 B), suggesting that the nitrogen in the incubation system was in unavailable forms. Ammonium concentration trends were associated with the high utilization of labile DOM by microbial metabolisms. In previous study of coastal microbial community incubation, ammonium levels dropped within the first three days and the nitrate and phosphate levels were much higher than in our incubation (ca. 10 mg L^{-1} and 0.15 mg L^{-1})[85]. The averaged concentrations of nutrients for the control sub-samples and SDOM-treated subsamples illustrated in figure 3.4 showed the chemical transformations of DOM rendered by microbial activity over the year-long incubation experiment. Overall, the microbial communities transformed the SDOM and produced FDOM from the initial materials.

Collaborator Yufeng Jia pointed out that any large discrepancies in nutrient concentrations between the two incubation studies are observed because of the environmental conditions of the microbial community collected from different regions. Our seawater was collected in the Gulf Stream which was extremely oligotrophic, and Zhao et al.[85] collected seawater from the Ocean City Inlet, Maryland, which was just off the coast where high nutrients input is expected. It is also unclear how significant nutrient limitation was in shaping microbial community structure under dark conditions. The implications of the findings of this chapter, support the idea that utilizing microbial ecology research is helpful in understanding FDOM research – of which includes the available published optical profiles. Given the diversity and range of datasets we have access, this information could better inform biogeochemists in profound ways in synthesizing marine microbial processing within the overall concept of the marine carbon cycle. The combination of FDOM concentrations, chemical structures, bioenergetics, and microbial diversity will unprecedented and increasingly important opportunities to understand marine carbon cycling in a changing world.

Chapter 4: Exploring the Weak Anion Exchange (WAX) Fraction of marine DOM in the Atlantic and Pacific Oceans using Liquid Chromatography Triple Quadrupole Mass Spectrometry

Abstract

Chapter four is a brief examination of marine DOM using HPLC paired with ESI QqQ MS/MS to detect ion transitions and investigate molecular masses of interest of interest. Solid phase extraction WAX cartridges were used in a sequential extraction, with the water already having passed through a PPL cartridge. Four nominal masses of interest found in the water column profiles at BATS were explored. These masses were not found at HOTS. NM 385 was the lowest and most consistent of the signals of interest observed at BATS but we did not observe any peak at the chlorophyl maximum as observed in the other signals. The behavior of NM 341 suggests it could be an aromatic glycoside, given the long retention time. The significant decreases in peak area seen in NM 341, NM 373, and NM 387 is suggests we can gather valuable information into processes within the marine DOM carbon cycle.

4.1 Introduction

In this chapter, I provide the results of a preliminary study of molecular signatures found in the WAX extracts of marine DOM at BATS and HOTS. The presence of aromatic glycosides has been hypothesized based on previous exploratory mass spectrometry data. The application of ESI LC-QqQ-MS has not often been applied to marine DOM because the immense complexity of DOM makes the selection of useful molecules difficult. Several previous studies have used information on chemical and physical environments, transformations, and degradation processes to assign molecular formulas to DOM extractions[9,88–90] based on direct infusion ultrahigh resolution MS. However, as Hertkorn et al.[49] remarked, DOM is very complex and each elemental formula could represent millions or more constitutional isomers depending on the mass[49]. As noted in the previous chapters, despite the importance of DOM – one of the most dynamic and complex carbon pools on earth, our understanding of it is limited. The sources, characterization, and structural nature of this material within the oceans remains unclear and continues to be a subject of debate across research[1,8,9]. This chapter is based on the analysis of solid phase WAX extracts by LC-ESI QqQ MS. This chapter discussed some preliminary molecular signatures and to describe differences in DOM composition extractable by this unique anion exchange fraction of DOM between the Pacific and Atlantic Ocean basins.

4.1.1 Fragmentation Studies for the Structural Characterization of Marine DOM

The synthesis/isolation of individual compounds from marine DOM is extremely challenging. Common metabolite databases are of limited use because the modifications by autotrophs and heterotrophs alike are uncatalogued. Hence, individual DOM molecules beyond known metabolites remain hidden behind the curtain of complexity, although some attempts have been undertaken[91]. This gives an idea of how unique and complex the DOM molecular composition might be.

4.2 Materials and Methods

This chapter uses the solid phase WAX extracts described in *Chapter 2*, sections 2.2.1 - 2.2.3b. As described previously, water samples were taken for extracting seawater DOM though the WAX cartridges in the first profile at each site, after the sample had already passed the PPL cartridge. Therefore, it is expected that Wax extracts have a very different composition with the majority of DOM removed by the PPL SPE method. This is the first study using this sequential use of the PPL followed by WAX in a high-resolution marine-DOM profile study to recover additional DOM constituents that were not extractable by the PPL resin. All these procedures and techniques used are described in detail in *Chapter* 2, sections 2.2.1 - 2.2.3b.

WAX extracts were analyzed by using an Agilent 1260 Infinity II LC interfaced with an Agilent 6420 QqQ MS. Initially, extracts were run in full ion scan mode to determine consistent high intensity signals. These specific m/z ions were then fragmented and consistent indictive fragments were isolated to see if they could be used for relative quantification of samples. Multiple m/z ions were successfully isolated that should consistent indicative fractions.

HPLC was then used to separate the m/z ions of interests out of the mixture. As chemical components arrive at the MS, precursor ions are mass filtered in the first quadrupole mass

analyzer (Q1), fragmented in the collision cell (q2), and then product ions are detected in the final quadrupole mass analyzer (Q3). Detecting ion transitions, instead of just the precursor ion mass, is typically used to select the chemicals of interest to confirm its structural identity. Without standards to compare our sample response factors and representative transitions to, the nature of this work is exploratory and is based on a relative comparison of very few specific mass to charge ratio (*m/z)* ions, their transitions and retention times without even knowing their exact structure at this stage.

The m/z ions and their specific transitions determined in the BATS WAX extracts are summarized in Table 4.1:

Table 4.1: Nominal mass (NM) fragmentation ions along with the specific ion transitions, average retention time (RT) and retention time standard deviation indicated in the BATS WAX extracts.

NM (+ESI mode)	1. fragment ion	2. fragment ion	Transitions	Avg. RT [min]	RT SD [min]
341	277	227	341 => 277; 341 => 227	8.45	0.11
373	337	210	373 => 337; 373 => 210	2.59	0.34
385	368	349	385 => 368; 385 =>349	9.14	0.12
387	369	337	387 => 369; 387 => 337	8.34	0.11

4.3 Results and Discussion

Four strong, reliable m/z ions were consistently found in the BATS profile (Figure 4.1), based on their specific transitions (see Table 4.1). Interestingly, none of these signatures could be found in the WAX extracts from the HOT samples. This finding alone is intriguing and may point for the first time to fundamental structural differences in DOM between these two major ocean basins. The *m/z* ions of interest in the BATS DOM-WAX-SPE are at nominal mass (NM) 341, 373, 385, and 387. NM 341 maintained the highest peak area, starting at 87,961 (arbitrary

units (au)) at the surface and peaked early at 147,364 at the chlorophyll maximum of 100 m. Below that there is a mirror-like decrease and increase in peak areas before substantially decreasing from 120,281 at 2,200 m to 6,624 at 2,400 m. From 2,800 m to our final depth 4,530 m, the peak area remained consistent with an average of 5,019 and a minimum of 2,690. The substantial sharp decrease in NM 341 peak area around 2,400 m is likely an indication of the transition of interest occurring in the water column at BATS. NM 373 produced the second highest signal in the surface extracts at 14,118 before increasing to a maximum of 32,868 at the chlorophyll maximum. There was a decrease before increasing again to 22,180 at 1,600 m, after which peak area decreased to 1642 by 2,200 m and by 2,400 m no more signal was detected. NM 385 is the lowest and most consistent of the signals of interest observed here. The peak area was 2,770 at the surface and consistently decreased down the water column to 503 at the bottom of 4,530 m, there was no peak or increase at the chlorophyl maximum as observed in the other signals. NM 387 produced the third highest signal in the surface extracts at 8,373 before increasing to a maximum of 20,541 at the chlorophyll maximum. The signal decreased until reaching 11,682 at 2,200 m except for a local maximum of 15,745 at 600 m. After 2,200 m, peak area decreased to 2,844 at 2,400 m and reached a minimum of 342 at 3,400 m. Peak area then slightly increased to 853 at the bottom. More research into the significant decreases in peak area seen in NM 341, NM 373, and NM 387 is needed to help build supporting information for structural analysis and this is the first evidence for specific compounds present in the weak anion exchange fraction of marine DOM. If you wanted to assume that these masses are types of compounds, it could mean that ecologically, they follow observed patterns unlike NM 385.

Research into production, consumption, or transformation processes of these highly specific signals is needed for structural elucidation, but it is beyond the scope of this thesis.

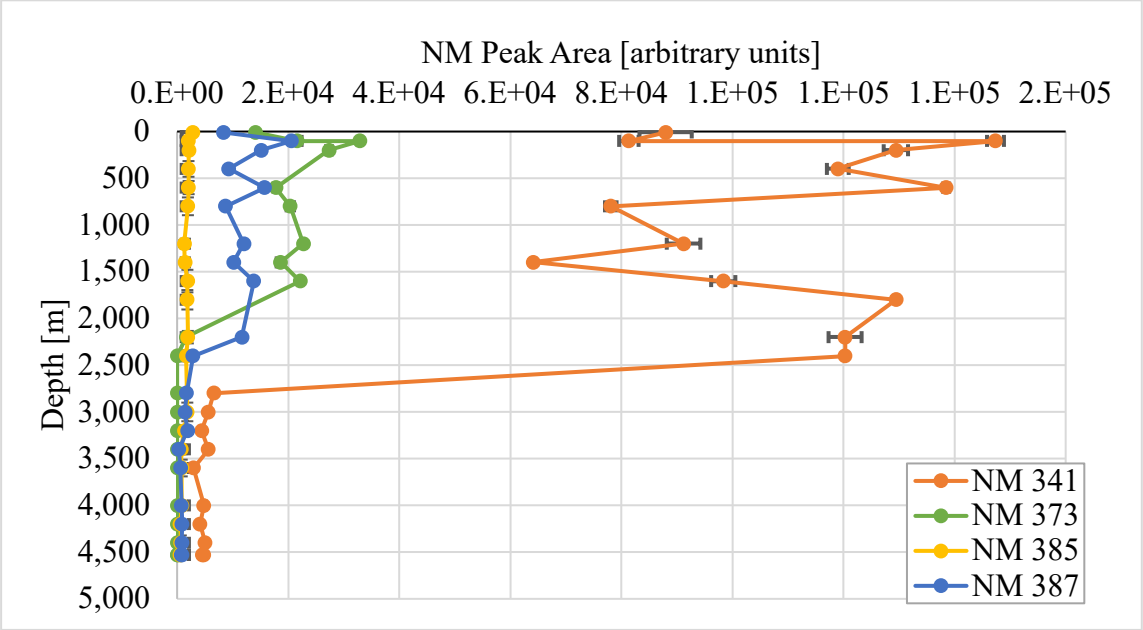

Figure 4.1 Depth profile of Nominal Mass (NM) Peak Area at BATS.

The retention time of NM 341 was at 8.45 minutes, which indicated substantial interaction with the used reversed phase column, which was not expected given that all extracted compounds are isolated by weak anion exchange. However, one explanation could be the supposition that aromatic glycosides might be present in the BATS depth profile, which could interact with the aromatic ring and the stationary phase of the column, but obviously more work is needed to determine structure. The retention time of NM 373 averaged the lowest at 2.59 minutes with the largest standard deviation of 0.34 minutes - about 20.4 seconds. The maximum retention time was 3.51 minutes, and the minimum was 1.64 minutes. This seems to be a compound that does only show very little interaction with the stationary phase and the variable retention time might indicate amphiphilic properties, but this is highly speculative at this point. The retention time of NM 385 was the highest at 9.13 minutes. The retention time of NM 387

was 8.34 minutes. Both, NM 385, and NM 387 once again had substantial interactions with the stationary phase similarly to NM341.

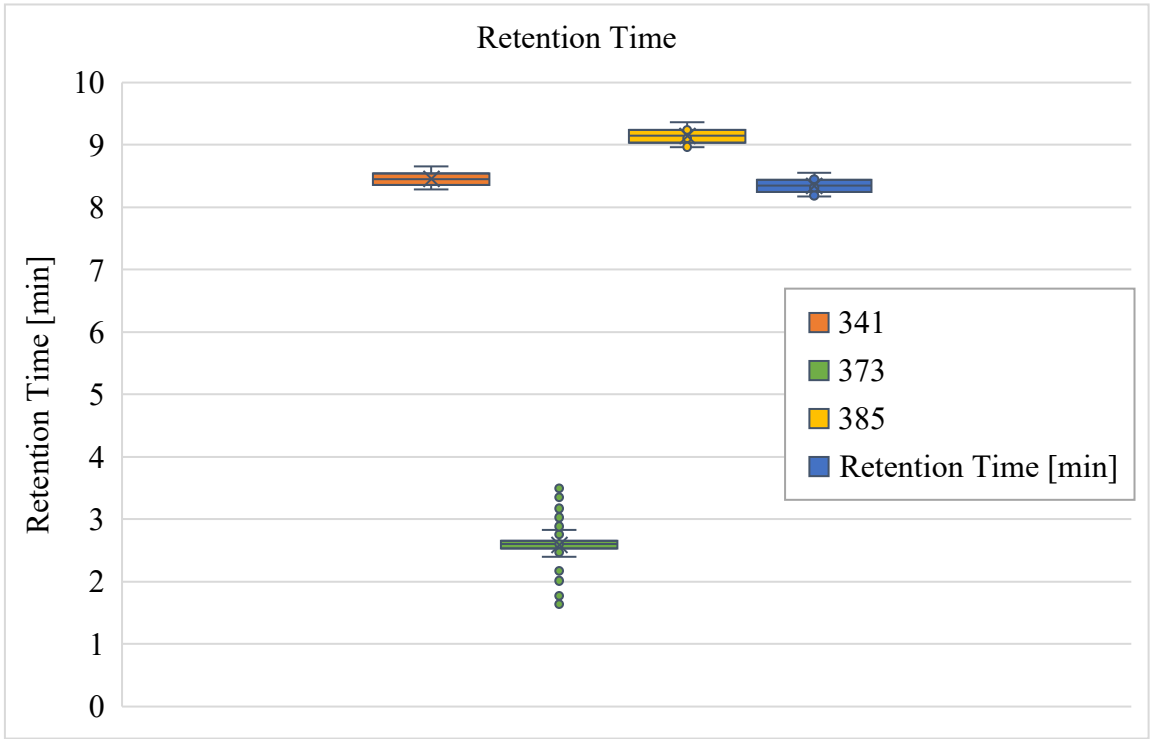

Figure 4.2 Retention times of fragments with distinct transitions observed in Figure 4.1.

This preliminary discussion of the data is intended to highlight the usefulness of DOM-WAX-SPE extracts and potentially expanding the toolbox of DOM molecular level exploration. These results are not based on any previously published study, but a preliminary study found that the Fourier-transform ion cyclotron resonance (FT-ICR-MS) results suggested exact molecular formulas that would fit aromatic glycoside structures. In this exploratory research, there was also a likely sulfonate structure present (NM 373). A sulfonate structure would be logical given the nature of the low pKa found in sulfonates that can be well-extracted with WAX and would not interact much with the stationary phase, but more convincing is the fragment used for relative quantification, which could reflect a sulfonate group. These possible explanations are preliminary and further research is needed to understand the full profile that SPE-DOM has to

offer, confirm the structural nature of WAX-SPE-DOM extracts, and why these results were found at BATS but not HOT. These findings at BATS and not HOT could even potentially be related to the findings in of lower heterotrophic microbial activity based on AOU and measured fluorescence at depths of BATS in Chapter 2 and the impact of substrates found in Chapter 3. Aside from contamination, any potential ecological or biogeochemical significance of these differences would it be interesting that glycoside and sulfonate compounds show up in this extract fraction in BATS and not HOT.

4.4 Conclusions

This chapter aimed to discuss molecular signatures and their specific fragmentations and to describe differences in DOM composition extractable by this unique anion exchange fraction of DOM between the Pacific and Atlantic Ocean basins. Diluted WAX sample extracts were compared by using HPLC paired with ESI-QqQ-MS/MS to detect ion transitions and investigate compounds of interest. The BATS DOM-WAX-SPE extracts produced four strong, consistent signals with transitions of interest at nominal masses 341, 373, 385, and 387, that could not be found at HOT. More research into structural elucidation and the significant decreases in peak area seen in NM 341, NM 373, and NM 387 is needed to help build supporting information for marine DOM dynamics in this unique DOM fraction. NM 385 was the lowest and most consistent of the signals of interest observed here and did not show any peak or increase at the chlorophyl maximum as observed in the other signals. The retention time of NM 373 averaged the lowest at 2.59 minutes with the largest standard deviation of 0.34 minutes was notable since all of the other retention times averaged at around 8.64 minutes with an overall standard deviation of 0.37 minutes.

Chapter 5: Research Summary, Conclusions, and Future Work

This study combined detailed optical properties analysis with DOM characterization using non-targeted mass spectrometric approaches to address the ongoing debate of sources of marine CDOM. Laboratory and mesocosm experiments have provided insight into the production of more stable DOM through microbial degradation. Preliminary results from globally distributed picocyanobacteria such as *Synechococcus* and *Prochlorococcus* have recently revealed that virus-induced cell lysis released CDOM that closely matched the "humic-like" appearance of marine CDOM[16]. In this thesis, I build on this work by investigating how picocyanobacteria-derived DOM is degraded, what role heterotrophic microbial communities play, and if we can further support the previously proposed concept of the microbial carbon pump based on a ubiquitously supplied but well constrained source of DOM.

Chapter 2 examined the differences in the Atlantic and Pacific depth profiles. The optical absorption was consistently higher at BATS than at HOT other than at 600 m (Figure 2.3 A). Trends of $S_{275–295}$ and SR values showed increases at HOT, further supporting the evidence that the MW of compounds were overall lower in the deep Pacific (Figure 2.3 B & D). The increasing absorption ratio E2/E3 at HOT also supported the idea that the CDOM was processed to smaller MW in the Pacific (Figure 2.3 E). PARAFAC modeled EEM fluorescence showed evidence of consistent $FDOM_H$ and $FDOM_P$ throughout the water column. The fluorescence values were higher in the Pacific than in the Atlantic (Figure 2.4 B & C) despite the higher absorbance in the Atlantic. At HOT, the relationships between Fmax 1 (446 nm): Fmax 2 (322 nm) and Fmax 2 (322 nm): Fmax 4 (453 nm) fall apart at lower depths indicating that the common component was likely subjected to remineralization (Figure 2.7 B & F). A ubiquitous strong correlation was found between all of the Fmax 4 (453nm) samples at BATS and HOT and

AOU at depths below 1,000m (Figure 2.10 H). $FDOM_H$ component comparisons showed high resolution profiles with higher linear regression slope at HOT than BATS, which could be explained by a higher FDOM production at HOT due to increased remineralization because of the dense, oxygen-rich bottom waters in the Pacific[33]. The $FDOM_P$ Fmax 3 (264 nm) showed only a weak overall negative correlation with AOU in the BATS and HOT profiles, but this seemed only to be present at shallower depth (<1,000 m) (Figure. 10 E). These findings support the idea that deep Pacific DOM is concurrently more accessible to the active carbon cycle and biological processes. This could mean that the Pacific supports more active or functionally efficient microbial populations which is supported by the higher Pacific AOU seen in Figure 2.9 and is depleted in a steady state equilibrium to a lower concentration. This supports the previous stipulation that the observed average DOC concentration difference in the subtropics and tropics (30° N to 30° S) between the Pacific and the Atlantic is only 2 μm (∼5%), based on the global DOC data set[8,92], and could be easily explained by differences in the DOM pool and its reactivity. Findings from the water column profiles, UV-Vis absorbance, PARAFAC model fluorescence values, AQY, and AOU analyses supported the idea that DOM in the Atlantic and Pacific oceanic basins are composed of fundamentally different molecules and hence reactivity and this is another piece of the puzzle to explain observed differences in bulk DOC.

Chapter 3 analyzes an alternative marine CDOM source that is derived from viral-lysed picocyanobacteria. The chromophores released from *Synechococcus*- lysed material might explain the “humic-like” signatures observed in open ocean environments, because of the global distribution of picocyanobacteria. Evidence of an effective transport from small picocyanobacteria to the deep ocean has been previously shown[83] and the optical analysis of $FDOM_H$ originating from picocyanobacteria has the potential to in part explain deep-sea CDOM.

The results give detailed information about the persistence of the UV protection properties and a more detailed molecular understanding of lysed and transformed SDOM. This chapter described the refractory nature of SDOM metabolites in the incubation treatments and observed the overall metabolite degradation process over time in the experiment. A humic-like PARAFAC component (Fmax 3) was initially absent but accumulated throughout the SDOM incubations. Decreases in PARAFAC components present at the beginning of incubations (Fmax 1 and 4) and the close inverse association between the accumulating component and the declining components suggest labile Synechococcus lysates are quickly transformed by heterotrophs into biologically refractory DOM. Refractory $FDOM_H$ may thus originate as cyanobacteria-derived DOM. Upon addition of SDOM on day 0, an increase in microbial biomass in the first three days corresponded with the sharp decrease of control of DOC, DON, and DOP levels, suggesting that microbes quickly take up nearly all the added cyanobacterial DOM (Figure 3.3 and 3.4 A-E). This result conflicts with the similar previous incubation experiment of coastal microbial community where quick consumption of DOC produced more DON and DOP[85]. Many aspects could factor in the dynamic difference of *S*DOM utilization in our experiment. For instance, nitrate concentration was extremely low (Figure 3.4 B), suggesting that the incubation system was in unavailable forms. Ammonium concentration greatly increased in the first ten days (Figure 3.4 B), which was associated with the high utilization of labile DOM by microbial metabolisms. Overall, the microbial communities transformed the SDOM and transformed FDOM from the initial materials. The diversity and range of datasets we have access to provide unprecedented opportunities to help determine the importance of these differences going forward in research on marine carbon cycling.

Chapter 4 investigates the addition of SPE-WAX to DOM-SPE techniques has the potential to discover additional fluorescent compounds that are viable to the unexplained but observed optical properties of marine DOM. The key to identifying independent molecular signatures and their specific fragmentations could be found in DOM composition extractions using the unique anion exchange fraction. Diluted WAX sample extracts of DOM from the Pacific and Atlantic Ocean basins were compared by using HPLC paired with ESI-QqQ-MS/MS to detect ion transitions and investigate compounds of interest. The BATS DOM-WAX-SPE extracts produced four strong, consistent signals with transitions of interest at nominal masses 341, 373, 385, and 387, that could not be found at HOT. More research into structural elucidation and the significant decreases in peak area seen in NM 341, NM 373, and NM 387 is needed to help build supporting information marine DOM dynamics in this unique DOM fraction. NM 385 was the lowest and most consistent of the signals of interest observed here and did not observe any peak or increase at the chlorophyl maximum as observed in the other signals. These findings have the potential to fundamentally advance our understanding of a presumably important marine CDOM source as well as addressing key issues in studying forms of marine organic carbon.

The analysis of optical properties of marine and picocyanobacteria-derived dissolved organic matter in the Atlantic, Pacific and during long-term incubation experiments continue to shine light on the large uncertainties in FDOM sources, structure, and sinks. The overall appearance of homogeneity of deep ocean DOM, when looked through the lenses of ultrahigh resolution mass spectrometry (MS) would suggest a convergence to a rather common pool of organic compounds and argue against fundamental differences in composition and reactivity. However, a recent study points to a more structurally diverse DOM composition in different

water masses[93]. Direct evidence is lacking in the process of integrating the chemical properties of DOM with microbial structure and activity. We also are still in the dark as to whether what we consider to be RDOM is derived directly from bacterially synthesized exudates fueling the microbial carbon pump or bacterially modified metabolites from autotrophs. Both mechanisms are likely, but the contribution of each pathway at any given location will determine the fate and degradation kinetics of the DOM. An understanding of the fate and transport of the light absorbing CDOM and hence the associated UV protection of marine life is important because even small changes can have profound effects. In particular, the ecological importance of picocyanobacteria has been widely acknowledged[83–85,87], but the extensive release of light absorbing chromophores from lysed cells into its surrounding water has not been adequately evaluated and may play an important role in microbial processes in the surface and deep ocean.

As with all analytical tools, trying to describe the overall composition, broad overlap of signals will likely dampen and mask small to moderate molecular changes, and hence, close attention needs to be paid to small but consistent differences observed using high resolution analytical techniques that describe the "fingerprint" of DOM. To further complicate the DOM fingerprinting, only a fraction of DOM is visible through this analytical window, and the "dark" DOM may be equally important to that what we currently observe, whether it is biased by extraction techniques (NMR and MS) or simply by ionization efficiency (MS) or broad overlap of incredibly structurally complex DOM (NMR, fluorescence, and UV−vis spectroscopy).

New Perspectives on the Marine Carbon Cycle – The Marine Dissolved Organic Matter Reactivity Continuum[8] highlights how our current understanding of the marine carbon cycle does not encompass robust ocean DOC inventories or accurate radiocarbon aging of DOC. This

perspective paper written by our team of Gonsior et al.[8] has sought to provide abundant evidence as to why we should question the assumption that all deep ocean DOM is thousands of years old and biologically inert. To overcome the large overall uncertainties in C sources and sinks, we suggest the identification of new and unique biomarkers to be used as model compounds not only to constrain the overall turnover of marine DOM and to define the DOM reactivity continuum but also to evaluate photochemical and microbial degradation pathways and processes both now and in the future. The proposed marine DOM reactivity continuum concept is much broader than the previously described and includes the degradation of molecules of comparable size but which degrade on drastically different time scales. Currently, the kinetic data to establish and validate such a marine DOM reactivity continuum model are still lacking, and their resolution depends on the discovery of new organic tracers that span large differences in reactivity and microbial degradation rates. Rather than compartmentalize DOM solely into vaguely defined reactivity brackets such as labile, semi-labile, or refractory DOM, we argue that it is time to apply the DOM reactivity continuum concept to the marine carbon pool and to begin to establish the slope of the marine DOM reactivity continuum defined by presumably multiple decay coefficients. In regard to this thesis, Chapter 2 demonstrates that the composition of DOM varies and that processes linking DOM composition to the marine carbon cycle processes might vary between basins - in other words, it is an example of the kind of problem this perspective article is trying to build from. Chapter 3 lays groundwork for future work in understanding transformations and the reactivity continuum modeling of specific picocyanobacteria lysates by identifying which fluorescence features go away and which form during incubation, so these can be the targets of future research. Chapter 4 shows the potential for novel MS work targeting specific masses which may be tied to functionally relevant compounds. To fundamentally

understand the marine DOM reactivity continuum, we must identify and quantify exact organic compounds from a range of potential sources and test their bio and photoreactivity across short (hours to days), medium (days to months), and long (decades) degradation time scales. Understanding these interplays and connecting them more inclusively with DOM composition research is likely the key to understanding the dynamics of marine DOM turnover and the effectiveness of marine carbon sequestration. Our perspective demonstrates reasonable doubts in the stability of the three pillars upholding our current framework of marine carbon cycling. This review and perspective is not meant to provoke controversy but to catalyze a collaborative effort to re-evaluate our current understanding of the marine carbon cycle and the marine DOM reactivity continuum. This pursuit is also an opportunity to reimagine the conceptualization of the marine carbon dynamics in a logically accessible way. We may need to refocus our efforts in deciphering the structure and reactivity of marine organic molecules in a kinetic context, including the microbial and physicochemical constraints on molecular reactivity that are present in the deep ocean. Resolving the kinetics of the proposed marine DOM reactivity continuum requires an interdisciplinary approach. By working together and across research disciplines, we can better constrain the turnover time of marine DOM and thus gain invaluable knowledge of global marine carbon cycling and oceanic carbon storage capacity as our planet continues to change. Collaborative studies will continue to advance our knowledge about the production, vertical transport, and dissolution of organic matter and is critical in quantifying anthropogenic alterations to the global carbon cycle. As mentioned in the introduction, increasing sea surface-based temperature projections are predicted to increase photosynthetic cyanobacterial cell numbers by 14% for Synechococcus[20]. These forecasted increases at the base of the oceanic food web suggest complex and interdependent changes in ocean ecosystems and increases in the

biological and microbial carbon pumps that will have significant implications for global biogeochemical cycles.

Afterword

Marine science is an incredibly inaccessible field and largely excludes women, racial minorities, non-binary, gender non-conforming, queer, and disabled people. Historical and institutional barriers—particularly racial bias and discrimination—play a role in the widening inclusivity gaps in marine sciences and determine who has access to opportunities in these fields. This means to get opportunities, these students have to work harder for access than their white, heterosexual, cis-gendered, able-bodied, and male peers. Students are expected to advocate for themselves throughout career advancement and navigate workplace challenges as systems in place continue to perpetuate barriers that may negatively impact productivity, innovation, and entrepreneurship. The weight and consequences of any conversation about equity and inclusion cannot be left to those already struggling for access, particularly because of the extra emotional labor already undertaken just to keep up with their peers.

Challenging traditional perceptions of identity in the marine science community is an important step in removing barriers for students and scientists with diverse physical, sensory, and cognitive abilities. The accessibility accommodations in place for most marine science opportunities are designed by abled scientists with little input or direction from the disabled community. This hinders disabled scientists from entering into the myriad fields that make up the discipline. “Academia and research are inherently designed for neurotypical, able-bodied people, everything from academia to labs to the field to conference[s] have been designed with abled people in mind. Workspaces are rarely ADA (Americans with Disabilities Act) compliant. How can we expect disabled people to succeed in this field when they can’t even get into the room?” Reilly Boyt, Marine Biologist with University of California San Diego and founder of Disabilities within Ocean Sciences (DWOS)[94].

In an ACS Chemical and Engineering News article, Daniel Lundberg, a Deaf chemistry professor at Gallaudet University, estimates that about 80% of chemistry terms have no established sign[95]. When a science teacher at the Florida School for the Deaf told hearing students and mentors at Harvard about the lack of signs for scientific terms in ASL, they were shocked. “They didn’t realize how many hurdles I had to be jumping over to understand the lecture”, Mandy Houghton says[95]. This isn’t new for Deaf scientists. A lack of signs for scientific terms significantly impedes deaf people’s entry into the sciences, as well as isolates deaf scientists from their hearing peers. This impedes collaborations between deaf and hearing scientists, including brainstorming new techniques, and helping colleagues troubleshoot problems. These limitations also affect a deaf scientist’s ability to have meaningful experiences at scientific conferences. “If you don’t see people that look like you, speak like you, live like you working and doing those things, you will assume it’s impossible,” Houghton says[95]. Fieldwork can also present challenges such as the harassment of underrepresented researchers, including, for example, marine science has recently begun to address the harassment of female scientists on research vessels and in other field settings[96]. A space that is limited to a narrow set of perspectives, experiences, and expertise due to the lack of inclusion in marine science profession and an associated academic space is likely to miss opportunities to illuminate critical questions, leading to poorly informed decisions and policymaking.

These barriers disproportionately affect entry of early career scientists such as myself and limits the success of marine conservation professionals from overburdened individuals.11% of undergraduate students and 7% of graduate students with a documented disability are pursuing STEM majors in the United States[97]. Together, there are ~75% fewer individuals with disabilities represented in the STEM workforce than in the general population[98]. Only 4.8% of

students entering the STEM workforce self-disclose a disability[99], and this number includes me. When physical requirements list: "Hearing requirements include the ability to hear and respond to instructions, communicate effectively in loud areas (pier/dock, warehouse)," I genuinely don't know if that includes me as a person that's considered "hard of hearing" to some and deaf to others. The job posting was for a lab work position with some fieldwork assistance which I have done without issues for the past three years here at the Chesapeake Biological Laboratory, or on research expeditions aboard R/V Atlantic Explorer and R/V Kilo Moana. During a job interview, I once explained that the extra effort it takes to include me as an employee also helps ensure that everyone understands their tasks/roles and the directions in preparation for jobs. My inclusion increases teamwork. If we are to begin addressing barriers to accessibility and inclusion within marine sciences, we should recognize that these efforts help the abled as well—hand signals on boats can be a useful resource when even those with good hearing can't hear over wind or machinery. Efforts intended for inclusivity can become more intentional efforts towards maximum safety when necessary.

It also allows for continued inclusion for those who were able-bodied until an accident (on the job or off the job) or medical event produced a barrier to their participation. I'm not just pointing to the "decades of experience" oceanographers who would fail a hearing or vision test – there are numerous examples of careers in which people are at risk of disability from injury or overuse and would benefit from better attempts at inclusivity in or outside the workplace. The majority of jobs aboard research vessels for marine science research are classified as a "safety concerned" position in some manner because there are so many physical risks that can impact an employee's ability to continue to work. Inclusion helps everyone.

Disabled people are time and time again being left out of these conversations, and everyone is falling further behind because of it. “Addressing the most compelling challenges of the twenty-first century and facilitating new avenues of discovery and innovation will require nurturing the careers of people from historically marginalized groups and recognizing their perspectives in ways that have not previously been fully appreciated and integrated” [100]. Wanda Diaz Merced Ph.D., a blind astronomer, argues that sonification could help astronomers to avoid methodological biases that come with only interpreting data visually[101]. After losing her sight in her twenties, Dr. Diaz Merced pioneered a technique called sonification which converts aspects of data, such as the brightness or frequency of electromagnetic radiation, into audible elements including pitch, volume, and rhythm[101]. This innovation could facilitate discoveries that conventional techniques would miss[101]. Amy Bower, Ph.D., of Woods Hole Oceanographic Institution is another blind scientist that is using data sonification to convey complex quantitative ocean science information, such as charts and graphs about ocean phenomena, that is challenging to express non-visually[102]. Bower and an interdisciplinary team of scientists and sound experts are working to design auditory displays of ocean data about phenomena such ocean-atmosphere exchange and underwater volcanic eruptions[102]. The innovative work that scientists such as Diaz Merced and Bower are doing is beneficial to everyone – our increasingly important science requires us to use untapped resources.

Being inclusive would be beneficial to the marine sciences, both for addressing ongoing workforce shortages in an increasingly urgent climate crisis and promoting innovations through diverse scientific perspectives. Furthermore, the lack of diversity deprives marine sciences and conservation efforts from serving the interests of the general public in an effective enough manner by limiting the improvements to human, social, and economic wellbeing. Specifically, a

future wherein the field standardizes and places value on not just who is doing conservation work, but the kind of work, the locations, and its inhabitants, and how the work is done and whom the results are shared with benefits everyone.

References

(1) Moran, M. A.; Kujawinski, E. B.; Stubbins, A.; Fatland, R.; Aluwihare, L. I.; Buchan, A.; Crump, B. C.; Dorrestein, P. C.; Dyhrman, S. T.; Hess, N. J.; Howe, B.; Longnecker, K.; Medeiros, P. M.; Niggemann, J.; Obernosterer, I.; Repeta, D. J.; Waldbauer, J. R. Deciphering Ocean Carbon in a Changing World. *Proc. Natl. Acad. Sci.* **2016**, *113* (12), 3143–3151. https://doi.org/10.1073/pnas.1514645113.

(2) Derrien, M.; Yang, L.; Hur, J. Lipid Biomarkers and Spectroscopic Indices for Identifying Organic Matter Sources in Aquatic Environments: A Review. *Water Res.* **2017**, *112*, 58–71. https://doi.org/10.1016/j.watres.2017.01.023.

(3) Jiao, N.; Robinson, C.; Azam, F.; Thomas, H.; Baltar, F.; Dang, H.; Hardman-Mountford, N. J.; Johnson, M.; Kirchman, D. L.; Koch, B. P.; Legendre, L.; Li, C.; Liu, J.; Luo, T.; Luo, Y.-W.; Mitra, A.; Romanou, A.; Tang, K.; Wang, X.; Zhang, C.; Zhang, R. Mechanisms of Microbial Carbon Sequestration in the Ocean – Future Research Directions. *Biogeosciences* **2014**, *11* (19), 5285–5306. https://doi.org/10.5194/bg-11-5285-2014.

(4) Herndl, G. J.; Reinthaler, T. Microbial Control of the Dark End of the Biological Pump. *Nat. Geosci.* **2013**, *6* (9), 718–724. https://doi.org/10.1038/ngeo1921.

(5) Hansell, D.; Carlson, C.; Repeta, D.; Schlitzer, R. Dissolved Organic Matter in the Ocean: A Controversy Stimulates New Insights. *Oceanography* **2009**, *22* (4), 202–211. https://doi.org/10.5670/oceanog.2009.109.

(6) Arrieta, J. M.; Mayol, E.; Hansman, R. L.; Herndl, G. J.; Dittmar, T.; Duarte, C. M. Dilution Limits Dissolved Organic Carbon Utilization in the Deep Ocean. *Science* **2015**, *348* (6232), 331–333. https://doi.org/10.1126/science.1258955.

(7) Hansen, A. M.; Kraus, T. E. C.; Pellerin, B. A.; Fleck, J. A.; Downing, B. D.; Bergamaschi, B. A. Optical Properties of Dissolved Organic Matter (DOM): Effects of Biological and Photolytic Degradation. *Limnol. Oceanogr.* **2016**, *61* (3), 1015–1032. https://doi.org/10.1002/lno.10270.

(8) Gonsior, M.; Powers, L.; Lahm, M.; McCallister, S. L. New Perspectives on the Marine Carbon Cycle–The Marine Dissolved Organic Matter Reactivity Continuum. *Environ. Sci. Technol.* **2022**, *56* (9), 5371–5380. https://doi.org/10.1021/acs.est.1c08871.

(9) Zark, M.; Dittmar, T. Universal Molecular Structures in Natural Dissolved Organic Matter. *Nat. Commun.* **2018**, *9* (1), 3178. https://doi.org/10.1038/s41467-018-05665-9.

(10) Pachiadaki, M. G.; Sintes, E.; Bergauer, K.; Brown, J. M.; Record, N. R.; Swan, B. K.; Mathyer, M. E.; Hallam, S. J.; Lopez-Garcia, P.; Takaki, Y.; Nunoura, T.; Woyke, T.; Herndl, G. J.; Stepanauskas, R. Major Role of Nitrite-Oxidizing Bacteria in Dark Ocean Carbon Fixation. *Science* **2017**, *358* (6366), 1046–1051. https://doi.org/10.1126/science.aan8260.

(11) Reinthaler, T.; van Aken, H. M.; Herndl, G. J. Major Contribution of Autotrophy to Microbial Carbon Cycling in the Deep North Atlantic's Interior. *Deep Sea Res. Part II Top. Stud. Oceanogr.* **2010**, *57* (16), 1572–1580. https://doi.org/10.1016/j.dsr2.2010.02.023.

(12) Ferreira, A. J. S.; Siam, R.; Setubal, J. C.; Moustafa, A.; Sayed, A.; Chambergo, F. S.; Dawe, A. S.; Ghazy, M. A.; Sharaf, H.; Ouf, A.; Alam, I.; Abdel-Haleem, A. M.; Lehvaslaiho, H.; Ramadan, E.; Antunes, A.; Stingl, U.; Archer, J. A. C.; Jankovic, B. R.; Sogin, M.; Bajic, V. B.; El-Dorry, H. Core Microbial Functional Activities in Ocean

Environments Revealed by Global Metagenomic Profiling Analyses. *PLoS ONE* **2014**, *9* (6), e97338. https://doi.org/10.1371/journal.pone.0097338.
(13) González-Benítez, N.; García-Corral, L. S.; Morán, X. A. G.; Middelburg, J. J.; Pizay, M. D.; Gattuso, J.-P. Drivers of Microbial Carbon Fluxes Variability in Two Oligotrophic Mediterranean Coastal Systems. *Sci. Rep.* **2019**, *9* (1), 17669. https://doi.org/10.1038/s41598-019-53650-z.
(14) D'Andrilli, J.; Junker, J. R.; Smith, H. J.; Scholl, E. A.; Foreman, C. M. DOM Composition Alters Ecosystem Function during Microbial Processing of Isolated Sources. *Biogeochemistry* **2019**, *142* (2), 281–298. https://doi.org/10.1007/s10533-018-00534-5.
(15) Jiao, N.; Herndl, G. J.; Hansell, D. A.; Benner, R.; Kattner, G.; Wilhelm, S. W.; Kirchman, D. L.; Weinbauer, M. G.; Luo, T.; Chen, F.; Azam, F. Microbial Production of Recalcitrant Dissolved Organic Matter: Long-Term Carbon Storage in the Global Ocean. *Nat. Rev. Microbiol.* **2010**, *8* (8), 593–599. https://doi.org/10.1038/nrmicro2386.
(16) Zhao, Z.; Gonsior, M.; Luek, J.; Timko, S.; Ianiri, H.; Hertkorn, N.; Schmitt-Kopplin, P.; Fang, X.; Zeng, Q.; Jiao, N.; Chen, F. Picocyanobacteria and Deep-Ocean Fluorescent Dissolved Organic Matter Share Similar Optical Properties. *Nat. Commun.* **2017**, *8* (1), 15284. https://doi.org/10.1038/ncomms15284.
(17) Chen, Q.; Chen, F.; Gonsior, M.; Li, Y.; Wang, Y.; He, C.; Cai, R.; Xu, J.; Wang, Y.; Xu, D.; Sun, J.; Zhang, T.; Shi, Q.; Jiao, N.; Zheng, Q. Correspondence between DOM Molecules and Microbial Community in a Subtropical Coastal Estuary on a Spatiotemporal Scale. *Environ. Int.* **2021**, *154*, 106558. https://doi.org/10.1016/j.envint.2021.106558.
(18) Wienhausen, G.; Noriega-Ortega, B. E.; Niggemann, J.; Dittmar, T.; Simon, M. The Exometabolome of Two Model Strains of the Roseobacter Group: A Marketplace of Microbial Metabolites. *Front. Microbiol.* **2017**, *8*, 1985. https://doi.org/10.3389/fmicb.2017.01985.
(19) Noriega-Ortega, B. E.; Wienhausen, G.; Mentges, A.; Dittmar, T.; Simon, M.; Niggemann, J. Does the Chemodiversity of Bacterial Exometabolomes Sustain the Chemodiversity of Marine Dissolved Organic Matter? *Front. Microbiol.* **2019**, *10*, 215. https://doi.org/10.3389/fmicb.2019.00215.
(20) Flombaum, P.; Gallegos, J. L.; Gordillo, R. A.; Rincon, J.; Zabala, L. L.; Jiao, N.; Karl, D. M.; Li, W. K. W.; Lomas, M. W.; Veneziano, D.; Vera, C. S.; Vrugt, J. A.; Martiny, A. C. Present and Future Global Distributions of the Marine Cyanobacteria Prochlorococcus and Synechococcus. *Proc. Natl. Acad. Sci.* **2013**, *110* (24), 9824–9829. https://doi.org/10.1073/pnas.1307701110.
(21) Coble, P. G. Marine Optical Biogeochemistry: The Chemistry of Ocean Color. *Chem. Rev.* **2007**, *107* (2), 402–418. https://doi.org/10.1021/cr050350+.
(22) Nelson, N. B.; Siegel, D. A. The Global Distribution and Dynamics of Chromophoric Dissolved Organic Matter. *Annu. Rev. Mar. Sci.* **2013**, *5* (1), 447–476. https://doi.org/10.1146/annurev-marine-120710-100751.
(23) Laane, R. W. P. M.; Kramer, K. J. M. Natural Fluorescence in the North Sea and Its Major Estuaries. *Neth. J. Sea Res.* **1990**, *26* (1), 1–9. https://doi.org/10.1016/0077-7579(90)90052-I.
(24) Miller, W. L.; Zepp, R. G. Photochemical Production of Dissolved Inorganic Carbon from Terrestrial Organic Matter: Significance to the Oceanic Organic Carbon Cycle. *Geophys. Res. Lett.* **1995**, *22* (4), 417–420. https://doi.org/10.1029/94GL03344.

(25) Gao, H.; Zepp, R. G. Factors Influencing Photoreactions of Dissolved Organic Matter in a Coastal River of the Southeastern United States. *Environ. Sci. Technol.* **1998**, *32* (19), 2940–2946. https://doi.org/10.1021/es9803660.
(26) Kieber, D. J.; McDaniel, J.; Mopper, K. Photochemical Source of Biological Substrates in Sea Water: Implications for Carbon Cycling. *Nature* **1989**, *341* (6243), 637–639. https://doi.org/10.1038/341637a0.
(27) Vione, D.; Minella, M.; Maurino, V.; Minero, C. Indirect Photochemistry in Sunlit Surface Waters: Photoinduced Production of Reactive Transient Species. *Chem. - Eur. J.* **2014**, *20* (34), 10590–10606. https://doi.org/10.1002/chem.201400413.
(28) *Aquatic Humic Substances: Influence on Fate and Treatment of Pollutants*; Suffet, I. H., MacCarthy, P., Eds.; Advances in Chemistry; American Chemical Society: Washington, DC, 1988; Vol. 219. https://doi.org/10.1021/ba-1988-0219.
(29) Gonsior, M.; Hertkorn, N.; Conte, M. H.; Cooper, W. J.; Bastviken, D.; Druffel, E.; Schmitt-Kopplin, P. Photochemical Production of Polyols Arising from Significant Photo-Transformation of Dissolved Organic Matter in the Oligotrophic Surface Ocean. *Mar. Chem.* **2014**, *163*, 10–18. https://doi.org/10.1016/j.marchem.2014.04.002.
(30) Timko, S. A.; Maydanov, A.; Pittelli, S. L.; Conte, M. H.; Cooper, W. J.; Koch, B. P.; Schmitt-Kopplin, P.; Gonsior, M. Depth-Dependent Photodegradation of Marine Dissolved Organic Matter. *Front. Mar. Sci.* **2015**, *2*. https://doi.org/10.3389/fmars.2015.00066.
(31) Tranvik, L. J.; Bertilsson, S. Contrasting Effects of Solar UV Radiation on Dissolved Organic Sources for Bacterial Growth. *Ecol. Lett.* **2001**, *4* (5), 458–463. https://doi.org/10.1046/j.1461-0248.2001.00245.x.
(32) Gonsior, M.; Schmitt-Kopplin, P.; Bastviken, D. Depth-Dependent Molecular Composition and Photo-Reactivity of Dissolved Organic Matter in a Boreal Lake under Winter and Summer Conditions. *Biogeosciences* **2013**, *10* (11), 6945–6956. https://doi.org/10.5194/bg-10-6945-2013.
(33) Jørgensen, L.; Stedmon, C. A.; Kragh, T.; Markager, S.; Middelboe, M.; Søndergaard, M. Global Trends in the Fluorescence Characteristics and Distribution of Marine Dissolved Organic Matter. *Mar. Chem.* **2011**, *126* (1–4), 139–148. https://doi.org/10.1016/j.marchem.2011.05.002.
(34) Tanaka, K.; Kuma, K.; Hamasaki, K.; Yamashita, Y. Accumulation of Humic-like Fluorescent Dissolved Organic Matter in the Japan Sea. *Sci. Rep.* **2015**, *4* (1), 5292. https://doi.org/10.1038/srep05292.
(35) Yamashita, Y.; Jaffé, R.; Maie, N.; Tanoue, E. Assessing the Dynamics of Dissolved Organic Matter (DOM) in Coastal Environments by Excitation Emission Matrix Fluorescence and Parallel Factor Analysis (EEM-PARAFAC). *Limnol. Oceanogr.* **2008**, *53* (5), 1900–1908. https://doi.org/10.4319/lo.2008.53.5.1900.
(36) Murphy, K. R.; Stedmon, C. A.; Graeber, D.; Bro, R. Fluorescence Spectroscopy and Multi-Way Techniques. PARAFAC. *Anal. Methods* **2013**, *5* (23), 6557. https://doi.org/10.1039/c3ay41160e.
(37) Helms, J. R.; Stubbins, A.; Ritchie, J. D.; Minor, E. C.; Kieber, D. J.; Mopper, K. Absorption Spectral Slopes and Slope Ratios as Indicators of Molecular Weight, Source, and Photobleaching of Chromophoric Dissolved Organic Matter. *Limnol. Oceanogr.* **2008**, *53* (3), 955–969. https://doi.org/10.4319/lo.2008.53.3.0955.

(38) Twardowski, M. S.; Boss, E.; Sullivan, J. M.; Donaghay, P. L. Modeling the Spectral Shape of Absorption by Chromophoric Dissolved Organic Matter. *Mar. Chem.* **2004**, *89* (1–4), 69–88. https://doi.org/10.1016/j.marchem.2004.02.008.
(39) Brown, M. Transmission Spectroscopy Examinations of Natural Waters. *Estuar. Coast. Mar. Sci.* **1977**, *5* (3), 309–317. https://doi.org/10.1016/0302-3524(77)90058-5.
(40) Vähätalo, A. V.; Wetzel, R. G. Photochemical and Microbial Decomposition of Chromophoric Dissolved Organic Matter during Long (Months–Years) Exposures. *Mar. Chem.* **2004**, *89* (1–4), 313–326. https://doi.org/10.1016/j.marchem.2004.03.010.
(41) De Haan, H.; De Boer, T. Applicability of Light Absorbance and Fluorescence as Measures of Concentration and Molecular Size of Dissolved Organic Carbon in Humic Lake Tjeukemeer. *Water Res.* **1987**, *21* (6), 731–734. https://doi.org/10.1016/0043-1354(87)90086-8.
(42) Peuravuori, J.; Pihlaja, K. Molecular Size Distribution and Spectroscopic Properties of Aquatic Humic Substances. *Anal. Chim. Acta* **1997**, *337* (2), 133–149. https://doi.org/10.1016/S0003-2670(96)00412-6.
(43) Fox, B. G.; Thorn, R. M. S.; Anesio, A. M.; Reynolds, D. M. The in Situ Bacterial Production of Fluorescent Organic Matter; an Investigation at a Species Level. *Water Res.* **2017**, *125*, 350–359. https://doi.org/10.1016/j.watres.2017.08.040.
(44) Goto, S.; Tada, Y.; Suzuki, K.; Yamashita, Y. Evaluation of the Production of Dissolved Organic Matter by Three Marine Bacterial Strains. *Front. Microbiol.* **2020**, *11*, 584419. https://doi.org/10.3389/fmicb.2020.584419.
(45) Shimotori, K.; Omori, Y.; Hama, T. Bacterial Production of Marine Humic-like Fluorescent Dissolved Organic Matter and Its Biogeochemical Importance. *Aquat. Microb. Ecol.* **2009**, *58*, 55–66. https://doi.org/10.3354/ame01350.
(46) Catalá, T. S.; Reche, I.; Fuentes-Lema, A.; Romera-Castillo, C.; Nieto-Cid, M.; Ortega-Retuerta, E.; Calvo, E.; Álvarez, M.; Marrasé, C.; Stedmon, C. A.; Álvarez-Salgado, X. A. Turnover Time of Fluorescent Dissolved Organic Matter in the Dark Global Ocean. *Nat. Commun.* **2015**, *6* (1), 5986. https://doi.org/10.1038/ncomms6986.
(47) Coble, P. G. Characterization of Marine and Terrestrial DOM in Seawater Using Excitation-Emission Matrix Spectroscopy. *Mar. Chem.* **1996**, *51* (4), 325–346. https://doi.org/10.1016/0304-4203(95)00062-3.
(48) Koch, B. P.; Witt, M.; Engbrodt, R.; Dittmar, T.; Kattner, G. Molecular Formulae of Marine and Terrigenous Dissolved Organic Matter Detected by Electrospray Ionization Fourier Transform Ion Cyclotron Resonance Mass Spectrometry. *Geochim. Cosmochim. Acta* **2005**, *69* (13), 3299–3308. https://doi.org/10.1016/j.gca.2005.02.027.
(49) Hertkorn, N.; Benner, R.; Frommberger, M.; Schmitt-Kopplin, P.; Witt, M.; Kaiser, K.; Kettrup, A.; Hedges, J. I. Characterization of a Major Refractory Component of Marine Dissolved Organic Matter. *Geochim. Cosmochim. Acta* **2006**, *70* (12), 2990–3010. https://doi.org/10.1016/j.gca.2006.03.021.
(50) D'Andrilli, J.; Dittmar, T.; Koch, B. P.; Purcell, J. M.; Marshall, A. G.; Cooper, W. T. Comprehensive Characterization of Marine Dissolved Organic Matter by Fourier Transform Ion Cyclotron Resonance Mass Spectrometry with Electrospray and Atmospheric Pressure Photoionization: Characterization of Marine Dissolved Organic Matter. *Rapid Commun. Mass Spectrom.* **2010**, *24* (5), 643–650. https://doi.org/10.1002/rcm.4421.

(51) Gonsior, M.; Peake, B. M.; Cooper, W. T.; Podgorski, D. C.; D'Andrilli, J.; Dittmar, T.; Cooper, W. J. Characterization of Dissolved Organic Matter across the Subtropical Convergence off the South Island, New Zealand. *Mar. Chem.* **2011**, *123* (1–4), 99–110. https://doi.org/10.1016/j.marchem.2010.10.004.
(52) Flerus, R.; Lechtenfeld, O. J.; Koch, B. P.; McCallister, S. L.; Schmitt-Kopplin, P.; Benner, R.; Kaiser, K.; Kattner, G. A Molecular Perspective on the Ageing of Marine Dissolved Organic Matter. *Biogeosciences* **2012**, *9* (6), 1935–1955. https://doi.org/10.5194/bg-9-1935-2012.
(53) Chen, H.; Stubbins, A.; Perdue, E. M.; Green, N. W.; Helms, J. R.; Mopper, K.; Hatcher, P. G. Ultrahigh Resolution Mass Spectrometric Differentiation of Dissolved Organic Matter Isolated by Coupled Reverse Osmosis-Electrodialysis from Various Major Oceanic Water Masses. *Mar. Chem.* **2014**, *164*, 48–59. https://doi.org/10.1016/j.marchem.2014.06.002.
(54) Lechtenfeld, O. J.; Kattner, G.; Flerus, R.; McCallister, S. L.; Schmitt-Kopplin, P.; Koch, B. P. Molecular Transformation and Degradation of Refractory Dissolved Organic Matter in the Atlantic and Southern Ocean. *Geochim. Cosmochim. Acta* **2014**, *126*, 321–337. https://doi.org/10.1016/j.gca.2013.11.009.
(55) Stubbins, A.; Lapierre, J.-F.; Berggren, M.; Prairie, Y. T.; Dittmar, T.; del Giorgio, P. A. What's in an EEM? Molecular Signatures Associated with Dissolved Organic Fluorescence in Boreal Canada. *Environ. Sci. Technol.* **2014**, *48* (18), 10598–10606. https://doi.org/10.1021/es502086e.
(56) Kellerman, A. M.; Kothawala, D. N.; Dittmar, T.; Tranvik, L. J. Persistence of Dissolved Organic Matter in Lakes Related to Its Molecular Characteristics. *Nat. Geosci.* **2015**, *8* (6), 454–457. https://doi.org/10.1038/ngeo2440.
(57) Dittmar, T.; Koch, B.; Hertkorn, N.; Kattner, G. A Simple and Efficient Method for the Solid-Phase Extraction of Dissolved Organic Matter (SPE-DOM) from Seawater: SPE-DOM from Seawater. *Limnol. Oceanogr. Methods* **2008**, *6* (6), 230–235. https://doi.org/10.4319/lom.2008.6.230.
(58) Schlitzer, R. Data Analysis and Visualization with Ocean Data View. *Can. Meteorlogical Oceanogr. Soc.* **2015**, No. 43, 9–13.
(59) Prasad, B. G.; Krishna, K. Muni. Response of Ocean Eddies to Monsoon Winds Over the Western Arabian Sea. *Open Access J. Phys.* **2020**, *4* (2), 9–16.
(60) Webb, P. *Introduction to Oceanography*; [publisher not identified]: [Place of publication not identified], 2019.
(61) Yamashita, Y.; Tanoue, E. Production of Bio-Refractory Fluorescent Dissolved Organic Matter in the Ocean Interior. *Nat. Geosci.* **2008**, *1* (9), 579–582. https://doi.org/10.1038/ngeo279.
(62) *Biogeochemistry of Marine Dissolved Organic Matter*, Second edition.; Hansell, D. A., Carlson, C. A., Eds.; Academic Press: Amsterdam ; Boston, 2015.
(63) Dalzell, B. J.; Minor, E. C.; Mopper, K. M. Photodegradation of Estuarine Dissolved Organic Matter: A Multi-Method Assessment of DOM Transformation. *Org. Geochem.* **2009**, *40* (2), 243–257. https://doi.org/10.1016/j.orggeochem.2008.10.003.
(64) Sharpless, C. M.; Blough, N. V. The Importance of Charge-Transfer Interactions in Determining Chromophoric Dissolved Organic Matter (CDOM) Optical and Photochemical Properties. *Env. Sci Process. Impacts* **2014**, *16* (4), 654–671. https://doi.org/10.1039/C3EM00573A.

(65) Boyle, E. S.; Guerriero, N.; Thiallet, A.; Vecchio, R. D.; Blough, N. V. Optical Properties of Humic Substances and CDOM: Relation to Structure. *Environ. Sci. Technol.* **2009**, *43* (7), 2262–2268. https://doi.org/10.1021/es803264g.
(66) Fichot, C. G.; Benner, R.; Kaiser, K.; Shen, Y.; Amon, R. M. W.; Ogawa, H.; Lu, C.-J. Predicting Dissolved Lignin Phenol Concentrations in the Coastal Ocean from Chromophoric Dissolved Organic Matter (CDOM) Absorption Coefficients. *Front. Mar. Sci.* **2016**, *3*. https://doi.org/10.3389/fmars.2016.00007.
(67) Grebel, J. E.; Pignatello, J. J.; Song, W.; Cooper, W. J.; Mitch, W. A. Impact of Halides on the Photobleaching of Dissolved Organic Matter. *Mar. Chem.* **2009**, *115* (1–2), 134–144. https://doi.org/10.1016/j.marchem.2009.07.009.
(68) Del Vecchio, R.; Blough, N. V. On the Origin of the Optical Properties of Humic Substances. *Environ. Sci. Technol.* **2004**, *38* (14), 3885–3891. https://doi.org/10.1021/es049912h.
(69) Santos, L.; Pinto, A.; Filipe, O.; Cunha, Â.; Santos, E. B. H.; Almeida, A. Insights on the Optical Properties of Estuarine DOM – Hydrological and Biological Influences. *PLOS ONE* **2016**, *11* (5), e0154519. https://doi.org/10.1371/journal.pone.0154519.
(70) Wünsch, U. J.; Murphy, K. R.; Stedmon, C. A. Fluorescence Quantum Yields of Natural Organic Matter and Organic Compounds: Implications for the Fluorescence-Based Interpretation of Organic Matter Composition. *Front. Mar. Sci.* **2015**, *2*. https://doi.org/10.3389/fmars.2015.00098.
(71) Yamashita, Y.; Tanoue, E. Chemical Characterization of Protein-like Fluorophores in DOM in Relation to Aromatic Amino Acids. *Mar. Chem.* **2003**, *82* (3–4), 255–271. https://doi.org/10.1016/S0304-4203(03)00073-2.
(72) Stedmon, C. A.; Nelson, N. B. *Biogeochemistry of Marine Dissolved Organic Matter*, 2nd ed.; Academic Press: Boston, 2015.
(73) Wünsch, U. J.; Murphy, K. R.; Stedmon, C. A. Fluorescence Quantum Yields of Natural Organic Matter and Organic Compounds: Implications for the Fluorescence-Based Interpretation of Organic Matter Composition. *Front. Mar. Sci.* **2015**, *2*. https://doi.org/10.3389/fmars.2015.00098.
(74) Yamashita, Y.; McCallister, S. L.; Koch, B. P.; Gonsior, M.; Jaffé, R. Dynamics of Dissolved Organic Matter in Fjord Ecosystems: Contributions of Terrestrial Dissolved Organic Matter in the Deep Layer. *Estuar. Coast. Shelf Sci.* **2015**, *159*, 37–49. https://doi.org/10.1016/j.ecss.2015.03.024.
(75) Bates, N. R.; Johnson, R. J. Acceleration of Ocean Warming, Salinification, Deoxygenation and Acidification in the Surface Subtropical North Atlantic Ocean. *Commun. Earth Environ.* **2020**, *1* (1), 33. https://doi.org/10.1038/s43247-020-00030-5.
(76) Montes, E.; Muller-Karger, F. E.; Cianca, A.; Lomas, M. W.; Lorenzoni, L.; Habtes, S. Decadal Variability in the Oxygen Inventory of North Atlantic Subtropical Underwater Captured by Sustained, Long-term Oceanographic Time Series Observations. *Glob. Biogeochem. Cycles* **2016**, *30* (3), 460–478. https://doi.org/10.1002/2015GB005183.
(77) Koslow, J. A.; Davison, P.; Ferrer, E.; Jiménez Rosenberg, S. P. A.; Aceves-Medina, G.; Watson, W. The Evolving Response of Mesopelagic Fishes to Declining Midwater Oxygen Concentrations in the Southern and Central California Current. *ICES J. Mar. Sci.* **2019**, *76* (3), 626–638. https://doi.org/10.1093/icesjms/fsy154.

(78) Arístegui, J.; Duarte, C. M.; Agustí, S.; Doval, M.; Álvarez-Salgado, X. A.; Hansell, D. A. Dissolved Organic Carbon Support of Respiration in the Dark Ocean. *Science* **2002**, *298* (5600), 1967–1967. https://doi.org/10.1126/science.1076746.
(79) Xilin Xiao. The Efficiency of the Microbial Carbon Pump as Seen from the Relationship between Apparent Oxygen Utilization and Fluorescent Dissolved Organic Matter, 2022. https://doi.org/10.17632/R96HJS8XV5.1.
(80) Yamashita, Y.; Hashihama, F.; Saito, H.; Fukuda, H.; Ogawa, H. Factors Controlling the Geographical Distribution of Fluorescent Dissolved Organic Matter in the Surface Waters of the Pacific Ocean: FDOM in the Surface Waters of the Pacific. *Limnol. Oceanogr.* **2017**, *62* (6), 2360–2374. https://doi.org/10.1002/lno.10570.
(81) Stanley, R. H. R.; Doney, S. C.; Jenkins, W. J.; Lott, III, D. E. *Apparent Oxygen Utilization Rates Calculated from Tritium and Helium-3 Profiles at the Bermuda Atlantic Time-Series Study Site*; preprint; Biogeochemistry: Open Ocean, 2011. https://doi.org/10.5194/bgd-8-9977-2011.
(82) Aytan, U.; Feyzioglu, A. M.; Valente, A.; Agirbas, E.; Fileman, E. S. Microbial Plankton Communities in the Coastal Southeastern Black Sea: Biomass, Composition and Trophic Interactions. *Oceanologia* **2018**, *60* (2), 139–152. https://doi.org/10.1016/j.oceano.2017.09.002.
(83) Lee, H.-W.; Noh, J.-H.; Choi, D.-H.; Yun, M.; Bhavya, P. S.; Kang, J.-J.; Lee, J.-H.; Kim, K.-W.; Jang, H.-K.; Lee, S.-H. Picocyanobacterial Contribution to the Total Primary Production in the Northwestern Pacific Ocean. *Water* **2021**, *13* (11), 1610. https://doi.org/10.3390/w13111610.
(84) Agawin, N. S. R.; Duarte, C. M.; Agustí, S. Nutrient and Temperature Control of the Contribution of Picoplankton to Phytoplankton Biomass and Production. *Limnol. Oceanogr.* **2000**, *45* (3), 591–600. https://doi.org/10.4319/lo.2000.45.3.0591.
(85) Zhao, Z.; Gonsior, M.; Schmitt-Kopplin, P.; Zhan, Y.; Zhang, R.; Jiao, N.; Chen, F. Microbial Transformation of Virus-Induced Dissolved Organic Matter from Picocyanobacteria: Coupling of Bacterial Diversity and DOM Chemodiversity. *ISME J.* **2019**, *13* (10), 2551–2565. https://doi.org/10.1038/s41396-019-0449-1.
(86) Scanlan, D. J.; West, N. J. Molecular Ecology of the Marine Cyanobacterial Genera Prochlorococcus and Synechococcus. *FEMS Microbiol. Ecol.* **2002**, *40* (1), 1–12. https://doi.org/10.1111/j.1574-6941.2002.tb00930.x.
(87) Agawin, N. S. R.; Duarte, C. M.; Agustí, S.; McManus, L. Abundance, Biomass and Growth Rates of Synechococcus Sp. in a Tropical Coastal Ecosystem (Philippines, South China Sea). *Estuar. Coast. Shelf Sci.* **2003**, *56* (3–4), 493–502. https://doi.org/10.1016/S0272-7714(02)00200-7.
(88) Zark, M.; Christoffers, J.; Dittmar, T. Molecular Properties of Deep-Sea Dissolved Organic Matter Are Predictable by the Central Limit Theorem: Evidence from Tandem FT-ICR-MS. *Mar. Chem.* **2017**, *191*, 9–15. https://doi.org/10.1016/j.marchem.2017.02.005.
(89) Hertkorn, N.; Harir, M.; Koch, B. P.; Michalke, B.; Schmitt-Kopplin, P. High-Field NMR Spectroscopy and FTICR Mass Spectrometry: Powerful Discovery Tools for the Molecular Level Characterization of Marine Dissolved Organic Matter. *Biogeosciences* **2013**, *10* (3), 1583–1624. https://doi.org/10.5194/bg-10-1583-2013.

(90) Riedel, T.; Dittmar, T. A Method Detection Limit for the Analysis of Natural Organic Matter via Fourier Transform Ion Cyclotron Resonance Mass Spectrometry. *Anal. Chem.* **2014**, *86* (16), 8376–8382. https://doi.org/10.1021/ac501946m.
(91) Witt, M.; Fuchser, J.; Koch, B. P. Fragmentation Studies of Fulvic Acids Using Collision Induced Dissociation Fourier Transform Ion Cyclotron Resonance Mass Spectrometry. *Anal. Chem.* **2009**, *81* (7), 2688–2694. https://doi.org/10.1021/ac802624s.
(92) Hansell, D. A.; Carlson, C. A.; Amon, R. M. W.; Álvarez-Salgado, X. A.; Yamashita, Y.; Romera-Castillo, C.; Bif, M. B. Compilation of Dissolved Organic Matter (DOM) Data Obtained from Global Ocean Observations from 1994 to 2020 (NCEI Accession 0227166), 2021. https://doi.org/10.25921/S4F4-YE35.
(93) Hansman, R. L.; Dittmar, T.; Herndl, G. J. Conservation of Dissolved Organic Matter Molecular Composition during Mixing of the Deep Water Masses of the Northeast Atlantic Ocean. *Mar. Chem.* **2015**, *177*, 288–297. https://doi.org/10.1016/j.marchem.2015.06.001.
(94) David Shiffman, Ph.D. How Accessible Are Marine Biology Careers for Disabled People? *Scuba Diving*. January 22, 2022.
(95) Krietsch Boerner, L. Expanding American Sign Language's Scientific Vocabulary. *American Chemical Society*. Chemical & Engineering News July 11, 2021.
(96) Orcutt, B.; Cetinic, I. Women in Oceanography: Continuing Challenges. *Oceanography* **2014**, *27* (4), 5–13. https://doi.org/10.5670/oceanog.2014.106.
(97) Ellis, R. A.; Babco, E. L.; Frehill, L. M.; Bell, N. A. Improving Federal Statistics on the Science, Technology, Engineering and Mathematics (STEM) Workforce, 2007.
(98) Atchison, C. L.; Libarkin, J. C. Professionally Held Perceptions about the Accessibility of the Geosciences. *Geosphere* **2016**, *12* (4), 1154–1165. https://doi.org/10.1130/GES01264.1.
(99) Burrelli, J. S.; Falkenheim, J. C. Diversity in the Federal Science and Engineering Workforce: Washington D.C., 2011.
(100) Behl, M.; Cooper, S.; Garza, C.; Kolesar, S.; Legg, S.; Lewis, J.; White, L.; Jones, B. Changing the Culture of Coastal, Ocean, and Marine Sciences: Strategies for Individual and Collective Actions. *Oceanography* **2021**, *34* (3). https://doi.org/10.5670/oceanog.2021.307.
(101) Gibney, E. How One Astronomer Hears the Universe. *Nature* **2020**, *577* (7789), 155–155. https://doi.org/10.1038/d41586-019-03938-x.
(102) Showstack, R. Accessible Oceans. *Oceanus*. October 13, 2021.